Design, Synthesis and Biological Assessment of Topoisomerase-I Inhibitors Targeting *Mycobacterium tuberculosis*

THESIS

Submitted in partial fulfilment

of the requirements for the degree of

DOCTOR OF PHILOSOPHY

by

PADMA SRIDEVI J

ID No. 2012PHXF539H

Under the supervision of

D. SRIRAM

BITS Pilani

Pilani | Dubai | Goa | Hyderabad

BIRLA INSTITUTE OF TECHNOLOGY AND SCIENCE, PILANI

2016

BIRLA INSTITUTE OF TECHNOLOGY AND SCIENCE, PILANI

CERTIFICATE

This is to certify that the thesis entitled "**Design, synthesis and biological assessment of topoisomerase-I inhibitors targeting *Mycobacterium tuberculosis***"and submitted by **PADMA SRIDEVI J** ID No.**2012PHXF539H** for award of Ph.D. of the Institute embodies original work done by her under my supervision.

Signature of the Supervisor **:**

Name in capital letters **: D. Sriram**

Designation **: Professor**

Date:

Acknowledgement

First and foremost I would like to thank almightyproviding me this opportunity and enough amount of strength in the accomplishment of this work.

I could not have completedmy PhD without the invaluable support of a several. Without these supporters, especially the select few I'm about to mention, I may not have been to where I am today.

I take this opportunity to sincerely acknowledge Department of science and Technology, Government of India, New Delhi, for providing me financial assistance by awarding me ***DST-INSPIRE fellowship****.*

My gratitude is also extended to my DAC members ***Prof. P. Yogeeswari****and****Dr.Sajeli begum****for their support and encouragement during this period.*

I'd also like to give a heartfelt, special thanks to ***Prof.V.S.Rao*** *(Director, Hyderabad campus)&Vice-Chancellor (BITS), for allowing me to carry out my doctoral research work in the institute.*

I am thankful to ***Prof. M. M. S.Anand,*** *Registrar and* ***Prof.S.K.Verma,*** *Dean, Academic Research (Ph.D. Programme), BITS Pilani for their support to do my research work.*

I would like to express my sincere thanks to ***Prof.M.B.Srinivas,*** *Dean, Administration and* ***Dr.Vidya Rajesh,*** *Associate Dean, Academic Research (Ph.D. Programme), BITS-Pilani, Hyderabad campus for their continuous support and encouragement during my research work.*

*Next I'd like to thank****Dr.Shrikanth Y. Charde****, Head of the Department, Pharmacy, for providing me with all the necessary laboratory facilities and for having helped me at various stages of my research work.*

I sincerely acknowledge the help rendered by ***Dr.Punna Rao Ravi,,Dr.Arthidhar, Dr. V. V. Vamsi Krishna,Dr.Balram Ghosh,, Dr. Swati Biswas*** *and* ***Dr.OnkarKulkherni,*** *faculty at Department of Pharmacy, BITS-Pilani, Hyderabad campus.*

I owe a great deal of appreciation and gratitude to ***Dr.Vinay Kumar Nandicoori****, Scientist, and his group at National Institute of Immunology, New Delhi, India for providing Mycobacterium tuberculosis Topo-I clone.*

I would feel pleasure to thank Dr.Vanajakumar, Former Deputy Director for Bacteriology division at National institute of Research in tuberculosis (NIRT), Chennai, for providing us Mycobacterium tuberculosis H37Rv and other resistant strains. I also thank them for providing me training to handle Mycobacterium tuberculosis strains.

In addition, I am very much grateful to all my friends ***Ganesh S, Manoj, Ganesh P, Jean, Sridhar, Parameshwar, Brindha, Mallika, Shalini, Reshma A, Reshma S, Vijay, Renuka, Koushik, Madhu, Saketh Sriram, Priyanka P, Priyanka S, Hasitha, Patrisha, Ram, Brahmam, Bobesh, Radhika, Gangadhar, Srikanth, Shubam, Praveen, Suman, Mahibalan, Rukaiyya, Shailendar, Poorna, Santosh, Preethi, Omkar, Anup, Shubmita, Vishnu, Rimpy, Reshma, Nikhila, Prashanthi, Himanshu****for the time they had spent for me and making my stay at campus a memorable one. I take this opportunity to thank one and all for their help directly or indirectly.*

I take this opportunity to thank the project students, especially, ***Sruthi, Shruthisingh and Sravan.***

I express my thanks to our laboratory assistants, ***Mrs. Saritha****,* ***Mr. Rajesh****,* ***Mr. Ramu****,* ***Mr.Seenu*** *and* ***Mrs. Rekha****.*

*Of course no acknowledgments would be complete without giving thanks to my parents. I would like to begin by dedicating this piece of work to my parents****Mr.J.Sriramamohan and Late Mrs. J. Annapurna devi****, whose dreams had come to life with me getting the highest degree in education. I owe my doctorate degree to my parents who kept with their continuous care, support and encouragement my morale high. Thanks are due if I don't dedicate this thesis to my brother* ***J.Srinivas and my family*** *whose constant and continuous support, love and affection made me reaching this height.*

Last but never least, I would like to thank my unbelievably supportive husband, ***Mr. Amaresh Murthiraju*** *for his immense support in each and every step of my PhD.*

This thesis is dedicated to the memory of my beloved mother, ***Mrs. J. Annapurna Devi.*** *It is your shining example that I try to reproduce in all that I do. Thank you for everything.*

Thanks to those who hated me,
You made me stronger.
Thanks to those who loved me,
You made my heat go fonder.
Thanks to those who cared,
You made me feel important.
Thanks to those who entered into my life,
You made who I am today.
Thanks to those who left,
You showed mw that nothing lasts forever.
Thanks to those who stayed,
You showed me true friendship.
Thanks to those who listened,
You made me like I was worth it.

Date: *PADMA SRIDEVI J*

Abstract

Tuberculosis (TB) is the leading infectious disease world-wide and is responsible for the greatest morbidity and mortality. In this study we have focused on developing novel leads for the enzyme target topoisomerase-I of tuberculosis in both active and dormant forms.

Mycobacterium tuberculosis (Mtb) topoisomerase I (Topo I), involved in the relaxation of negatively supercoiledDNA, plays an important role in the viability of pathogen Mtb. Being one of the most significantenzymes; it also takes part in crucial biological pathways such as transcription and replication of the pathogen. The present study aims at the development of MtbTopo I 3D protein structure which in turn was employed for the virtual screening of compound libraries in a process of identification of a hit molecule. Three lead molecules hydroxycamptothecin, amsacrine and tryptanthrin were identified. Lead-I,hydroxycamptothecin, was active with an IC_{50} of 6.25 µM which was further derivatized synthetically into fifteen novel analogues. Among these, four compounds (**3b**, **3g**, **3h** and **3l**) emerged to be active displaying IC50 values ranging from 2.9 to 9.3 µM against MtbTopo I and were non-cytotoxic at 25 µM. These four compounds also proved their efficacy when tested against active, dormant and resistant forms of Mtb. The most potent inhibitor **3b** was screened for *in vivo* anti-mycobacterial activity using adult zebrafish model and was found to be more effective when compared to first line anti-tubercular drugs, isoniazid and rifampicin. The binding affinity of this compound towards MtbTopo I was analysed by differential scanning fluorimetry which resulted in a positive shift in melting temperature when compared to the native protein thereby proving its stabilization effect over protein.

Lead-II, amsacrine was active at 25 µM which was further derivatized into twenty four analogues. Out of which, three compounds **6b**, **6d** and **7d** were found to be active with IC50 values 12.3, 14.8 and 22.8 µM. These three compounds were further tested for their activity on active, dormant and resistant forms and these compounds exhibited good active against the same. The most active compounds **6b** and **6d** were screened for *in vivo* anti-mycobacterial activity using adult zebrafish and compound **6d** was found to be more effective than standard compound Moxifloxacin with ~3.1 bacterial log reduction.

Lead-III, tryptanthrin was active at 42.3 µM on MtbTopo I. This was further derivatised into thirteen analogues using medicinal chemistry approach. Out of these 13 compounds, three compounds **TR07**, **TR11** and **TR12** were found to potent than the lead compound exhibiting and IC50 of 20.2, 21.6 and 35.8 µM respectively. These compounds were further screened for

their anti-tubercular activity on active, dormant and resistant TB and were found to be active on all the three forms. The most active compounds **TR00** and **TR11** were tested for *in vivo* anti-mycobacterial activity using adult zebrafish. Compound **TR11** exhibited promising activity and was found to be more potent than standard compound Moxifloxacin with ~3.0 bacterial log reduction.

Thus, with an urgent need of anti-mycobacterial drugs for dormant forms, we believe that the present class of drugs could be useful as potential leads for further optimization through mutagenesis, and pharmacokinetic approaches.

Table of Contents

List of Tables

List of Figures

List of Abbreviations

μM	:	Micromolar
δ	:	Chemical shift
^{13}C NMR	:	Carbon Nuclear Magnetic Resonance
^{1}H NMR	:	Proton Nuclear Magnetic Resonance
ATP	:	Adenosine Triphosphate
BCG	:	Bacillus Calmette-Guerin
BLAST	:	Basic Local Alignment Search Tool
CFU	:	Colony Forming Unit
CHN	:	Carbon Hydrogen Nitrogen
CNS	:	Central Nervous System
CoA	:	Coenzyme A
D	:	Hydrogen bond Donor
d	:	Doublet
dd	:	Doublet of Doublet
DMSO	:	Dimethyl Sulphoxide
DMSO d_6	:	Dimethyl Sulphoxide deuterated
DOTS	:	Directly Observed Treatment, Short course
DSF	:	Differential Scanning Flourimetry
EF	:	Enrichment Factor
FBS	:	Fetal Bovine Serum
FDA	:	Food and Drug Administration
GH	:	Goodness of Hit
GLIDE	:	Grid based Ligand Docking and Energetics
HEPES	:	4-(2-Hydroxyethyl)piperazine-1-ethanesulfonic acid
HIV	:	Human Immunodeficiency Virus
HPLC	:	High Pressure Liquid Chromatography
HTVS	:	High-throughput Virtual Screening
IC_{50}	:	Half maximal Inhibitory Concentration
IPTG	:	Isopropyl β-D-1-thiogalactopyranoside
J	:	Coupling constant
kDa	:	Kilo Daltons

K_i	:	Inhibitor constant
K_m	:	Kinetic constant
LCMS	:	Liquid Chromatography-Mass Spectrometer
LTBI	:	Latent Tuberculosis Infection
m	:	Multiplet
m-Amsa	:	m-Amsacrine
M.P	:	Melting point
MABA	:	Microplate Alamar Blue Assay
MDR TB	:	Multidrug Resistant Tuberculosis
mg	:	Milligram
MIC	:	Minimum Inhibitory Concentration
ml	:	Milliliter
mM	:	Millimolar
mmol	:	Millimole
MPN	:	Most Probable Number
Mtb	:	*Mycobacterium tuberculosis*
MTT	:	(4,5-dimethylthiazol-2-yl)-2,5-diphenyltetrazolium bromide
N	:	Negative ionisable
NaCl	:	Sodium chloride
NaOH	:	Sodium hydroxide
Ni-NTA	:	Nickel-nitroloacetic acid
nM	:	Nanomolar
nm	:	Nanometre
NRP	:	Non-Replicating Persistant
ns	:	Nanoseconds
OADC	:	Oleic acid, Albumin, Dextrose, Catalase
OPLS		Optimised Potentials For Liquid Simulations
PAGE	:	Polyacrylamide Gel Electrophoresis
PCR	:	Polymerase Chain Reaction
PDB	:	Protein Data Bank
PHASE	:	Pharmacophoric Search Engine
pM	:	Picomolar

q	:	Quadruplet
QPlogBB	:	QuickProp predicted Blood Brain partition coefficient
QPlogCaco	:	QuickProp predicted Caco-2 cell permeability
QPlogHERG	:	QuickProp predicted the human Ether-a-go-go-Related gene
QPlogP	:	QuickProp predicted Partition coefficient
R	:	Aromatic ring
RFU	:	Relative Fluorescence Units
RMSD/rmsd	:	Root Mean Square Deviation
RNI	:	Reactive Nitrogen Intermediate
ROI	:	Reactive Oxygen Intermediate
rpm	:	Rotation per minute
RPMI	:	Roswell Park Memorial Institute
rt	:	Room Temperature
RT-PCR	:	Real time Polymerase Chain Reaction
s	:	Singlet
SAR	:	Structure-Activity Relationship
SD	:	Standard Deviation
SDS	:	Sodium Dodecyl Sulphate
SEM	:	Standard Error of the Mean
SP	:	Standard Precision
t	:	Triplet
TAE buffer	:	Tris base, Acetic acid and EDTA buffer
TB	:	Tuberculosis
TIP_3P		Three-site Transferable Intermolecular Potential
Topo I	:	Topoisomerase I
TLC	:	Thin Layer Chromatography
T_m	:	Melting temperature
V_{max}	:	Maximum velocity
WHO	:	World Health Organisation
XDR-TB	:	Extensively Drug Resistant Tuberculosis
XP	:	Extra Precision

Chapter 1

Introduction

1.1. Tuberculosis

Koch's disease or tuberculosis (TB) caused by *Mycobacterium tuberculosis* (Mtb), a facultative intracellular organism discovered by Robert Koch in 1882 is an ancient contagious disease that currently presents an immense global health challenge. The fate of the initial exposure to *Mycobacterium tuberculosis* varies from immediate elimination of the organism by the host's innate immune response to infected individuals developing active primary TB [Flynn J.L., *et al.,* 2001]. The initial acute infection in immunocompetent individuals is controlled by the immune system, and living bacteria are limited in a peculiar confined pulmonary structure called granuloma. There the bacteria endures indefinitely in a latent non-virulent form, and gets reactivated whenever an immunosuppressive condition occurs [Ferraris D.M., *et al.,* 2011]. However, these patients have the risk of 5-10 % to develop active form during their life even with the absence of any cause of immunosuppression (Figure 1.1) [Clark-Curtiss., *et al*., 2003]. The increasing emergence of drug resistant TB and HIV co-infection, which compromises host defence and allows latent infection to reactivate or render individuals more susceptible to TB, pose as further challenge for effective control of the disease [Corbett E.L., *et al.,* 2003].

An estimate by World Health Organization (WHO) in 2014 shows that about 9 million people developed TB and 1.5 million died from the disease (3,60,000 of whom were HIV-positive), with the overwhelming majority of these from developing parts of the world [WHO Global Tuberculosis Report 2014]. An estimated 1.1 million (13%) of the 9 million people who developed TB in 2013 were HIV-positive. In 2013, an estimated 5,10,000 women died as a

result of TB. From 2000 to 2013, 37 million lives were saved through effective diagnosis and treatment. Out of 9 million people who developed TB in 2013, more than half (around 56%) were in the Western Pacific regions and South-East Asia. India and China alone accounted for 24% and 11% of total cases, respectively. This situation highlights the relative shortcomings of the current treatment strategies for TB and the limited efficacy of public health systems; particularly in resource-poor countries where the main TB burden lies.

1.2. Physiology of Mtb

Mtb is a non-motile rod shaped bacterium distantly related to actinomycetes. The rods are of 2-5 μm in length and 0.2-0.5 μm in width. Since it is an obligate aerobe, Mtb complexes are found in upper lobes of lungs in human. Mtb is a facultative intracellular parasite that has slow doubling time, i.e 15-20 hrs, and a characteristic feature that contributes to its virulence. Mtb is classified as neither as Gram-positive nor as Gram-negative because it do not have corresponding characteristics. Hence Mtb is classified specifically as acid-fast bacteria due to their impermeability of specific dyes and stains. Anti-tuberculosis agents in current development trigger a large panel of biological pathways such as cell wall synthesis, DNA replication, protein synthesis or membrane energy production [Zhang Y., *et al*., 2005].

1.3. Pathogenesis of TB

Nearly 2 billion people are estimated to be latently infected with Mtb, in a non-replicating or dormant stage. TB can affect any organ but mostly affects lungs. Mtb is transmitted *via* air and reaches pulmonary alveoli where the bacteria are phagocytized by non-activated macrophages. Within the macrophage the bacteria inhibit many cellular mechanisms preventing the fusion between phagosomes and lysosomes [Houben E.N., *et al*., 2006]. The ability of the bacteria to circumvent phagolysosomal degradation allows it to replicate freely and eventually when macrophage lyses the bacteria could invade new macrophage. When large number of

macrophage gets infected, they fuse and form multinucleated giant cells called Langhans cells. Other immune cells surround the infected macrophage forming a barrier to the surrounding tissue, thereby creating a compartment called granuloma [Pieters J., *et al*., 2008]. In most cases, the immune system overwhelms the infection and the bacteria enter a dormant state (stop to replicate) within the granulomas. In these granulomas there is a balance between the host immune response and pathogen virulence factors. Suppression of immune system at later state could result in reactivation of bacterial multiplication and continuation of Mtb infectious cycle.

Bacteria inside the granulomas could survive for long time and hence requires longer antibiotic treatment. Most of the commonly available antibiotics are directed towards different parts of replication machinery which are not targeted as effectively in dormant bacteria. Within granulomas the microenvironment could be characterized by hypoxia, nutrient starvation and exposure to reactive oxygen intermediates (ROI) and reactive nitrogen intermediates (RNI) [Vergne I., *et al*., 2004]. These compounds are used by phagocytic cells to eliminate internalized bacteria, yet some pathogenic bacteria like *S. typhimurium* and Mtb were found to avoid elimination, leading to long term survival and the establishment of persistent infection [Zahrt T.C., *et al*., 2002]. The peptidoglycan layer was found to play an important role in the maintenance of dormancy in bacteria and variation in specific cross-link during stationary phase adaptation of Mtb.

There is strong evidence that Mtb uses lipids as their major energy source for persistence in the host. Mtb uses the host triacylglycerol to accumulate lipid droplets intracellularly and acquire dormancy phenotype inside macrophage [Fattorini L., *et al*., 2014]. Recently it was reported that, dormant bacteria may be eradicated with antibiotics generated with hydroxyl radicals, suggesting that stimulation of reactive oxygen species provide potential strategy to manage persistent infections [Grant S.S., *et al*., 2012]

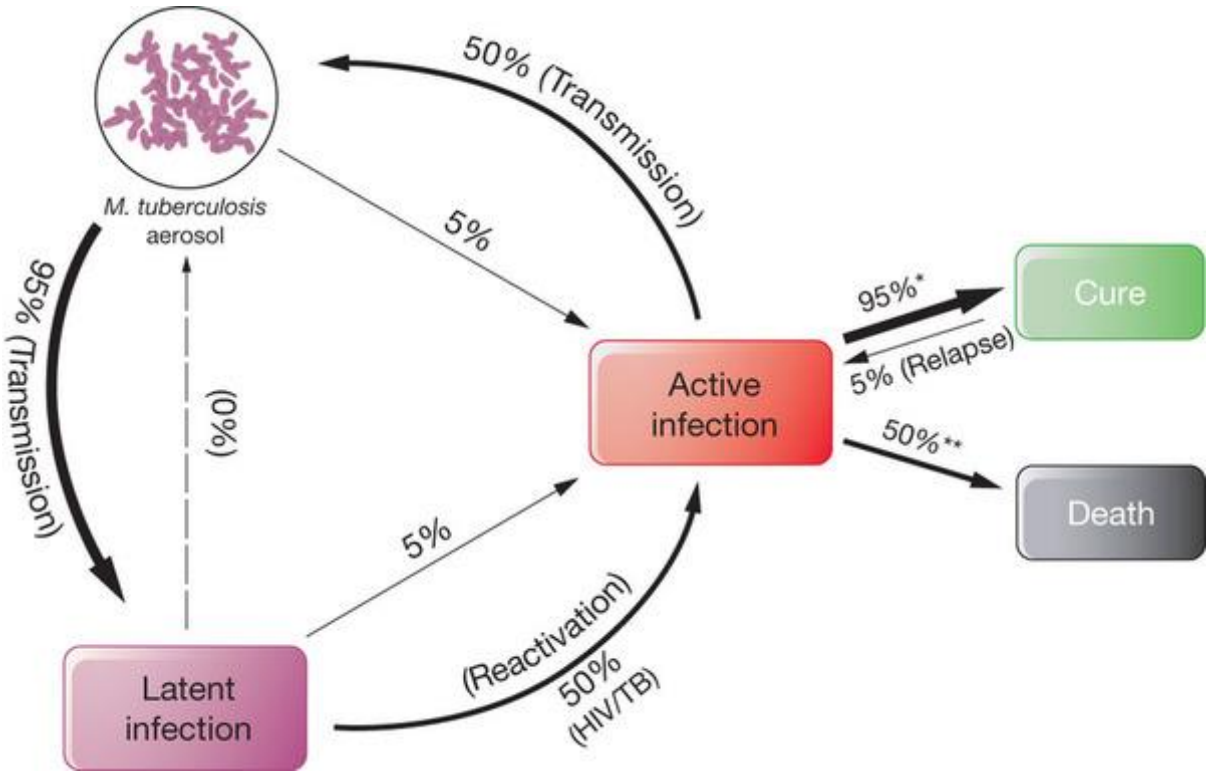

Figure 1.1: Dormant Mtb and active TB differentiation inside the macrophage [Koul A., et al., 2011]

Most of the TB drugs in first-line were discovered in 1950's and 1960's. Streptomycin was first discovered as an effective anti-TB agent [Vilemagne D., *et al*., 2012]. This aminoglycoside interfere with protein biosynthesis through interaction with 30S ribosome subunit [Schatz A., *et al*., 1944; Jones D., *et al*., 1944]. Discovery of mycolic acid synthesis inhibitor INH was one of the most active TB drugs till date [Bernstein J., *et al*., 1944]. The discovery of pyrazinamide, a major breakthrough in TB treatment made significant reduction in treatment period from 9 months to 6 months. In 1961, investigation of polyamines and diamines led to production of a series of diamine analogues that gave rise to discover of ethambutol [Thomas J.P., *et al*., 1961]. Finally rifampicin (RIF) [Binda G., *et al*., 1971] the last member of present first-line drugs was found effective against replicating and non-replicating Mtb. This class of drugs inhibited RNA synthesis by binding to the B-subunit of DNA-dependent polymerase.

In-spite of significant efficiency by these drugs, it was observed that the bacteria rapidly developed resistance to these drugs and stable cure was unattainable with single dose therapy. Inorder to prevent the development of resistance and produce stable cure, combination therapy was introduced. WHO recommended DOTS (Directly observed treatment, short course) anti-TB therapy using combination of four drugs: isoniazid, ethambutol and pyrazinamide for two months followed by rifampicin and isoniazid for four months [Kimerling M.E., *et al*., 1999]. The combination therapy cure rates were found to be 90% in HIV-negative patients which was a globally accepted standard treatment of active TB. Treatment with these first-line drugs when carried for two months led to destruction of bacteria in all stages of growth and when the treatment continued with rifampicin and isoniazid for four months, residual dormant bacilli was eliminated using rifampicin and any rifampicin resistant mutant was killed by isoniazid.

1.4. Limitations of TB drug therapy and emergence of Drug resistant TB

Due to emergence of drug resistant TB and association between HIV and Mtb, DOTS became rapidly ineffective in controlling TB [Kimerling M.E., *et al*., 1999]. The combination of drugs was very expensive and has to be administered for a longer duration which led to significant side effects. The length of therapy makes the patient compliance difficult and these patients would become susceptible to drug-resistant strains. The second major problem was that the current therapies available today were ineffective against persistent bacilli except rifampicin and pyrazinamide. Rifampicin was active against both actively growing and slow metabolizing non-growing bacilli whereas pyrazinamide was active against semi-dormant non-growing bacilli. However there are still dormant bacilli populations not killed by any of the available drugs [Chopra P., *et al*., 2003]. Therefore, there is a need for new drugs that are more active against slowly growing and persistent bacilli to treat populations of bacteria at risk of developing active disease through reactivation. Also, it is important to achieve shortened therapy to slow down the development of drug resistance in mycobacteria.

MDR-TB is resistant to the first-line anti-TB drugs isoniazid and rifampicin. The term MDR-TB was associated with high mortality rates occurred among HIV-infected patients [WHO report, 2013]. The treatment is quite complicated and it requires second-line drugs some of which are less effective, more toxic and expensive than first-line drugs. XDR-TB is resistant to at least isoniazid and rifampicin and also to fluoroquinolones, capreomycin, kanamycin and amikacin. XDR-TB requires longer treatments with drugs are very costly with limited efficacy and increased side effects. XDR-TB is reported in 77 countries and its prevalence is not clear. Only two of 27 burden MDR-TB countries are routinely testing for the resistance of second-line drugs; since XDR-TB is resistant to first and second-line drugs. The genetic diversity of drug-resistant Mtb indicates that the drug resistance has been evolving due to inappropriate drug treatment [Trauner A., *et al*., 2014]. The ongoing evolution of Mtb, provide excellent opportunity to explore genetic determinants of drugs resistance to Mtb. Unlike other bacterial pathogens, resistance plasmids and horizontal gene transfer plays no role in drug resistance to Mtb. Efflux mechanism seem to play vital role in developing resistance to this pathogenic bacterium. Due to genetic mutations could be helpful for reliable molecular markers for drug susceptibility testing. The application of this technology to clinical research led to the development of diagnostic tool based on nucleic acid amplification [Trauner A., *et al*., 2014].

1.5. TB drug pipeline

A major advance in the screening efficacy for novel targets was achieved by shifting from enzyme targets to phenotypic screening of whole bacterial cell. Whole bacterial cell screening identified diarylquinolones (bedaquiline), benzothiazines (BTZ-043 and PBTZ-169), and imidazopyridine amide (Q-203) [Zumla A.I., *et al*., 2014] (Figure 1.2).

Bedaquiline (TMC-207), an adenosine triphosphate synthase inhibitor was recently approved by U.S. FDA for the treatment of MDR-TB as a part of new combination therapy. Also, IOC-

67683 (delamanid) and TBA-354, a second generation nitroimidazole has also entered phase 3 trials for the treatment of MDR-TB.

Q-203, a compound made from imidazopyridines inhibits the mycobacterial growth by blocking respiratory cytochrome essential for maintaining the proton gradient and ATP synthesis. This drug also has similar property as bedaquiline and inhibits both replicating and non-replicating Mtb. It is active against MDR-TB, XDR-TB and *in vivo* data shows there is 100-1000 fold reduction of CFU and blocking of granuloma formation.

Benzothiazinones derivatives, PBTZ-169 and BTZ-043 are in late stage of clinical development. Both drugs inhibits the enzyme, decaprenylphosphory-β-D-ribose 2' epimerase (DprE1) in Mtb. Inhibition of this enzyme prevents the formation of decaprenylphosphoryl arabinose- a key precursor for biosynthesis of cell wall arabinans, resulting in cell lysis and bacterial death. Both the compounds show 100-1000 fold reduction in CFU *in vivo*.

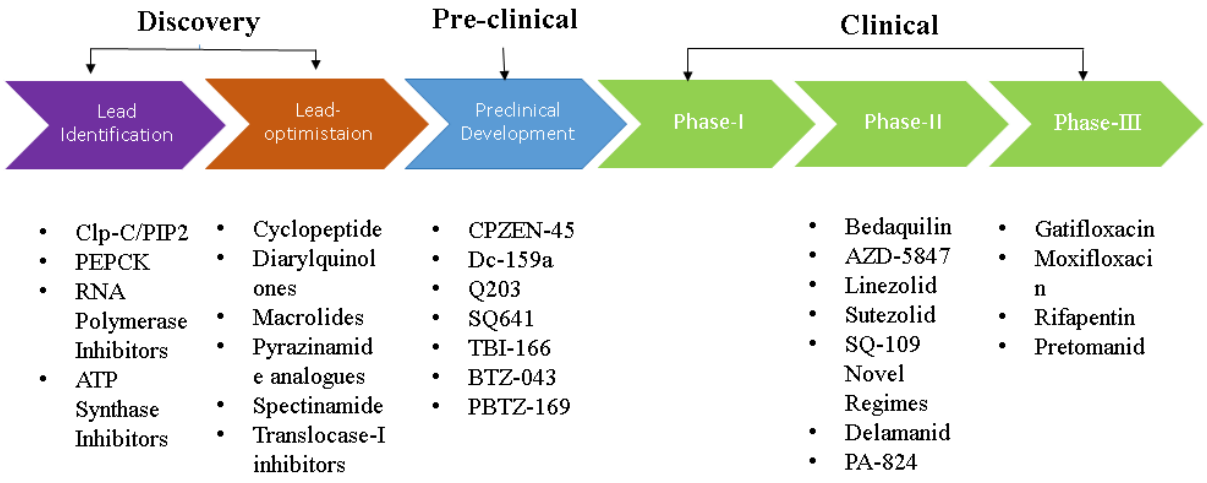

Figure 1.2: Global pipeline of new TB drugs.

Chapter 2
Literature Review

DNA molecules forms negative or positive supercoils, due to alterations in topology when they bend and coil in space. The enzymes which control the topology of DNA, function at several different steps in replication in both prokaryotic and eukaryotic cells. DNA topoisomerases are a class of enzymes involved in the regulation of DNA supercoiling. Type I topoisomerases, to cause change in the degree of supercoiling of DNA, causes single-strand breaks and re-ligation, whereas type II topoisomerases (such as DNA gyrase) cause double stranded breaks. Topoisomerase I has also been associated in unknotting and knotting DNA and in linking complementary rings of single stranded DNA into double stranded rings [Lodish H., *et al*., 2000].

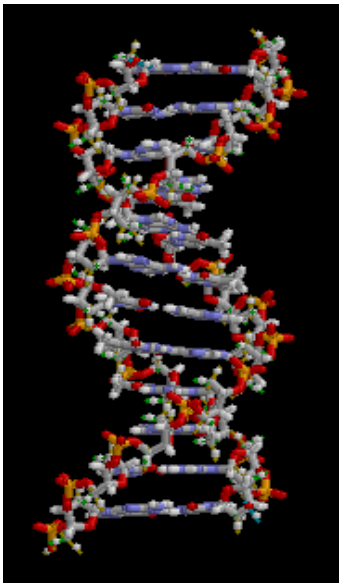

Figure 2.1: Structure of part of DNA helix

DNA Topoisomerases as the biological target has aroused a general interest in developing inhibitors as potential antibacterial drugs for several reasons as such as:

1) These are essential components of all bacteria.

2) These proteins are essential for bacterial viability involved in bacterial cell division and DNA replication as well.

3) There are many distinct structural differences when compared to the mammalian enzyme counterparts to allow for bacterial specificity.

4) Multiple target sites have been identified within the enzymes, insisting a broad range for the drug action with the enzyme.

5) Inhibition of their function in many bacteria usually leads to a bactericidal event, revealing the importance of the enzyme.

2.1. Topoisomerase I

Topoisomerases are enzymes that regulate the underwinding or overwinding of DNA. This winding problem of DNA arises due to the entwined nature of its double-helical structure. In order to help overwhelm these types of topological problems caused by the double helical structure, topoisomerases bind to either single-strand or double-strand DNA and cut the phosphate backbone of the DNA. The intermediate break allows the DNA to be untangled and at the end of these processes, the DNA backbone is resealed again. Since the complete connectivity and chemical composition of the DNA do not change, the interwined and uninterwined DNAs are chemical isomers, differing only in their total topology, thus their

name, Topoisomerases. Topoisomerases are isomerase enzymes that act on the topology of DNA [Champoux J.J., 2011].

Topoisomerases can fix these topological problems and are separated into two types separated by the number of strands cut in one round of action [Wang J.C., 1991]. Type I topoisomerase cuts one strand of a DNA double helix, allows the other strand to pass through it and then the cut strand is resealed. Cutting one strand allows the part of the fragment on one side of the cut to move around the uncut strand, thereby reducing stress from too much or too little wind in the helix. This kind of stress is introduced when the DNA strand is "supercoiled" or unwound to or from higher orders of winding. Type II topoisomerase breaks both strands of one DNA double helix, passes another unbroken DNA helix through it, and then reanneals the cut strands.

Topo I appears to reverse supercoiling by breaking a segment of single-stranded DNA, passing a whole single- or double-stranded strand of DNA through the broken segment, then re-joining the broken segment. Topo I has several unusual features. Topo I catalyses the complex topological rearrangements of DNA and does not require ATP hydrolysis for this reaction. Topo I appear to be a fully functional monomer, whereas most enzymes involved in complex rearrangements of DNA are oligomeric [Wang J.C., 1991].

The catalytic mechanism of this type of topoisomerase involves a covalent linkage between a tyrosine residue in the active site of enzyme's N-terminal domain and the 5' phosphoryl group of the cleaved DNA strands and is ATP independent [Fude Y., *et al*., 1996].

The existence of at least one type I topoisomerase in every bacteria designates that the enzyme plays important role(s) in cellular functions [Wang J.C., 2002].

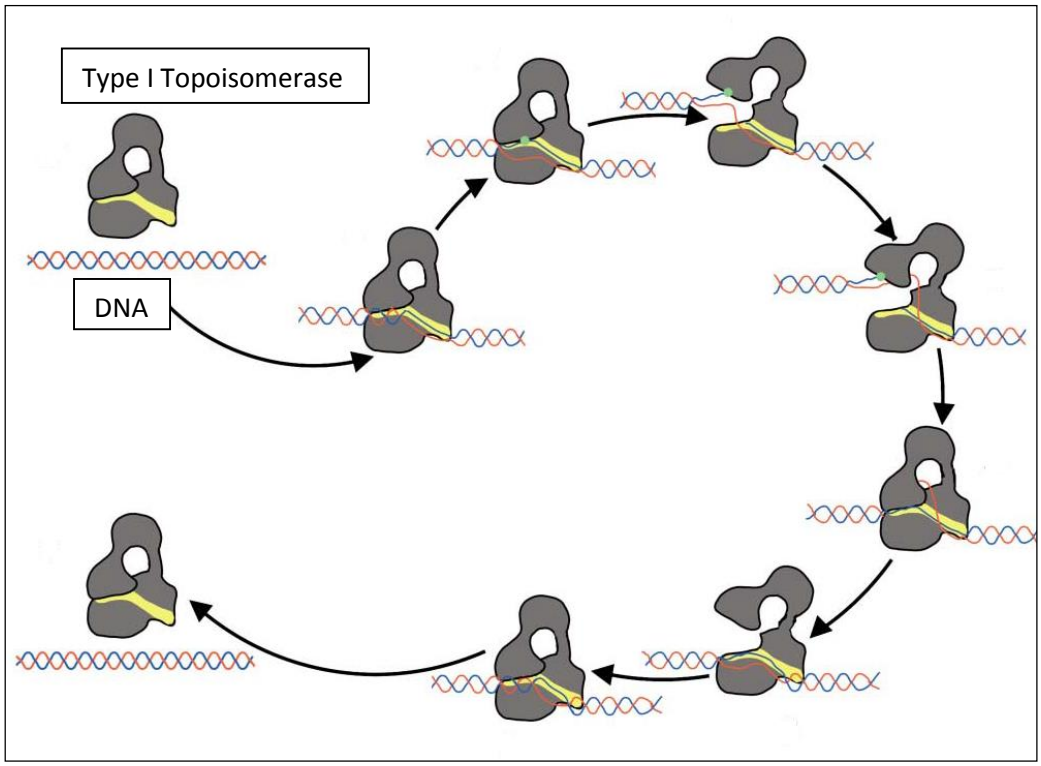

Figure 2.2: Diagram Illustrating the Proposed Mechanism of DNA Relaxation Catalyzed by Type I DNA Topoisomerases [Kay P., *et al*., 2003].

2.2. Mycobacterium tuberculosis Topoisomerase I

Recombinant Mtb Topo I is enzymatically active, relaxing negatively supercoiled DNA in ATP-independent and magnesium-dependent reaction [Lodish H., *et al*., 2000]. The enzyme has several properties which are not shared by either type IA or IB enzymes with respect to DNA sequence specificity, recognition, binding and interaction pattern. A large number of bacteria contains Zn++ fingers in topoisomerase I. The first identified member without Zn++ finger is from Mtb Topo I. Apart from this, the enzyme exhibits a unique property not shared by other topoisomerases. The enzyme identifies both single and double stranded DNA with very high affinity. However, this high affinity binding is at the specific recognition sequence. In contrast, eukaryotic type I enzymes are known to recognize only double stranded DNA [Nagaraja V., et al., 2002].

2.3. Topoisomerase I as a potential target for tuberculosis

According to Ahmed W., et al., 2014, the conditional knockdown mutant of Topo I in Mtb exhibited delayed growth on agar plate. In liquid culture, the growth was drastically reduced when Topo I expression was suppressed. Moreover, novobiocin and isoniazid showed greater inhibitory potential against the conditional mutant. The same study was also carried out in *Mycobacterium smegmatis*. The Topo I depleted strain exhibited tremendously slow growth and drastic changes in phenotypic features. The impaired growth indicates the essentiality of the enzyme for the organism although having other DNA relaxation enzymes in the cell. Especially, the imbalance in Topo I level led to the altered expression of topology modulatory proteins, resulting in a dispersed nucleoid architecture. Transcript and proteomic analysis of the conditional knockdown mutant of Topo I indicated reduced expression of the genes involved in core DNA transaction processes and central metabolic pathways [Ahmed W., et al., 2015]. These studies establish the essentiality of TopoI for the M. tuberculosis growth and open up new avenues for targeting the enzyme.

2.4. Known inhibitors for Mtb Topo I

The search for new TB drugs that can overcome the increasing spread emerging drug resistant tuberculosis. It can be approached from two directions: the identification and validation of new targets for the development of novel antibiotics with no pre-existing resistance mechanisms; or assessment of known and clinically confirmed targets for new chemical series or modification of current drug classes to abolish the possibility of cross resistance with present drugs for which resistances has developed [Skrahin A., *et al*., 2014]. The second approach has had significant success identifying newer and more effective generation of compounds based on older drugs (isoniazid, rifampin, pyrazinamide, and ethambutol) from a variety of classes. This kind of

approach also benefits from aiming fully validated molecular targets whose biochemical inhibition is known to cause inhibition of bacterial growth.

There are less known small molecule inhibitors for DNA Topo I against MTB. However, there are certain inhibitors for *Mycobacterium smegmatis* Topo I. Monoclonal antibodies that inhibit *Mycobacterium smegmatis* Topo I have been characterized and 2F3G4 inhibits *M. smegmatis* at nano molar concentration [Leelaram M.N., *et al*., 2012]. The same monoclonal antibody 2F3G4 also inhibited the relaxation activity of Mtb Topo I. The monoclonal antibody bound with the enzyme stimulated the first transesterification reaction leading to improved DNA cleavage, without significantly altering the religation activity of the enzyme. [Adwait A.G., *et al*., 2012].

The oligonucleotides containing STS effectively inhibit the *M. smegmatis* Topo I DNA relaxation activity. Synthetic oligonucleotides having the consensus sequence were used as substrates for DNA clevage and binding reactions of the enzyme [Tisha B., *et al*., 2000].

2.4.1. m-AMSA as Mtb Topo I inhibitor

Recently, m-AMSA (type-II eukaryotic topoisomerase inhibitor), was identified as inhibitors for DNA Topo I from Mtb [Godbole A.A., *et al*., 2014].

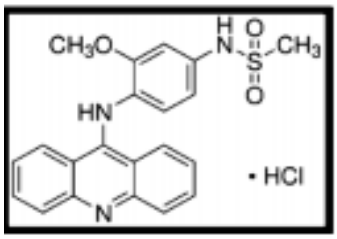

Fig 2.3: Stucture of m-Amsacrine

When the compound was pre-incubated either with the DNA or the enzyme, a complete inhibition of the reaction was observed at 25 µM and 10 µM respectively. But, the inhibition was not complete even at 50 µM when the compound was added to the pre-formed DNA–enzyme complex. From this data, it appears that the compound needs to first interact either with the DNA or the protein, prior to the formation of the Topo I–DNA complex for inhibition of the reaction.

2.4.2. Imipramine and Norclomipramine as Mtb Topo I inhibitors

Imipramine, used clinically as anti-depressant and Norclomipramine inhibited Topo I enzyme of both *Mycobacterium tuberculosis* and *Mycobacterium smegmatis* [Godbole A.A., *et al*., 2015].

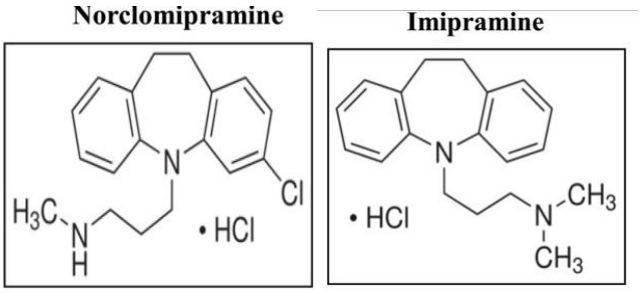

Figure 2.4: Structure imipramine and Norclomipramine (IC50 on Mtb Topo I – 0.1 µM)

Norclomipramine and imipramine inhibited Mtb Topo I activity at 0.1 µM concentration, not reported so far for any bacterial type I topoisomerases. Norclomipramine inhibited Mtb H37Ra at 60 µM and clomipramine at 250 µM.

2.5. Gap in existing research

Clinical studies indicate that a significant number of the strains are resistant to isoniazid, rifampin and pyrazinamide. However, there are still persistent bacterial populations that are not killed by any of the available TB regimens. Therefore, there is a need to design new drugs

that are more active growing non-persistent bacilli to treat the population at risk of developing active disease through reactivation. As there are a limited number of effective inhibitors available in the market to MDR-TB and XDR-TB, there is an urgency to develop additional therapeutically useful inhibitors. There are no small molecule inhibitors of topoisomerase I explored till date against TB. So there is an urgent need to develop some novel inhibitors against MTB targeting Topo I.

Chapter 3
Objectives and Plan of work

3.1. Objectives

From the above literature evidences it was clear that TB is a major health problem affecting the global population both in developed and developing countries. In order to accelerate the development of new anti-TB drugs, several strategies have been developed, which could help in shortening the therapy and be effective against both active and latent form of Mtb. The important role of Topo I in Mtb was thoroughly reviewed from various sources. Design of inhibitors for Mtb Topo I was considered as prime importance and hence the below mentioned strategy was followed. Clinical studies indicated that a significant number of the strains are resistant to isoniazid, rifampin and pyrazinamide. However, there are still persistent bacterial populations that are not killed by any of the available TB drugs. Therefore, there is a need to design new drugs for actively growing non-persistent bacilli to treat the population at risk of developing active disease through reactivation. As there are only few successful inhibitors available in the market to MDR-TB and XDR-TB, there is an urgency to develop additional therapeutically useful inhibitors. There are limited number of inhibitors against Mtb Topo I reported till date and those inhibitors were found to be effective towards TB. Hence for development of novel inhibitors against Mtb Topo I, with effectiveness against dormant and active forms of TB was considered important.

The main objectives of the proposed work were:

1. **Optimization of adult zebrafish model for *in vivo* anti-mycobacterial screening**
    I. Optimisation study
    II. Validation study
2. **Mtb Topo I inhibitors**

A. To design Mtb Topo I inhibitors by:

- Homology modelling of Mtb Topo I protein structure.
- High throughput virtual screening of In-house database (BITS-database) towards the active site of developed Topo I model.

B. *In vitro* enzymatic screening of designed molecules for Mtb Topo I

C. Development of various analogues of Mtb Topo I inhibitors based on *in vitro* enzymatic screening data.

D. *In vitro* anti-tubercular screening for both active and latent forms of Mtb.

E. *In vitro* cytotoxicity screening to check the safety profile of the compounds.

F. *In vivo* anti-mycobacterial screening using adult zebrafish.

G. Bio-physical characterisation using differential scanning flourimetry to determine the thermal stability of protein and protein-ligand complexes.

3.2. Plan of work

The plan of work has been classified into following categories,

3.2.1. Optimization of adult zebrafish model for *in vivo* anti-mycobacterial screening

It was done by following approach:

- The concentration of bacteria (*Mycobacterium marinum*) required to produce a reproducible phenotype of oraganism was optimised.
- Optimised the dose of standard compounds to treat the infected fish.
- Design of *in vivo* protocol for screening the standard compounds using zebrafish.

3.2.2. Mtb Topo I inhibitors

3.2.2.1. Design of novel inhibitors for Mtb Topo I using Homology modelling and Virtual screening

For designing the New Mtb Topo I inhibitors we followed below approach

- There is no crystal structure reported in Protein Data Bank (PDB). So, Homology modelling was done by using PRIME application from Schrödinger.
- The model obtained was checked for the stability using Molecular dynamic stimulations.
- Docking of In-house database molecules were done using GLIDE module.
- The compounds were shortlisted based on their docking score, Hydrogen bond and interacting amino acids.
- The shortlisted compounds were screened for *in vitro* Mtb Topo I enzyme activity and further derivatives were prepared using Medicinal chemistry approach

3.2.2.2. *In vitro* enzyme inhibition assay

- NdeI and PmlI restriction enzymes were used for cloning.

- E.coli arctic express (DE3) RP strains were used for the overexpression of MTB topoisomerase I.
- Supercoil pUC19 plasmid DNA will be used as substrate for the enzyme inhibition assay.

The synthetic and designed compounds will be evaluated *in vitro* for the inhibition of topoisomerase I from MTB at suitable concentration. Recombinant MTB topoisomerase I is enzymatically active, relaxing negatively supercoiled DNA in a magnesium-dependent, ATP-independent reaction. The protocol for the assay is

- Negatively supercoiled pUC19 DNA will be incubated with varying amounts of enzyme in Tris-HCL(pH 8.0) containing 20mM NaCl, 1mM EDTA, 5mM $MgCl_2$ at 37°C for 30min.
- The reaction will be terminated using 0.1% SDS.

The reaction products will be resolved in 1.2% agarose gel and visualised by staining with Ethidium bromide after electrophoresis.

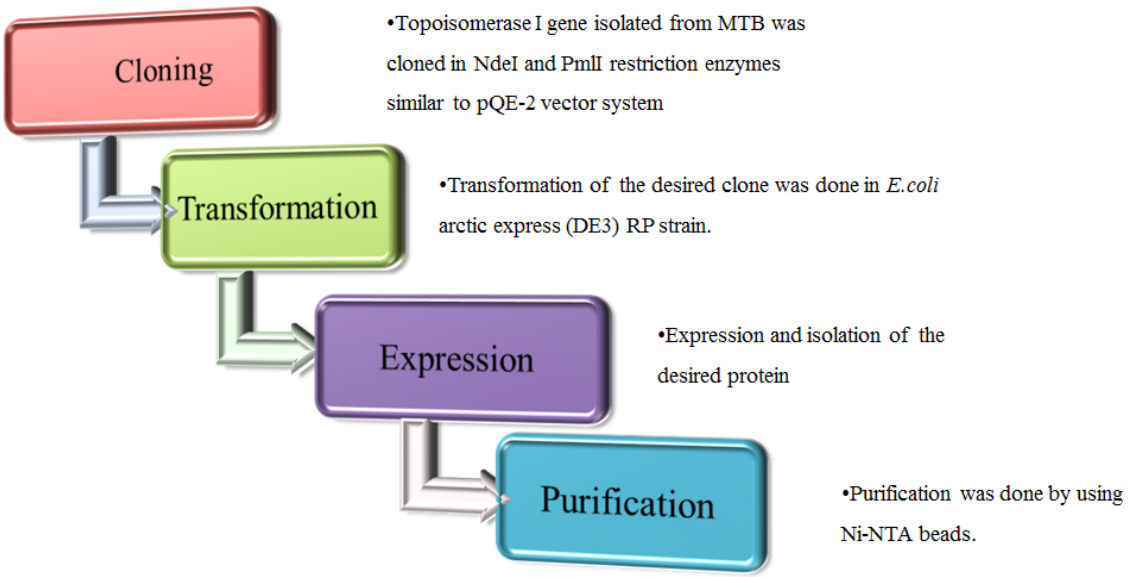

Figure 3.1: Work flow for biological evaluation

3.2.2.3. Lead modification using synthetic chemistry

The top active molecules were further derivatized using synthetic chemistry utilizing novel/previously reported methodologies as a lead expansion strategy. The synthesis was outsourced to the medicinal chemistry research group at the department of pharmacy.

3.2.2.4. *In vitro* anti-tubercular screening

Lead compounds synthesized for Mtb Topo I were evaluated for anti-tubercular screening using different methods as follows.

- Using MABA to determine the MIC's.
- Determination of inhibitory effect on dormant bacilli using Nutrient starvation, Oxidative stress and Nitrosative stress models.

3.2.2.5. *In vitro* toxicity studies

To evaluate the toxicity of the designed and synthesized compounds against HEK 293 cells were utilized and tested at 25 μM concentration using MTT assay to evaluate their toxicity profile.

3.2.2.6. *In vivo* anti-mycobacterial screening using adult zebrafish

The zebra fish is a commonly used laboratory animal for the study of development and disease. The relatively rapidly growing human and animal pathogen *Mycobacterium marinum*, a close genetic relative of MTB, was used to study the pathogenesis of tuberculosis. *M. marinum* causes systemic granulomatous infections and disease in its natural hosts, ectotherms such as fish and frogs, and peripheral chronic granulomatous disease (fish tank granulomas) in humans. Zebra fish become infected with *M. marinum* in fish facilities and also develop disease upon experimental inoculation. The synthetic compounds were screened by injecting them to the infected fish and the bacterial count was determined using MPN assay.

3.2.2.7. Biophysical characterization

To evaluate the stabilization of protein-ligand complexes of promising leads, thermal shift assay was performed using differential scanning flourimetry for Mtb Topo I inhibitors.

Chapter 4
Materials and Methods

4.1 Optimization of adult zebrafish model for *in vivo* anti-mycobacterial screening

4.1.1. Zebrafish maintenance

Zebrafish were maintained as per Guidelines for Use of Zebrafish in the NIH Intramural Research Program and the Zebrafish Book. Zebrafish were obtained from Vikrant Aquaculture, Mumbai, India, and were maintained at BITS-Pilani, Hyderabad campus, India as per the procedures mentioned earlier. Briefly, all the fish were taken care to acclimatize for a week at 26–28 °C and at conditions of 14:10 hr. (light: dark) every day. The fish were allowed to swim in separate chambers filled with filtered water containing 0.2% sea salt and were fed with dry food (procured from the same vendor) at three regular intervals daily. Fish were observed to be healthy through their feeding and swimming activities and with a weight range of 500 mg. The healthy fish were further selected to conduct the study.

4.1.2. *M. marinum* strains, culture condition and inoculation

M. marinum strains used for this study were derived from a human clinical isolate, strain M (ATCC BAA-535), and were grown at 30 °C in Middlebrook 7H9 broth (HiMedia) supplemented with Middlebrook OADC Growth supplement (HiMedia) and 0.05% Tween 80 or on Middlebrook 7H10 agar (HiMedia) supplemented with Middlebrook OADC Growth supplement (HiMedia). Infected fish homogenates were plated in 48 well plates using Middlebrook 7H9 broth (HiMedia) supplemented with amphotericin B (10 mg/liter) and polymyxin B (20 mg/liter), to avoid contamination with normal flora. Cultures used in

infections were grown to an optical density at 600 nm of 1.0 and maintained at 80 °C in 1-ml aliquots with 10% glycerol [Flynn J.L., 2006]. Intraperitoneal administration (i.p.) was used for bacterial inoculation, wherein a maximum volume of 15 µl/fish was injected using a 29-gauge insulin syringe to avoid injury-induced stress based on methods described in the literature [Chaudari G.H., *et al*., 2013, Kinkel M.D., *et al*., 2010].

4.1.3. Drug, vehicle and drug administration

The standard drugs Isoniazid, Rifampicin, Ethambutol, Moxifloxacin, and Amoxicillin were procured from Sigma Aldrich, and Tween 80 was procured from NICE laboratories. All other routine chemicals were procured locally. All drugs were administered orally using a recently reported method [Banote R.K., *et al*., 2013, Kulkarni P., *et al*., 2014]. This method allows the calculation of the oral dose of the drugs in terms of milligrams per kilograms (mg/kg), which is very useful in ascertaining the vital parameter of drug dosage required for ranking of molecules and taking decisions in a screening program. The authors that proposed this method have demonstrated the credibility of the method by substantiated pharmacokinetics and pharmacology data.

4.1.4. Optimization study

A study was conducted to optimize the concentration of bacteria needed to produce a reproducible phenotype of zebrafish TB. Healthy fish were grouped in to four groups (n=15/group) and *M. marinum* cultures were injected into the fish (inside a BSL-II hood) at inoculums of 0.5 (Group I), 0.6 (Group II) and 0.75 (Group III) million bacteria respectively. Two time points viz. day 7 and 14 were used to sacrifice the fish and results were determined using Most Probable Number (MPN) assay (n = 6) and body weight (n=10). Before sacrificing, the fish were allowed to swim in 1.5 mg/ml of Kanamycin Sulfate for 45 min at 27 °C, to prevent any cross-infection [Swaim L.E., *et al*., 2006]. Thereafter, the fish were homogenized

and processed for MPN assay as per a published protocol [Salina E., *et al*., 2014]. MPN values were finally calculated using standard statistical methods [de Man J.C., 1975]. The survival probability curve of Group III fish was also plotted by conducting a separate experiment on 90 fish based on Kaplan–Meier survival analysis.

4.1.5. Validation study

An *in vivo* protocol using the standard drugs was further designed. It was performed as a two-week study: infection stage (0–7th day) and treatment stage (8th–14th day). Eighty fish were inoculated with an optimized count of M. marinum. A dose optimization study resulted in finalizing the following drug doses: amoxicillin (10 mg/kg), isoniazid (10 mg/kg), rifampicin (5 mg/kg), moxifloxacin (5 mg/kg), ethambutol (10 mg/kg) and a combination of isoniazid (5 mg/kg) + rifampicin (2.5 mg/kg). The drug solutions (diluted with vehicle Tween 80) were prepared considering the average body weights of the fish in each group. 5 µl of each drug (n = 10 in each group) was administered orally. This dosing was done for a week (8th–14th day), and the results were determined using MPN assay (n = 6) and body weight (n = 10).

4.2. Mtb Topo I inhibitors

In search of novel inhibitors for Mtb Topo I for the treatment of TB, we employed computational strategy for screening of large data sets of molecules and evaluated *in vitro* for the identification of promising molecules. Virtual screening, a computational method where large libraries of compounds could be assessed for their potential to bind specific sites on target molecules such as proteins, was employed in the study.

As there is no reported crystal structure for Mtb Topo I, we have used PRIME from Schrodinger to develop a homology model using E.coli Topo I (PDB ID: 3PX7) as template. We utilised this developed model for virtual screening of in-house database (BITS-Database) consisting of around 1000 molecules.

4.2.1. Computational methodology

4.2.1.1. Computational Details

All computations were carried out in an Intel Core 2 Duo E7400 2.80 GHz capacity processor with memory of 2GB RAM running with the RHEL 5.2 operating system. PHASE 3.3 implemented with Maestro 9.3 software package (Schrodinger, LLC) was used to generate pharmacophore models. The virtual screening options for HTVS (High Throughput Virtual Screening), SP (Standard Precision) and Glide XP (Extra Precision) docking were all checked to be executed. Glide XP (extra precision) module of Schrodinger 9.3 (Glide, version 5.7, Schrodinger, LLC, New York, NY, 81 2011) was utilised for docking. Bond orders and formal charges were added to the hetero groups and hydrogen atoms were added to all atoms in the system.

4.2.1.2. Homology modeling of Mtb Topo 1

The amino acid sequence for Mtb Topo 1 was retrieved from UniProt (accession id P9WG49) [Yang F., *et al.*, 1996]. This sequence was run for protein BLAST (BLASTp) against non-redundant database (Protein Data Bank (PDB)) to identify the most identical template [Altschul S.F., *et al*., 1990]. Suitable template required for the generation of homology model of Topo I was selected based on the identity compared to the query sequence. The model was built using Prime 3.1 of Schrödinger 2012 molecular modeling package [Prime v3.1, Schrödinger suite, 2012]. The energy based mode of modeling was operated for model generation employing OPLS_2005 force field [Petrovic A.G., *et al*., 2010]. The generated model was subjected to loop refinement and was energy minimized using the same OPLS_2005 force field. The stereo chemical quality of the constructed model was analyzed with Ramachandran plot using PROCHECK [Laskowski R.A., *et al.*, 1993]. The active site analysis of the model was carried out based on the sequence alignment of Topo I over the template.

4.2.1.3. MD simulation

MD simulations were run for the model using Desmond 3.1 from D. E. Shaw research employing explicit solvent conditions [Desmond v3.1, Maestro v3.1, Schrödinger suite, 2012]. The solvent system for the protein model was setup using an orthorhombic solvent box using TIP3P water model [Jorgensen W.L., *et al.*, 1983]. The solvent system was setup with a cutoff of 10 Å from any protein atom and was neutralized by the addition of appropriate number of counter ions. An initial minimization of the total system was operated with a convergence threshold of 1 kcal mol^{-1} $Å^{-1}$ employing OPLS_2005 force field. Following this, minimization of the system was performed both with and without restraints on the solute atoms for 12 ps time scale at 10 K temperature using Berendsen thermostat (isothermal–isobaric ensemble) [Mudi A., *et al*., 2004]. Additionally, the system temperature was raised up to 300 K at 1 atm pressure for 24 ps time. A cutoff of 12 Å was used for calculating the non-bonded interactions.

M-SHAKE algorithm was used with integration time step of 2 fs for the purpose of reordering the hydrogen bonds during simulation [Kräutler V., *et al.*, 2001]. The total MD simulation continued for 10 ns with the trajectory frames recording at an interval of 4.8 ps. In a way to compare and analyze the behavior of both the model and template during simulation, a 10 ns MD was also run for the template.

4.2.1.4. Preparation of ligands

The in-house database (BITS-database) with 1000 molecules were processed through redundancy checking and Lipinski filters to select compounds that had better drug property [Knox A.J., *et al*., 2005]. All the structures were prepared using LigPrep (LigPrep v2.2, Schrodinger LLC, New York, NY) along with Epik (Epik v1.6, Schrodinger, LLC, New York, NY) to expand protonation and tautomeric states at 7.0 ± 2.0 pH units. Conformational sampling was also performed for all database molecules using the ConfGen search algorithm. Confgen with OPLS 2005 force field was applied for the generation of conformers with duplicate poses eliminate if the RMSD was less than 2.0 Å. A distance-dependent dielectric constant of 4 and maximum relative energy difference of 10 kcal mol^{-1} were applied. Using Phase, the database was indexed with automatic creation of pharmacophore sites for each conformer to allow rapid database alignments and screening.

4.2.1.5. Molecular docking studies

The active site pocket of the developed Mtb Topo 1 model was identified based on the sequence alignment over the template used. Also the probable binding pockets of protein were identified using SiteMap version 2.6 [SiteMap v2.6, Schrödinger suite, 2012]. The active site was selected based on the above analysis and the grid for docking was generated targeting the selected pocket using Glide [Glide v5.8, Schrödinger suite, 2012]. The generated protein grid was subjected for high throughput virtual screening (HTVS) against asinex database (commercial chemical database with 5,00,000 molecules) and in-house BITS database

(containing 930 compounds) using Glide module, for identifying novel compounds which can be used as Mtb Topo 1 inhibitor [Asinex, http://www.asinex.com/]. Further, the compounds with considerable docking score and better interactions at the active site were selected for standard precision (SP) and extra precision (XP) docking [Friesner R.A., *et al.*, 2004, Friesner R.A., *et al.*, 2006]. Compounds from both databases with effective binding ability were selected, also considering their docking score compounds shortlisted. The compounds were carried forward to *in vitro* enzyme inhibition studies.

4.2.1.6. ADME prediction

All the selected hit compounds were subjected to in-silico ADME analysis using QikProp module of Schrödinger. Various properties like LogP (octanol water coefficient), % human oral absorption, Lipinski's rule of five, QPlogBB (Predicted brain/blood partition coefficient), QPlogHERG (Predicted IC50 values for blockage of HERG K+ channels) and QPPCaco (Predicted apparent Caco-2 cell permeability in nm/s) were predicted for the compounds and were checked for any violations.

4.2.2. Synthesis

Synthesis of promising leads (Topo-I) and their analogues were performed by our medicinal chemistry research group at the Department of Pharmacy. Hit expansion of the lead identified was achieved using the following synthetic protocols (Figure 4.1-Figure 4.3).

4.2.2.1. Synthesis of Hydroxycamptothecin derivatives

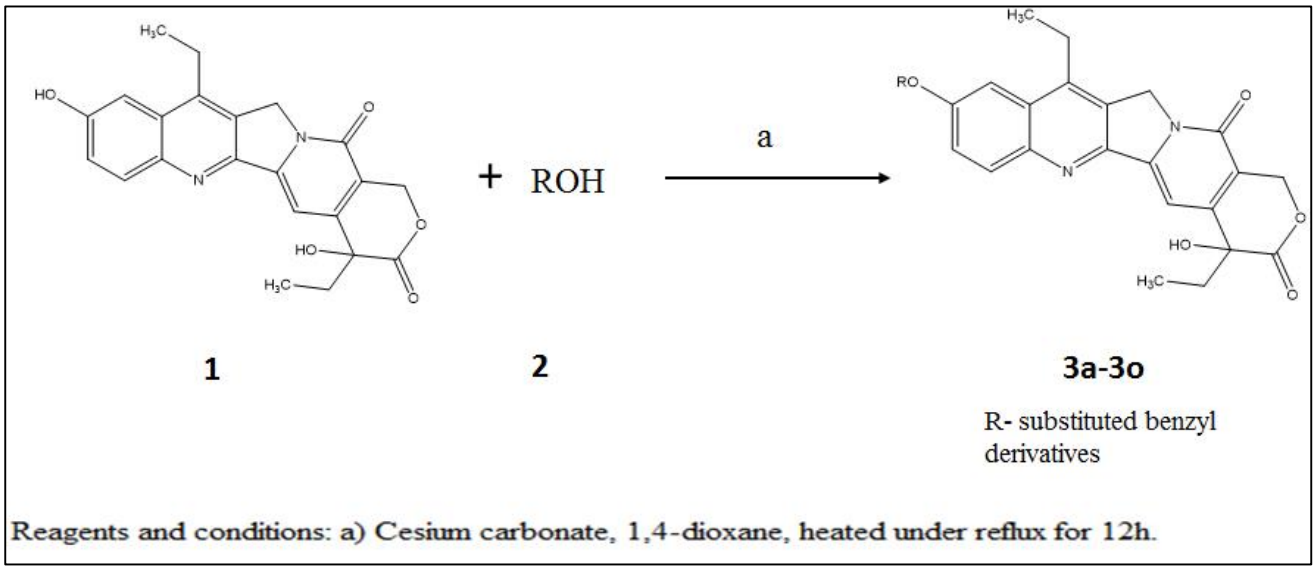

Figure 4.1: Synthetic scheme for Hydroxycamptothecin derivatives.

4.2.2.2. Synthesis of Amsacrine derivatives

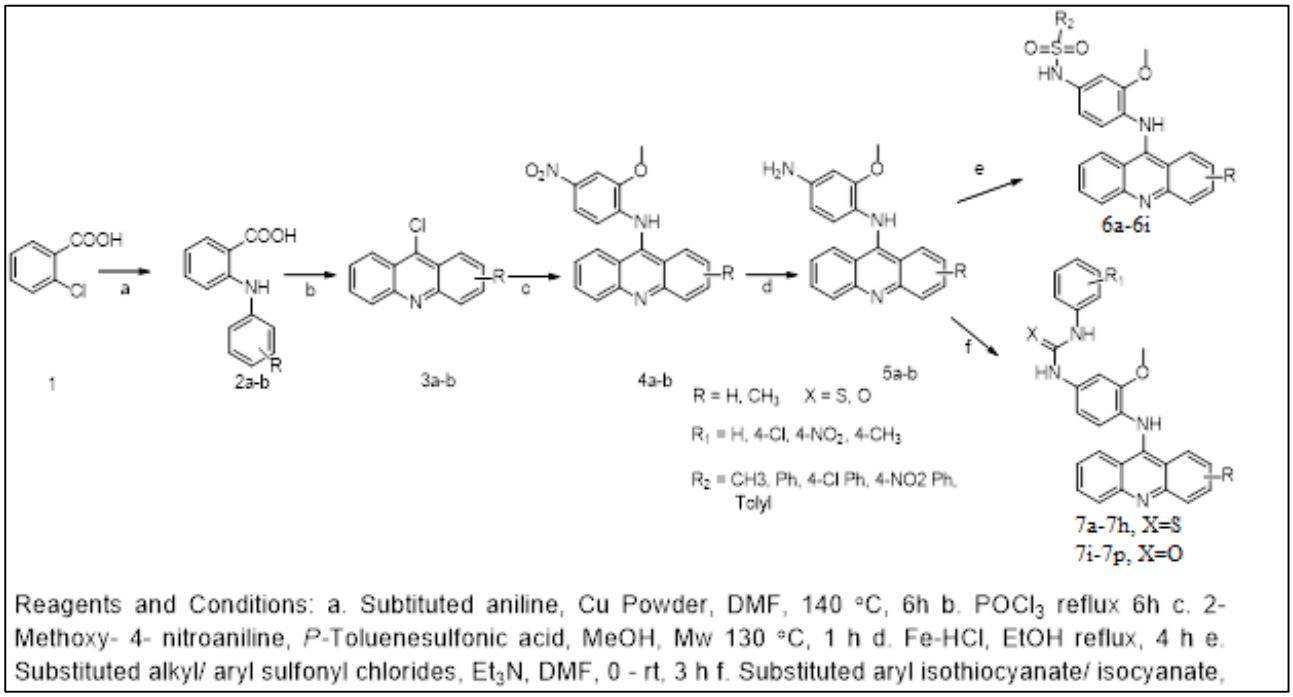

Figure 4.2: Synthetic protocol for Amsacrine derivatives.

4.2.2.3. Synthesis of Tryptanthrin derivatives

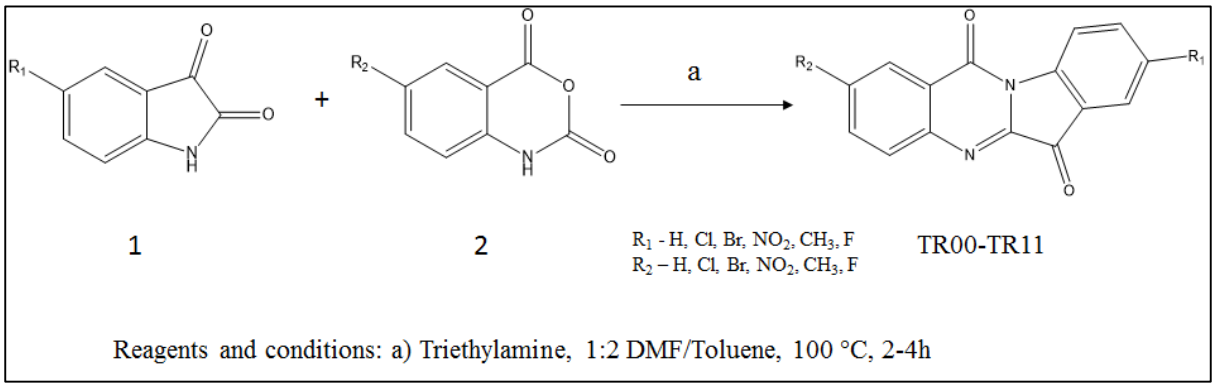

Figure 4.3: Synthetic protocol for Tryptanthrin derivatives.

All commercially available chemicals and solvents were used without further purification. TLC experiments were performed on aluminimum-backed silica gel 40 F254 plates (Merck, Darmstadt, Germany). The homogeneity of the compounds was monitored by thin layer chromatography (TLC) on silica gel 40 F254 coated on aluminum plates, visualized by UV light and KMnO4 treatment. Purifications were done on Biotage Isolera purification system on silica gel (MPLC grade) by using either hexane: ethylactetae or dichloromethane: methanol as eluent. All 1H and 13C NMR spectra were recorded on a Bruker AM-300 (300.12 MHz, 75.12 MHz) NMR spectrometer, (BrukerBioSpin Corp, Germany). Chemical shifts are reported in ppm (δ) with reference to the internal standard TMS. The signals are designated as follows: s, singlet; d, doublet; dd, doublet of doublets; t, triplet; m, multiplet. Molecular weights of the synthesized compounds were checked by SHIMADZU LCMS-2020 series in ESI mode. Elemental analyses were carried out on elementar vario MICRO CUBE, CHN Analyser. All commercially available chemicals and solvents were used without further purification.

4.2.3. Biological assessments

All the designed leads and synthesized analogues were evaluated for *in vitro* biological assessments Mtb topo-I enzymatic assays, MIC against both active and dormant Mtb, resistant tb, *in vivo* studies in adult zebrafish model and cytotoxicity studies in eukaryotic cell lines.

4.2.3.1. Mtb topo-I assay

4.2.3.1.1. Cloning and expression of Mtb topoisomerase 1

Mycobacterium tuberculosis H37Rv strain possess *topA* gene Rv3646c which encodes for topoisomerase I (Mtb Topo I) protein with 934 amino acids and an approximate molecular weight of 102.3 kDa [Yang F., *et al.*, 1996]. A set of forward primer 5'CACCCATATGTTGGCTGACCCGAAAACGAA 3' and reverse primer 5'AGCTCACGTGCTAGTCGCGCTTGGCTGCCT 3' were used for PCR amplification. The PCR product was further digested with NdeI and PmlI restriction enzymes similar to the pQE2 vector. The final PCR amplicons were ligated with the help of T4 DNA ligase at 25 ^{o}C for 2 h. Further, sequence confirmation was done to verify the final clone. Initially, the transformation and expression was done into BL21 (DE3) CODON PLUS cells as per Yang *et al*. But difficulties in the solubility of the expressed protein along with very less yield of the protein have been encountered in our laboratory similar to other researchers [Yang F., *et al.*, 1996, Manjunatha U.H., *et al.*, 2006]. The difference in codon usage was investigated to be one of the possible reasons behind the solubility and efficiency of the protein expressed. As per Thirunavukkarasu Annamalai *et al* expression of mycobacterium topoisomerase I from a recombinant plasmid pLIC-MTOP in an *E.coli*arctic express (DE3)RP strain (Agilent Technologies) at low temperatures of about 12°C to 14°C for 24 h according to the manufacturer's (Agilent Technologies) protocol solved the solubility issues. The mechanism behind this compatibility is because of the strains chromosomally integrated T7 RNA polymerase which was expressed from the *lacUV5* promoter and furthermore Arctic express

strain also expresses cold chaperonin proteins and high copies of tRNAs (recognizing arginine and proline codons) that facilitated the expression proteins by overcoming issues of protein solubility and also codon bias respectively. Furthermore, on induction of this T7 RNA polymerase with inducibleisopropyl β-d-thiogalactopyranoside (IPTG) resulted in the high expression of the T7 promoter-driven recombinant MtTOP protein [Annamalai T., *et al.*, 2009].

4.2.3.1.2. Purification of Mtb topoisomerase I

As the clone was tagged by a hexa-histidine tag, the purification was carried out by Ni-NTA column. After 24 hours IPTG induction, the cells were collected and subjected to centrifugation at 5000 rpm, 20 min. The pellet was dissolved in lysis buffer (50 mM NaH_2PO_4, 300 mM NaCl, 10 mM imidazole, 1 mg/ml lysozyme, pH 8) until an homogenous mixture is obtained. The recombinant Mtb Topo I protein in the soluble lysate was allowed to bind to Ni-NTA sepharose column (Qiagen) and packed. Further, the column is washed overnight with wash buffer (50 mM NaH_2PO_4, 300 mM NaCl, 20 mM imidazole, pH 8.0), Subsequently, the topoisomerase protein was eluted with an elution buffer (50 mM NaH_2PO_4, 300 mM NaCl, 25 to 500 mM imidazole, pH 8.0). Gradual increase in the concentration of imidazole elutes the protein. Subsequently pooled the 250 mM and 300 mM eluate fractions and was dialyzed thrice against the dialyses buffer (15% glycerol, 300 mM NaCl in 50 mM NaH_2PO_4 (pH 8)), aliquoted and stored at -80 ^oC. Fractions containing the desired Mtb Topo I protein was confirmed by running an SDS–PAGE (Sodium dodecyl sulfate–polyacrylamide gel electrophoresis) against a pre-stained protein ladder (Genetix Biotech Asia Pvt. Ltd.) with a broad range (10-150 kDa). Mtb Topo I protein had about 99-100 kDa [Yang F., *et al.*, 1996].

4.2.3.1.3. Mtb Topoisomerase I relaxation assay

In nature, usually plasmids exist as negatively supercoiled forms. Supercoiled pUC 19 was used as the substrate for relaxation assays. IU of enzyme was defined as the least quantity of the Mtb Topo I enzyme required for complete relaxation of 0.5 μg of negatively supercoiled

plasmid pUC 19 DNA in 30 min at 37 °C [23]. The DNA relaxation assay was performed in a standard reaction volume of 30 µL assay buffer with 10 mM Tris-HCl (pH 8.0), 50 mM NaCl, 6 mM $MgCl_2$, 0.1 mg/ml gelatin and 0.5 µg of supercoiled pUC 19 plasmid DNA (HiPurA plasmid DNA maxiprep purification spin kit, HiMedia). Reactions were initiated by adding 800ng Mtb Topo I protein. Later, after incubation at 37°C for 30 min, the reactions were quenched by adding 5 µL of Stop buffer (50 mM EDTA (pH. 8; 50% glycerol and 0.5 % (v/v) bromophenol blue). Subsequently, the DNA was electrophoresed in a 1% (w/v) agarose gel with TAE buffer (40 mM Tris-acetate, pH 8.1, 2 mM EDTA). The gels were stained after the electrophoresis to prevent any differences in mobility of DNA due to chelation; gel was stained with ethidium bromide and photographed over UV light using GelDoc imager (Bio-Rad). The supercoiled plasmid was considered as blank; the supercoiled DNA with the Mtb Topo I enzyme was used as control with 100% relaxation. Different concentrations of the drugs tested were assayed to know the percentage inhibitions on the enzyme [Godbole A.A., *et al.*, 2012].

4.2.3.2. Anti-tubercular screening

4.2.3.2.1. *In vitro* active and resistant Mtb assay

The bacterial inoculums for both H37Rv (active TB) and XDR (resistant TB) strain were prepared from fresh LJ medium and re-suspended in Middlebrook 7H9 broth (HiMedia Laboratories) which was supplemented with Middlebrook OADC growth supplement (HiMedia Laboratories). Both H37Rv and XDR strain were obtained from National Institute of Research in Tuberculosis (NIRT), Chennai. XDR-TB strain obtained is resistant to first line anti-tubercular drugs isoniazid and rifampicin, second line injectable amikacin and fluoroquinolone ofloxacin. The growth supplement included oleic acid, albumin, dextrose and catalase and the above broth was diluted to 1:20 with media of which 100 µL was used as an inoculum. Each drug stock solution were thawed and diluted in Middlebrook 7H9-OADC at four-fold the final highest concentration tested. Serial two fold dilutions of each drug were

prepared directly in a sterile 96-well microtiter plate using 100µL Middlebrook 7H9-OADC. A growth control containing no drug and a sterile medium as control were also prepared on each plate. Sterile water was added to all outer wells to avoid evaporation during the incubation. The plate was covered, sealed in plastic bags and incubated at 37 °C. After 7 days of incubation, 50 µL of 1:1 mixture of alamar blue solution (Sigma Aldrich) and sterile tween 80 (Nice chemicals) were added to each well and the plate was re-incubated overnight. A change in color from blue (oxidized state) to pink (reduced) indicated the growth of bacteria and the MIC (minimum inhibitory concentration) was defined as the lowest concentration of drug that prevented this change in colour [Franzblau S.G., *et al.*, 1998, Collins L.S., *et al.*, 1997].

4.2.3.2.2. *In vitro* dormant Mtb assay

Mycobacterium tuberculosis dormant cultures were prepared using three well established models: nutrient starvation, oxidative stress and nitrosative stress [Joanna C., *et al.*, 2002, Kawaji S., *et al.*, 2010]. In nutrient starvation model, culture of *Mycobacterium tuberculosis* H37Rv (NIRT, Chennai) grown in Middlebrook 7H9 medium supplemented with OADC(nutrient rich medium) was pelleted and washed twice with PBS(Phosphate Buffer Saline, obtained from HiMedia Laboratories). The pellet was resuspended in PBS in sealed bottles and was incubated at 37 °C for 6 weeks [Joanna C., *et al.*, 2002]. In oxidative stress model, the culture was exposed to 0.05% (v/v) hydrogen peroxide (H_2O_2) for 7 days incubated at 37 °C. For nitrosative stress, the culture was exposed to 50 mM sodium nitrate ($NaNO_2$) (final concentration of 1 mM) for 7 days incubated at 37 °C [Kawaji S., *et al.*, 2010]. These cultures were treated with standard drugs like isoniazid, rifampicin and moxifloxacin along with the synthesized compounds for 7 days at a concentration of 10 µg/ml. The treated cell suspensions were diluted 10-fold up to 10^{-6} using Middlebrook 7H9 medium supplemented with OADC and 100 µl of each dilutions were plated in 48 well plates in triplicates along with 900 µl of Middlebrook 7H9 medium (HiMedia Laboratories) supplemented with OADC

(HiMedia Laboratories). The plates were incubated at 37 °Cfor 3-4 weeks the wells with visible bacterial growth were counted as positive. The bacterial count was down by using standard statistical methods using MPN assay [de Man J.C, 1975, Salina E., *et al.*, 2014].

4.2.3.3. Anti-mycobacterial screening for most active compound using adult zebrafish

The most active compound was further evaluated for its *in vivo* activity using adult zebrafish model established by us in a laboratory setup. We used *Mycobacterium marinum* strain (ATCC BAA-535) grown at 30 °C in Middlebrook 7H9 broth. Fish were initially weighed and monitored for its locomotor activities and were divided into control and treatment groups (n=6). All the fish were injected by intra-peritonial injection with 20 µl of thawed bacterial stocks (around 0.75 million bacteria). They were observed for lesions, reduction in swimming activities and squamous eruptions in the initial 7 day infection stage which was followed by treatment stage. The drug solutions were prepared based on the fish's body weight and oral dosing amount of 5 µL. Fish were then administered drug orally using micropipette, on each day during the treatment phase and were noted for their recovery symptoms. They were allowed to swim in 1.5mg/mL solution of kanamycin sulphate before proceeding for sacrifice at the end of study i.e., 14^{th} day. Finally, all of them were sacrificed using homogenization technique and the tissue sample was prepared in Middlebrook 7H9 broth. The collected homogenate was serially diluted to 10^{-6} times and plated into 48-well plates, incubated at 30 °C for 24 h. The plates were checked for the bacterial counts using MPN bacterial count software [de Man J.C, 1975, Salina E., *et al.*, 2014].

4.2.3.4. *In vitro* cytotoxicity screening

The synthesized compounds were further screened for cytotoxic activity using Human Embryonic cell line HEK 293 at 25µM. The cells were grown in RPMI medium with 10% FBS. The activity was carried out using MTT assay. The enzymes in the viable cell have the

capability of reducing the tetrazolium dye MTT 3-(4,5-dimethylthiazol-2-yl)-2,5-diphenyltetrazolium bromide to its reduced form formazon, which has purple color. The cells were grown in RPMI-1640 medium supplemented with 10% FBS (Fetal bovine serum), 100 IU/ml penicillin, 100 mg/ml streptomycin and 2 mM glutamine. Cell line was maintained at 37 °C in a humidified 5% CO_2 incubator (Thermo scientific). Cells were scrapped and were seeded into wells approx 5,000 cells per well in poly-L-lysine coated plates. The plates were incubated at 37°C in humidified CO_2incubator and then treated with the synthesized compounds at 25µM concentration and incubated for 48 h. 10 µL of 0.5mg/ml concentration of MTT was added and incubated for 3 h at 37 ^oC and the final product formazon crystals were dissolved in 100µL of DMSO and the viability was measured at 595nm [vanMeerloo J., *et al.*, 2011]. Relative to the control wells the percent growth was calculated for each well. The percentage of cells killed was calculated from the formula,

$$\% \text{ of cells killed} = 100 \left[\frac{\text{Mean OD sample}}{\text{Mean OD day 0}}\right]$$

4.2.3.5. Biophysical characterization using differential scanning fluorimetry

The most active compound was further investigated using a biophysical technique. The ability of the compound to stabilize the Mtb Topo I protein was assessed using this technique by measuring fluorescence of the native protein and the protein-ligand complexes in the presence of a fluorescent dye SYPRO-orange whose fluorescence increases when exposed to non-polar residues of the protein and reaches a maximum when the protein denatures, this happens as it binds with maximum number of residues in uncoiled state [Niesen F.H., *et al.*, 2007]. Complex with the compound was heated stepwise from 25 to 95 ^oC in steps of 0.1 ^oC in the presence of the fluorescent dye, whose fluorescence increases as it interacts with protein. A right side positive shift of T_m in comparison to native protein means higher stabilization of the protein-

ligand complex, which is a consequence of the thermally stable inhibitor binding profile [Jeankumar V.U., *et al.*, 2013].

Chapter 5

Result and Discussion for optimization of adult zebrafish model for *in vivo* anti-mycobacterial screening

5.1. Optimization study

The lesions observed in infected fish were redness with squamous eruptions (in the form of white fibres) (Figure 5.1).

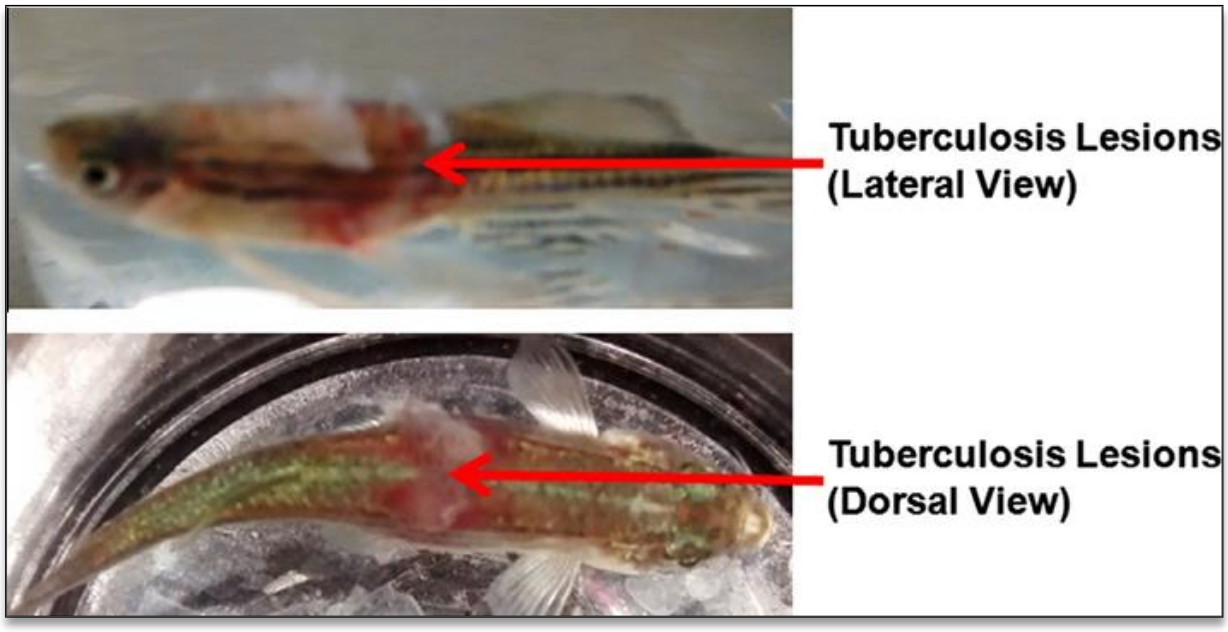

Figure 5.1: *M. marinum*-induced adult zebrafish with red lesions & squamous eruptions on dorsal and lateral sides observed during the study.

The MPN assay showed a clear dose response in the increase of the bacterial counts (Figure 5.2). Group I showed approximately 1.2 and 1.8-fold increase in MPN on days 7 and 14 respectively. Group II showed an increase of 1.5 and 3.1-fold increase in bacterial counts on the days of sacrifice (days 7 and 14). The highest increase was seen in Group III with an

increase of 4.1 on day 7 post infections and a huge 12.8-fold increase on day 14 post infection. Body weight reduction was seen in a dose response manner (Figure 5.3). The mean body weight reduction in the control group was 1.7 ± 2% and 0 ± 1.8% on days 8 and 14 post infection, respectively. Whereas, in the infected groups, the reduction was significantly higher within 8 days post infection and was observed to be 18.5 ± 1.5%, 29.5 ± 1.8% and 31.7 ± 1.4% in Groups I, II and III, respectively. On day 14, there was a further reduction in body weights in all three groups by 22.3 ± 1.6%, 33.2 ± 1.8% and 41.2 ± 1.1% in Groups I, II and III, respectively. In order to ensure that Group III was suitable for conduct of screening experiments, a survival probability assessment (Figure 5.4) was conducted on 90 fish after inoculation of 0.75 million bacteria and observation for 14 days for survival.

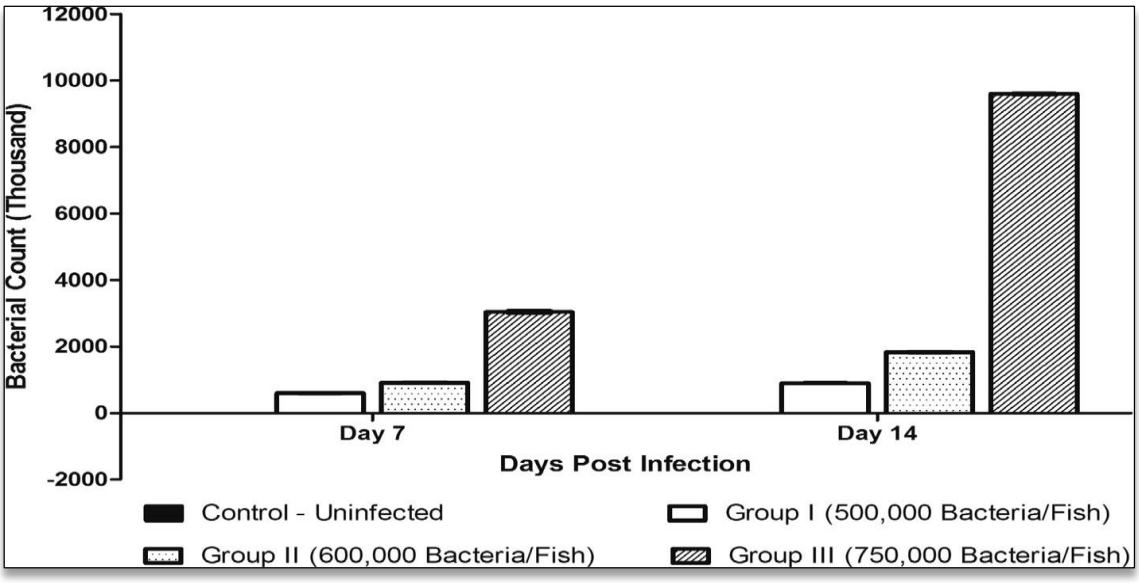

Figure 5.2: Bacterial counts of groups I, II, III (Mean ± S.E.M., n = 6) on days 7 and 14 during the optimization study of *M. marinum* induced adult zebrafish model.

At the end of 14 days, a survival probability of 0.71 suggested this dose to be robust and suitable for conducting screening experiments with a substantial sample size surviving for measuring the response of test drugs. It is reported that almost half (47%) of the experiments conducted on murine models of TB are based on the criterion of lethality [Franco N.H., *et al.*, 2012], and

the biological significance for efficacy in such models is generally considered to be a 20% improvement in survival. Therefore, the survival probability of >0.7 in this model ought to be sufficiently ‘‘humane’’ for the purpose of drug efficacy evaluation.

Therefore, Group III was the group that showed substantial symptoms and a high lesion score, >10-fold increase in MPN, >40% reduction in body weight, and >0.7 survivability. Thus, an intra-peritoneal inoculation of 0.75 million bacteria/fish was selected as the suitable paradigm for *M. marinum* infection model in adult zebrafish.

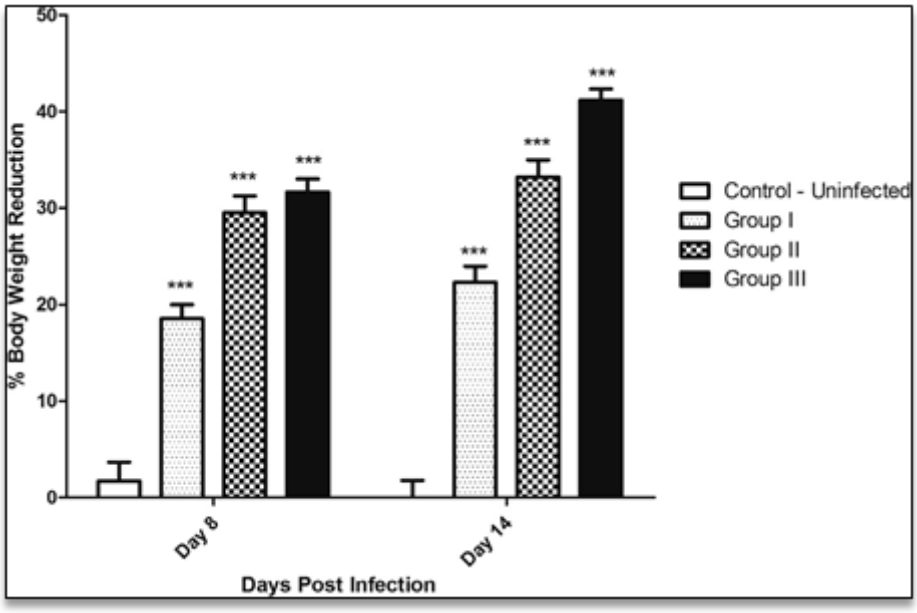

Figure 5.3: Percentage body weight reduction observed in groups control-uninfected, I, II, III (Mean ± S.E.M., n = 10) on days 7 and 14 during the bacterial optimization study *of M. marinum*-induced adult zebrafish model. The statistical significance (*p < 0.05, **p < 0.01 and ***p < 0.001) with respect to un-infected control group has been analyzed by one-way ANOVA using Graph Pad Prism software

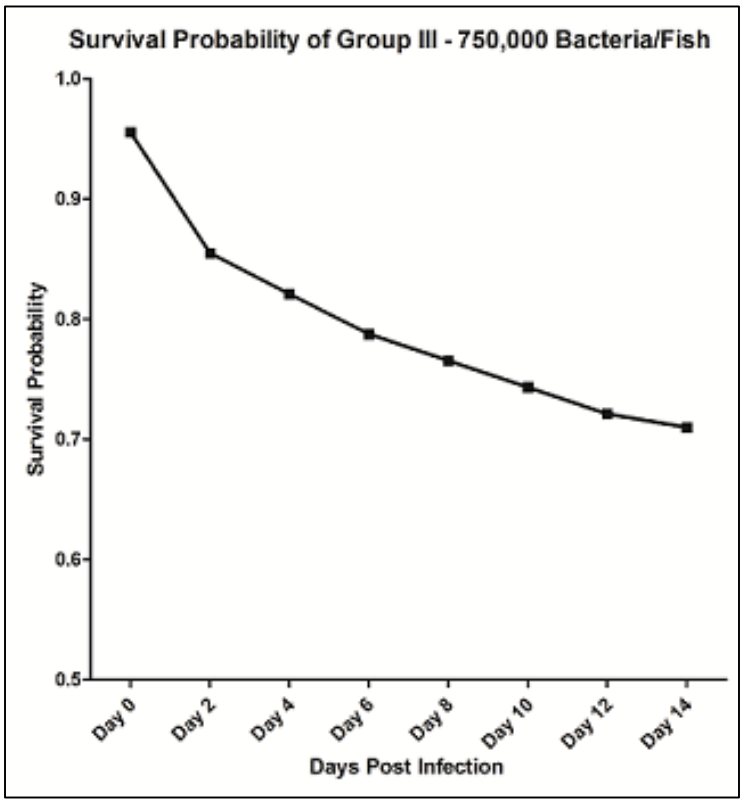

Figure 5.4: Kaplan–Meier survival analysis performed to know survival probability of Group III fish induced with 750,000 bacteria.

5.2. Validation study

All the parameters, i.e., MPN assay results (Figure 5.5) and body weight reduction observations (Figure 5.7) demonstrated that the antituberculosis drugs were efficacious in this model whereas the negative control Amoxicillin did not show any signs of efficacy in reversing the parameters of *M. marinum* infection.

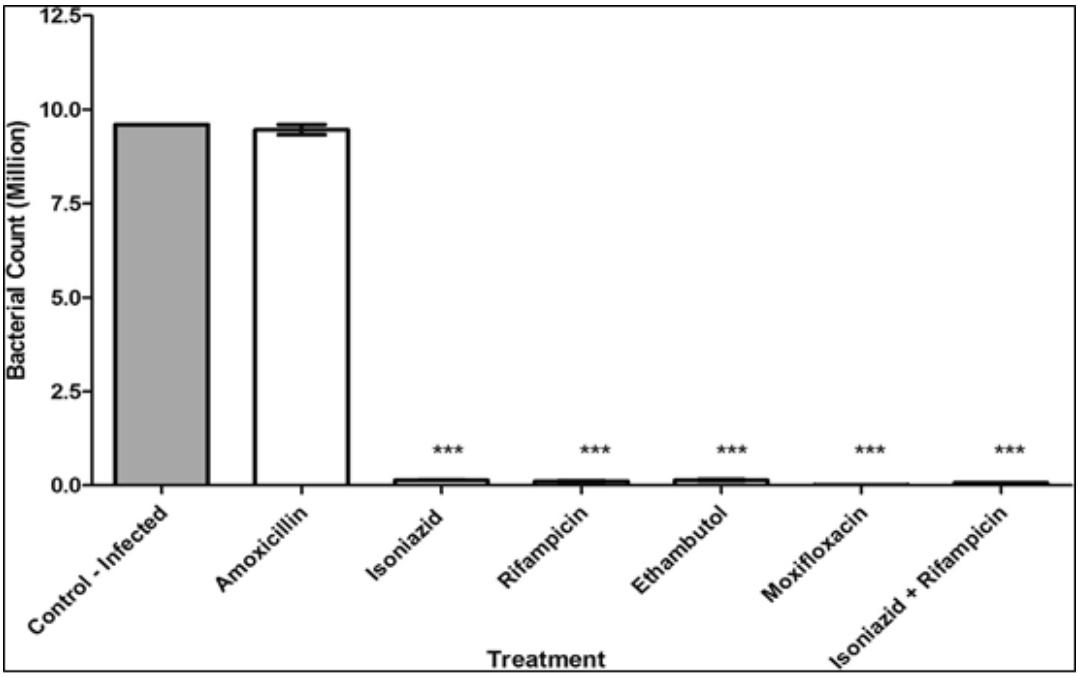

Figure 5.5: Bacterial count estimation (Mean ± S.E.M., n = 6) for control and treated groups conducted by using MPN (most probable number) assay. The statistical significance (*$p < 0.05$, **$p < 0.01$ and ***$p < 0.001$) with respect to infected control group.

The average bacterial counts were >12-fold higher in the infected group and the data was consistent with the results seen in the optimization study. The Amoxicillin treated group also showed MPN equivalent to the infection control fish. Fish treated with all the drugs showed almost complete elimination of bacteria with a very high statistical significance.

The data on body weight reduction showed that fish treated with Moxifloxacin and the combination of Isoniazid + Rifampicin did not show any significant reduction in body weight as compared with the untreated control on day 14 of the study. Furthermore, there was a reduction in body weights for the first seven days of the infection phase which improved in the treatment phase (Figure 5.6). Fish treated with Isoniazid, Rifampicin and Ethambutol showed a statistically significant reduction in body weight as compared with the untreated control;

however, the reduction seen in the infected control group and the Amoxicillin treated group was over 50%, which showed a severe infection in these fish.

Overall, the evaluation that the anti-tuberculosis could be ranked for efficacy in the following order is based on various parameters summarized in Table 5.1:

(a) Moxifloxacin

(b) Isoniazid + Rifampicin

(c) Rifampicin

(d) Ethambutol

(e) Isoniazid

It is known that Moxifloxacin and a combination therapy of Isoniazid + Rifampicin are more efficacious in human TB followed by the other three studies in this experiment. This result suggests that the efficacy profile observed in the zebrafish model is similar to the one seen in a clinical situation, demonstrating the predictive value of this model in drug screening.

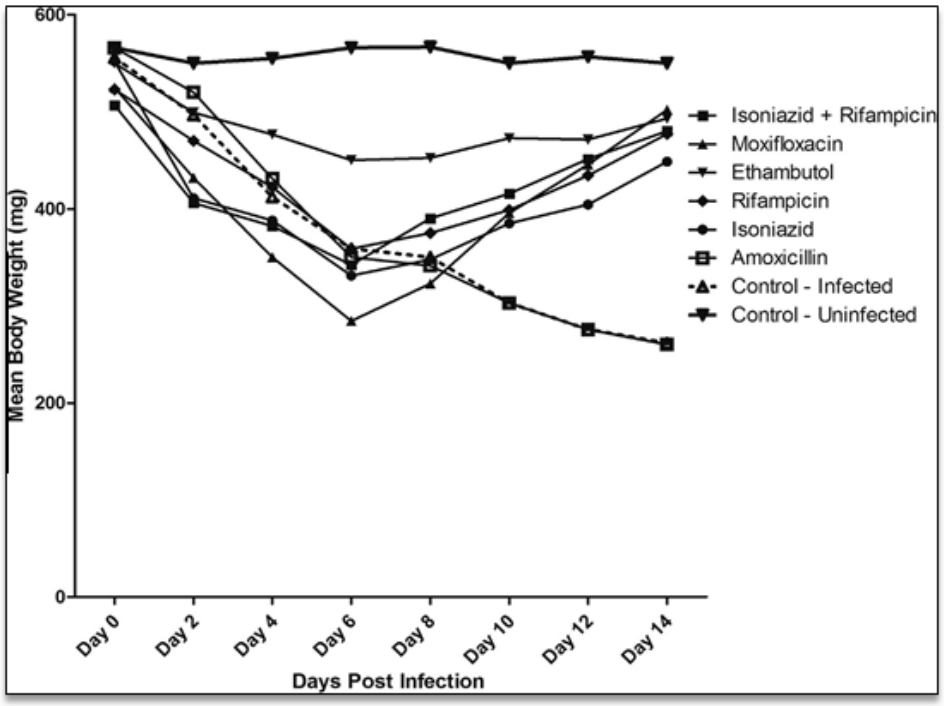

Figure 5.6: Mean body weight changes observed (Mean ± S.E.M., n = 10) with respective days post infection for all the groups during the study of *M. marinum*-induced adult zebrafish model.

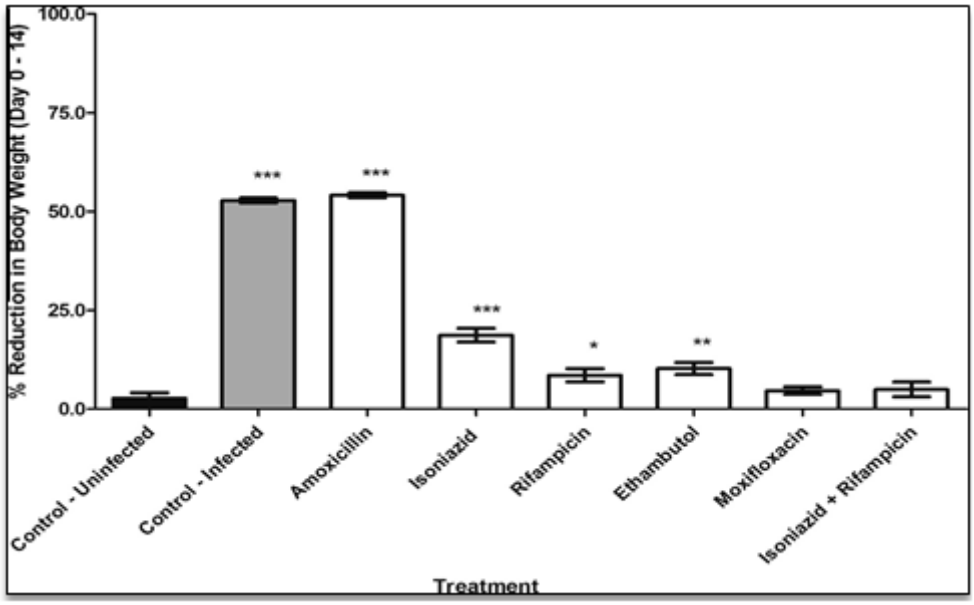

Figure 5.7: Percentage body weight reduction (Mean ± S.E.M., n = 10) over the study period for control and treated groups of *M. marinum*-induced adult zebrafish model. The statistical significance (*$p < 0.05$, **$p < 0.01$ and ***$p < 0.001$) with respect to uninfected control group has been analyzed by one-way ANOVA using GraphPad Prism Software.

Table 5.1: Ranking of antituberculosis drugs based on various parameters of efficacy in *M. marinum*-induced adult zebrafish model of tuberculosis.

Rank	Anti-tuberculosis Drug	Dose	Parameter Values (Day 14 Post Infection)		
			MPN (million/fish)	% Body Weight Reduction	Survivability
1	Moxifloxacin	5 mg/kg	0.01 ± 0.00	4.4 ± 1.0	0.6
2	Isoniazid + Rifampicin	5 mg/kg + 2.5 mg/kg	0.07 ± 0.00	5.3 ± 1.8	0.6
3	Rifampicin	5 mg/kg	0.12 ± 0.01	8.8 ± 1.6	0.7
4	Ethambutol	10 mg/kg	0.14 ± 0.01	10.3 ± 1.6	0.7
5	Isoniazid	10 mg/kg	0.14 ± 0.01	18.7 ± 1.7	0.7

5.3. Discussion

The use of adult zebrafish as a surrogate model for assessing drug efficacy in TB research has not been fully exploited by either academicians or by the industry. Important aspects of establishment of a screening tool for evaluation of pharmacological activity of drugs include genetics and physiology rationale, predictivity and reproducibility of protocol. The genetic and physiological relevance of *M. marinum*-induced adult zebrafish models of TB has been well established in the literature [Ramakrishnan L., 2013]. Various methods and models of *M. marinum* have been reported in the literature. A rapid high-throughput platform wherein zebrafish larva infected with fluorescently labeled *M. marinum* are monitored using automated plate fluorometry (APF) has been developed to assess both efficacy and safety [Takaki K., *et*

al., 2012]. A similar high-throughput larval model using larval zebrafish has been reported recently [Veneman V.J., *et al.*, 2014]. The adult zebrafish model of *M. marinum* infection has been reported [Swaim L.E., *et al.*, 2006], however, the report deals with the study of pathology with respect to adaptive immunity and this model has not been validated for drug screening. The present protocol has been inspired by this report, and an attempt to modify and refine the protocol has been made in order to make it reproducible and simple to conduct.

A flow chart for standardization of the protocol for *M. marinum* based adult zebrafish TB model has been suggested in Figure 5.8. It provided for criterion for each step of standardization and validation of the model. This flow chart will be very useful for the development of such a model in laboratories across academia and the industry.

It was proposed that the use of adult zebrafish model should take precedence over the larval model (which has been more popular) based on the following rationale: adult zebrafish have optimally developed organs required for drug metabolism [Alderton W., *et al.*, 2010, Wang Z., *et al.*, 2010]; poorly soluble drugs may precipitate and will be unabsorbed in the larval assay and hence cannot be tested in larval zebrafish; using the oral dosing paradigm, the dosage of the drugs can be ascertained in terms of mg/kg. Therefore, even though the larval models can be useful for early high- throughput screening, the adult model holds greater promise for the establishment of *in vivo* proof-of-concept. An alternative to the oral method of administration, the intraperitoneal (i.p.) method can also be used for precision drug administration [Stewart A., *et al*., 2012] and for arriving at a dose in terms of mg/kg. The use of the adult zebrafish model helps us have a fully grown organism with optimally functioning systems of ADME (absorption, distribution, metabolism and excretion) and precise methods for drug administration. This can ensure that the effect of candidate drugs can be determined to take decisions in preclinical research. This protocol would further help researchers to correlate drug efficacy data between zebrafish and other mammalian models.

The methods reported so far using larval zebrafish require fluorescently labeled organisms and sophisticated visualization techniques. Moreover, micro-injections for the inoculation of infection will require specific equipment and trained manpower. Small academic laboratories and start-up companies may not be in a position to make these investments for a small library-based screening program. Even larger organizations that are not interested in high-throughput screening would prefer a protocol which can be used in low-resource settings. This protocol is resource-efficient, inexpensive, involves simple techniques like bacterial count, body weight change and survivability.

Literature reports have suggested the use of zebrafish as a model organism to study various other bacterial infections like *Burkholderia cenocepacia*, *Pseudomonas aeruginosa*, *Staphylococcus aureus*, *Streptococcus pyogenes* and *Francisella* species, the fungal pathogen *Candida albicans* and the viral pathogen *Herpes simplex* virus type 1 [Brannon M.K., *et al.*, 2009, Chao C.C., *et al.*, 2010, Clatworthy A.E., *et al.*, 2009, Prajsnar T.K., *et al.*, 2008, Szabady R.L., *et al.*, 2009, Vergunst A.C., *et al.*, 2010, Wiles T.J., *et al.*, 2009]. It is believed that these methods can be modified suitably and applied to these infections as well.

A possible improvement in the present protocol could be the addition of pharmacokinetic assessment of test drugs in order to develop pharmacokinetic-pharmacodynamic correlation of efficacy. Drug metabolism can also be assessed in the same study. In conclusion, the use of adult zebrafish and the involvement of simple phenotypic parameters ensure obtaining the maximum data about compounds from one study, a possibility that makes this protocol very useful in drug discovery decision-making.

5.4. Summary and Conclusion

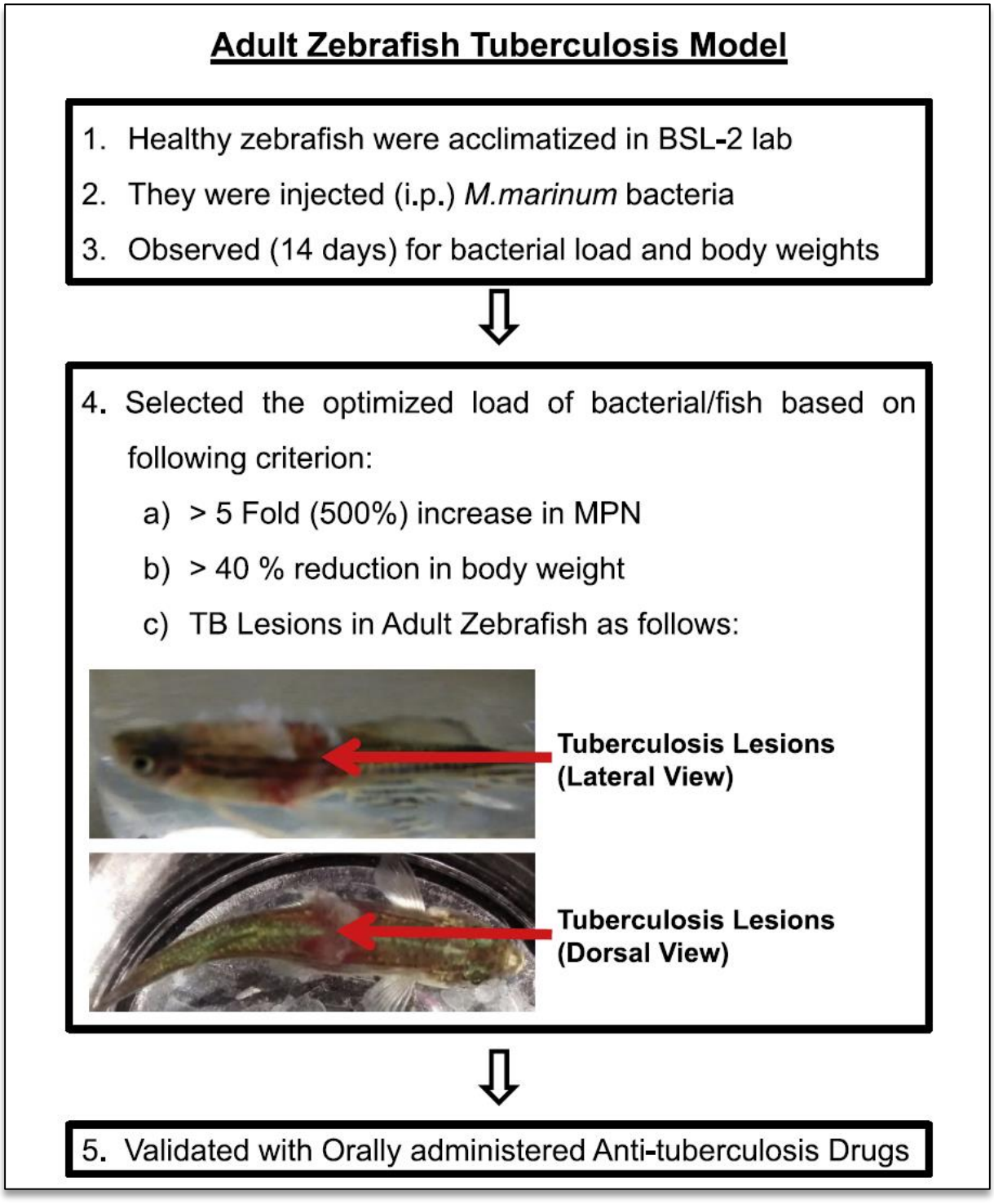

Figure 5.8: Flow chart demonstrating the standardization process followed in developing adult Zebrafish tuberculosis model for evaluation of oral antituberculosis drugs

Chapter 6

Result and Discussion for Development of Mycobacterial Topoisomerase I Inhibitors

6.1 Homology modeling and design of inhibitors for Mtb Topo I

6.1.1. Mtb Topo I model structure

The absence of crystal structure for Mtb Topo I impelled us to develop its tertiary protein model which can be further used in docking studies. The retrieved Topo I amino acid sequence was run for BLASTp against protein data bank (PDB) and suitable template was selected based on its identity and query coverage. The crystal structure of *Escherichia coli* Topo I with cleaved DNA (3PX7) was chosen for this purpose which was found with 42% identity with Mtb Topo I. The alignment for both the sequences is given in supporting information Figure 6.1. Initially, missing loops and side chains were added to the template based on its sequence as some gaps in crystal structure were noticed. This processed structure was employed as template for generating 3D protein model for Mtb Topo I. Energy based model generation was employed in model development using OPLS_2005 force field. The loops in the generated model were found with residues falling in the generously allowed and disallowed regions of Ramachandran plot which were corrected by loop refinement. The final protein model was energy minimized, shown in Figure 6.2, and its quality was finally evaluated by using Ramachandran plot. The Ramachandran plot, Figure 6.3 given in supporting information, showed statistics of 82.7% residues in most favoured region, 15.1% residues in additional allowed region, 1.9% residues in generously allowed region and 0.4% in disallowed region making the model highly acceptable.

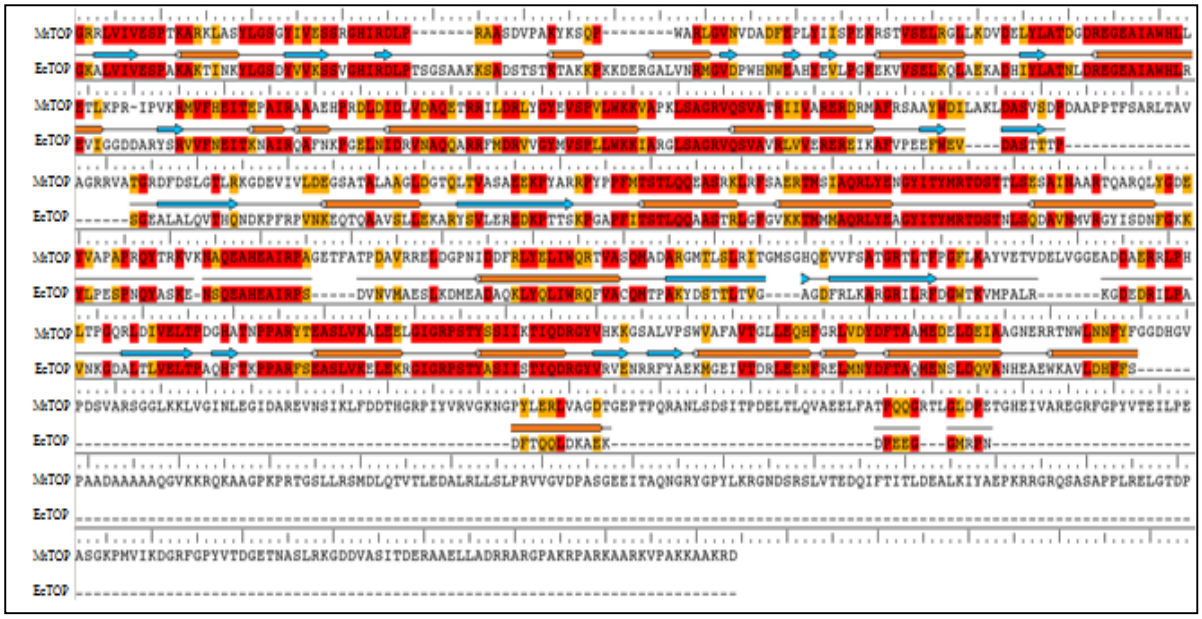

Figure 6.1: Sequence alignment of Mtb Topo I over *E. coli* topoisomerase. Red colour indicates similar amino acids in both the sequences.

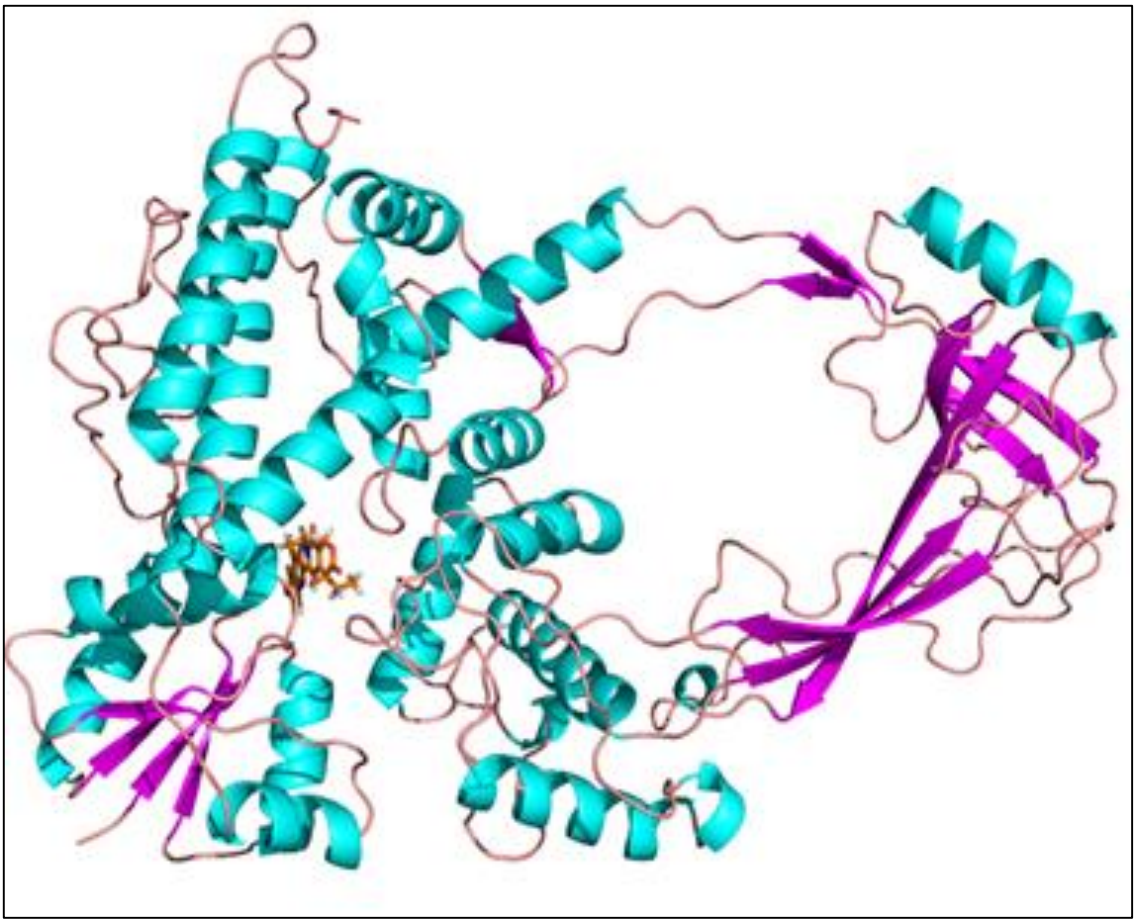

Figure 6.2: Homology model of Mtb Topo I developed showing hydroxycamptothecin (orange) at the binding pocket.

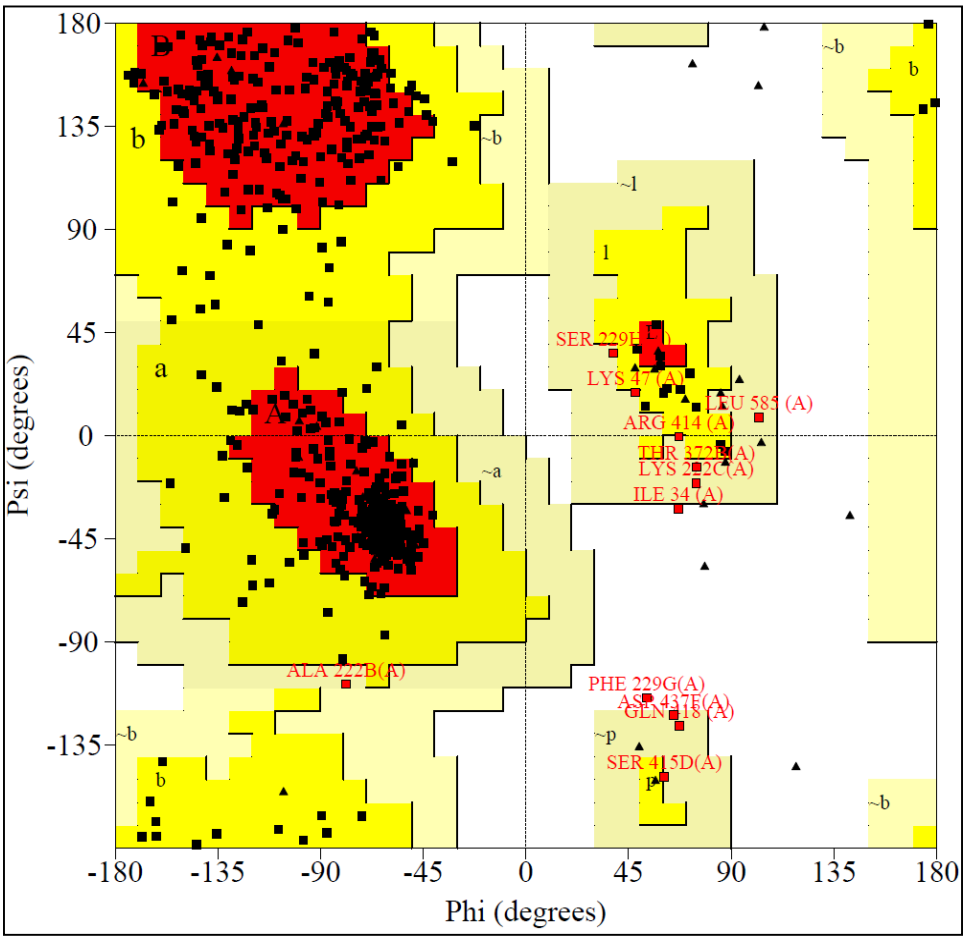

Figure 6.3: Ramachandran plot for Mtb Topo I model developed using crystal structure of *E. coli* (PBD code – 3PX7).

6.1.2. Molecular Dynamic simulation analysis

The model developed was further simulated for 10 ns under explicit solvent conditions employing TIP3P water model. The trajectory was analyzed for evaluating the behavior of the model like stability, flexibility etc under dynamic conditions. The root mean square deviation (rmsd) of the model during the simulation was plot as a function of time (as shown in Figure 6.4). The figure shows the rms deviation of total protein atoms (blue line) and only backbone atoms (red line). The initial jump in the rmsd can be reasoned for the relaxation of the model when minimized. After a time scale of 2.5 ns, the plot was seen to be stable maintaining the

rmsd less than 2 Å at any considered frame till a time period of 10 ns. Plots for both all atoms and backbone atoms of the model showed almost similar deviations. The rms deviation for the model was compared with that of template rmsd plot (not incorporated in the manuscript) so as to analyze the model stability. Identical deviations were found with both the model and template with lesser fluctuations showing the consistency of the model. The MD simulation analysis shows the protein to be with least fluctuations thereby strongly supporting its stability even in dynamic conditions. Hence this model was considered further for molecular docking studies.

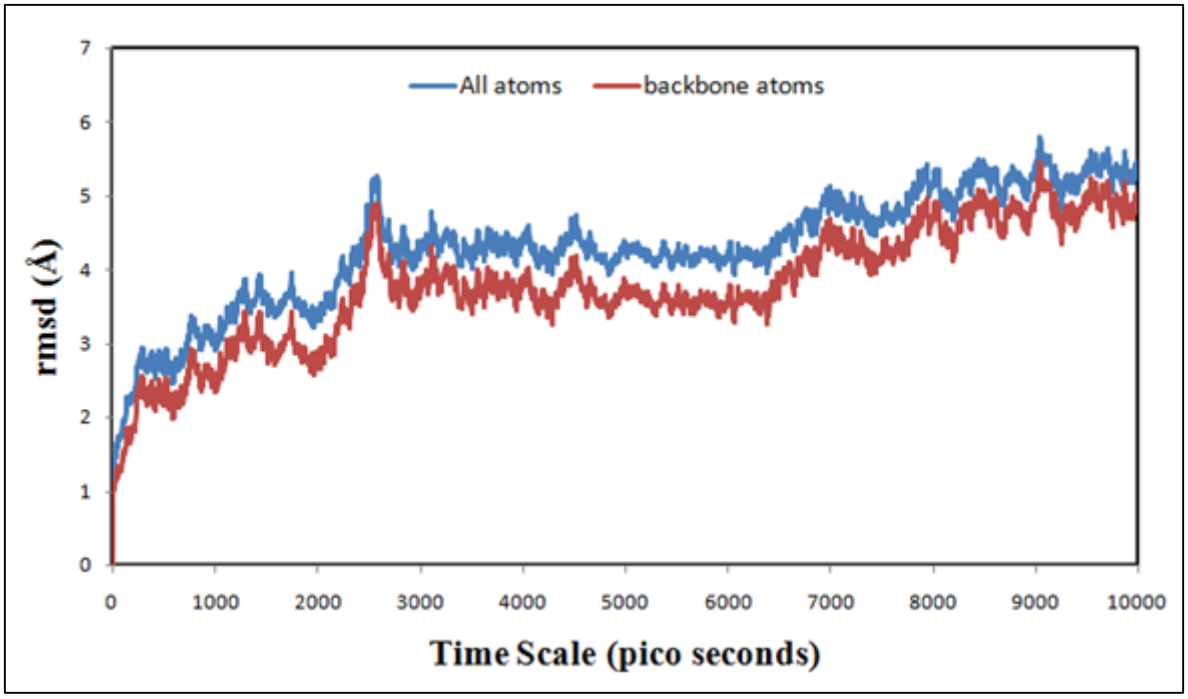

Figure 6.4: Root mean square deviation (rmsd) plot for Mtb Topo I model simulated for 10 ns.

6.1.3. Docking calculations

The active site of the model was identified by overlapping the tertiary protein structure of template (crystal structure of *E. coli* Topo I) over the constructed model and the active site conserved residues were identified. The sequence alignment of topoisomerase I of both *M.*

tuberculosis and *E. coli* is shown in Figure 6.1. Almost 75% of the active site residues were found to be conserved in Mtb Topo 1 compared to the template. The probable binding pocket of the model was also determined by using SiteMap, which also resulted in the same pocket identification as of that from alignment. Residues Pro11, Asp111, Asp113, Phe139, Tyr319, Arg321, Thr322, Asp323, ser324, Ala367, Ser495 were found to be lining the Mtb Topo I active site.

The identified active site was targeted for grid generation for docking calculations of the model. The protocol followed for the molecular docking studies has been documented in detail in supporting information. A high throughput virtual screening (HTVS) docking was run with both in-house (BITS database) and asinex databases so as to identify compounds with good affinity of binding. The compounds with better interaction pattern were selected further for standard precision and extra precision docking. The compounds showing considerable polar and non-polar bonding at the active site were selected for further *in vitro* enzyme inhibition studies. Total 15 compounds were selected and ADME predictions were done for the selected compounds using QikProp module in Schrödinger (Table 6.1).

Table 6.1: ADME predictions for the designed compounds.

Compound ID	QPlogPo/w[a]	QPlogHERG[b]	QPPCaco[c]	QPlogBB[d]	% Human oral absorption[e]	Rule of 5[f]
Lead-I	2.39	-4.83	153.01	-1.4	80.02	0
Lead-II	3.42	-6.51	701.99	-0.9	100	0
Lead-III	1.01	-5.09	763.96	-0.4	84.44	0
Lead-IV	3.25	-6.13	798.61	-0.56	100	0
Lead-V	3.30	-5.90	911.99	-0.71	100	0
Lead-VI	3.17	-6.10	792.75	-0.43	100	0
Lead-VII	3.38	-6.11	800.54	-0.39	100	0
Lead-VIII	3.43	-6.13	799.39	-0.38	100	0
Lead-IX	4.81	-7.79	466	-0.04	100	0
Lead-X	5.50	-7.71	465.58	0.13	93.98	1
Lead-XI	3.16	-3.78	29.02	-1.92	71.63	0
Lead-XII	3.94	-5.23	21.48	-2.61	73.87	0
Lead-XIII	2.58	-4.33	23.11	-1.96	66.51	0
Lead-XIV	3.96	-5.15	26.95	-2.40	75.74	0
Lead-XV	4.31	-5.37	21.48	-2.73	76.07	0

[a]Predicted octanol/water partition coefficient logP (acceptable range: −2.0 to 6.5); [b]Predicted IC_{50} value for blockage of HERG K+ channels.(below -5); [c]Predicted apparent Caco-2 cell permeability in nm/sec (<25 poor; >500 great); [d]Predicted brain/blood partition coefficient (-3.0 to 1.2); [e]Percent human oral absorption (<25% is poor and >80% is high); [f]Rule of 5 violation (mol_MW < 500, QPlogPo/w < 5, donorHB ≤5, accptHB ≤10)

6.1.4. Design of compounds

A total of 15 compounds were selected from the database after the docking studies and the compounds were tested for *in vitro* Mtb Topo I inhibitory activity. Initially, these fifteen compounds were screened at 200 µM concentration which resulted in 3 compounds showing more than 90% inhibition. Further, these 3 compounds were screened at lower concentrations of from 100 µM to 1.5 µM and their IC_{50}s were calculated (given in Figure 6.5). The structures

of the remaining 12 inactive compounds are shown in Figure 6.6. All the three compounds selected were found with Mtb Topo I inhibitory activity below 50 µM with hydroxycamptothecin (lead 1) being the top one with an IC_{50} of 6.25 µM. The docking pattern of the compound revealed the polar interactions with Val196 and Gln97. The compound was oriented such that the hydroxyl group of the compound was facing towards the opening of active site and residues Ala41, Pro181, Trp184 and Ala193 at this position were involved in hydrophobic interactions with the compound. The compound was seen to be involved in hydrogen bonding with active site residues Asp113 and Ser495 as seen in Figure 6.7. This compound was further derivatized replacing the terminal hydroxyl group, facing towards outside of the pocket, with some hydrophobic moieties so as to study the influence of the substituents over the residues in the vicinity such as Pro11 and Gly32, thereby monitoring the activity fluctuations of the compounds.

The docking pattern of Lead-II amsacrine (Figure 6.7) shows the hydrogen bonding interactions with active site residues Ser495 and Asp113. This compound was further derivatised and 24 derivatives were prepared by replacing the methyl group in N-substituted methanesulphonamide and checked for their activity on Mtb Topo I.

The ligand interaction picture of Lead-III tryptanthrin (Figure 6.7) shows polar contact with Arg321, an active site residue. 13 synthetic derivatives were prepared for the lead compound to further improvise the activity on Mtb Topo I.

.

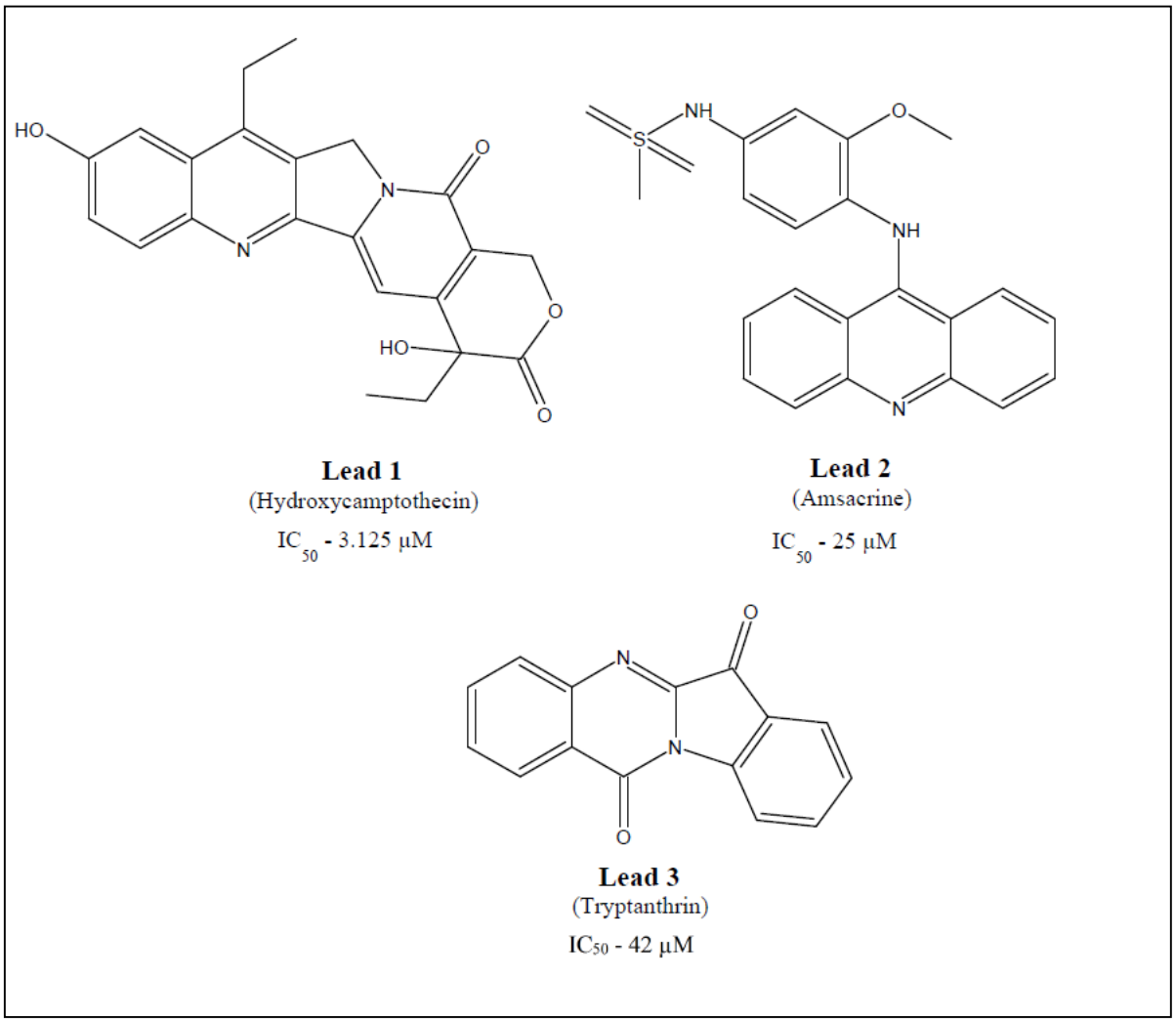

Figure 6.5: Three compounds out of 15 that resulted from virtual screening studies found with Mtb Topo I inhibitory activity below 50 µM.

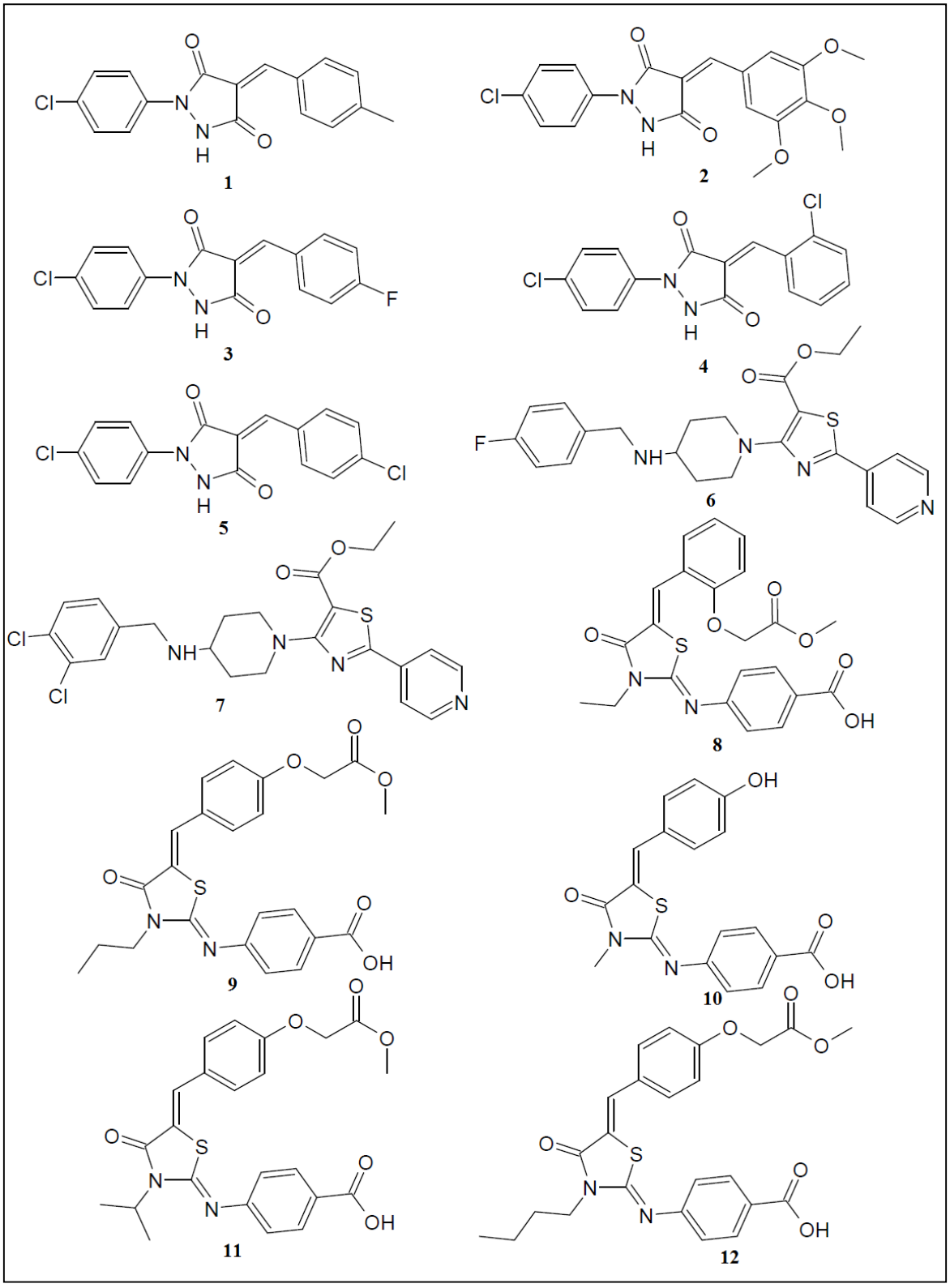

Figure 6.6: Twelve compounds inactive against Mtb Topo I below 100 µM concentration

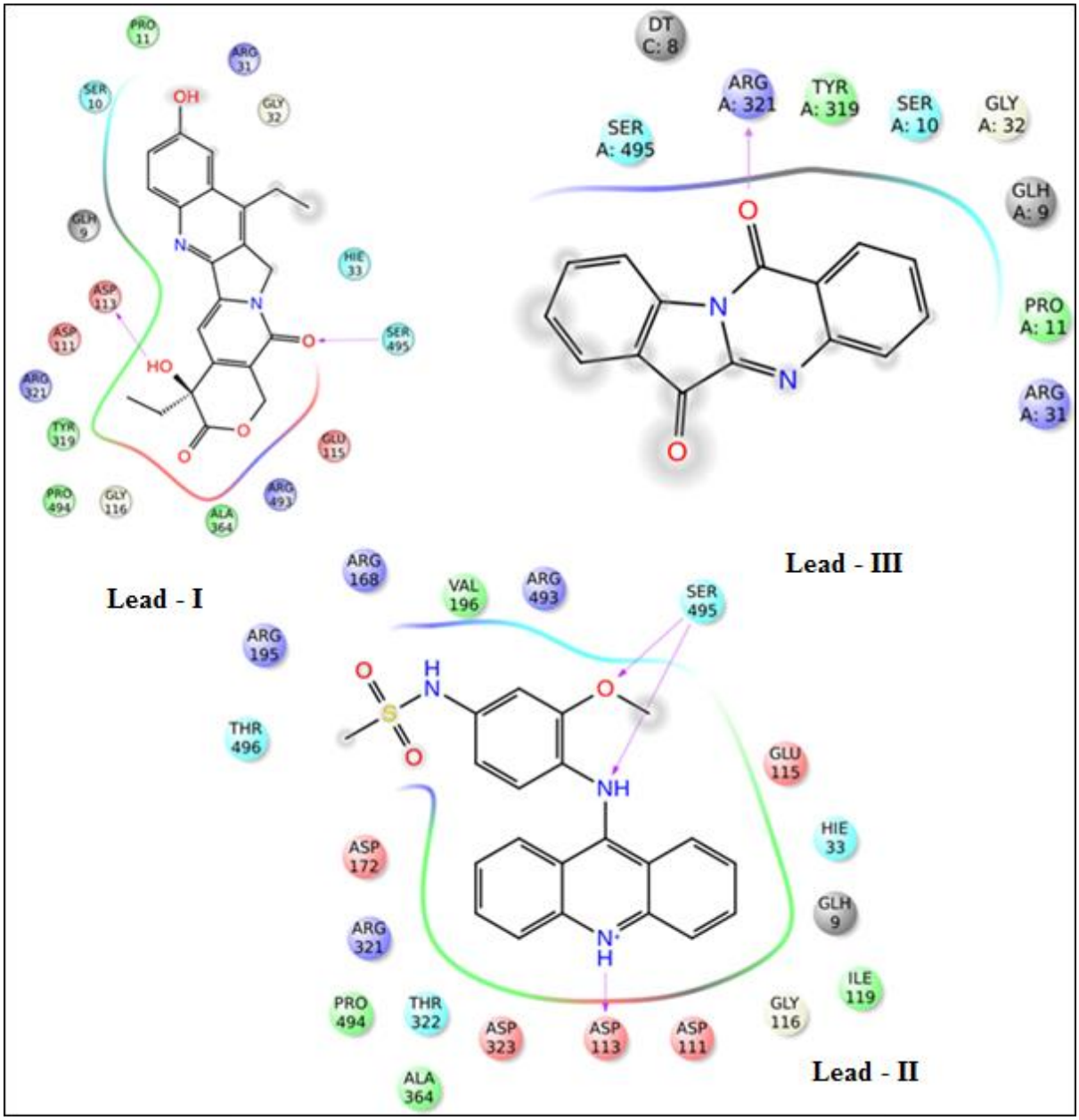

Figure 6.7: Ligand interaction pictures of Lead I (Hydroxycamptothecin), II (Amsacrine) and III (Tryptanthrin).

6.2. Synthesis and biological assessment of Lead-I camptothecin derivatives

6.2.1. Lead optimization using Medicinal chemistry

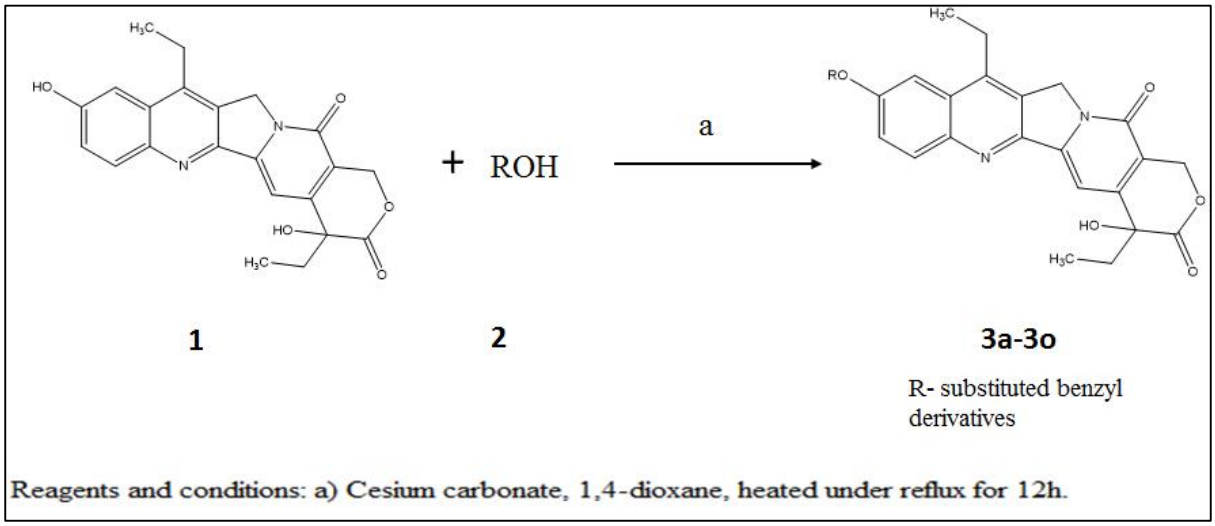

Figure 6.8: Synthetic protocol for hydroxycamptothecin derivatives (3a-3o).

To a solution of 7-Ethyl-10-hydroxycamptothecin (0.02 g, 0.0510 mmol) in 1, 4-dioxane (5 mL) was added Cs_2CO_3 (0.019 g, 0.0612 mmol) followed by corresponding benzyl bromide derivative (0.0561 mmol) and the resulting solution was heated under reflux for 12 h under inert atmosphere. The reaction mixture was filtered and the filtrate was concentrated to get crude compound. Crude compound was triturated by using diisopropyl ether and dried to afford compound **3a – 3o**.

6.2.2. *In vitro* enzymatic assay of synthesized compounds

Further, 103 KDa Mtb Topo I protein was cloned and purified using Ni-NTA column in low pressure liquid chromatography from Bio-Rad as described in the experimental section. The protein was eluted at 250 mM and a sharp protein peak was observed. The Mtb Topo I assay was performed by gel based assay, with a range of inhibitor concentrations from 200 to1.5 µM. The synthesized 15 compounds were screened at 200 µM, of which compounds **3a**, **3b**, **3e**, **3i**, **3j**, **3n** and **3o** showed more than 60% inhibition, whereas the other compounds showed lesser

inhibitions. Further, all the compounds were screened at lower concentrations and their inhibitory concentrations (IC_{50}s) were determined and given in Table 6.2. Of fifteen, compound **3b**was found with better Mtb Topo I inhibitory profile followed by the other compounds. At a lower concentration of 100 and 50 µM, only six compounds excluding **3n**, showed a better activity against the enzyme. Finally, when tested at lower concentrations of 25 µM,12.5 µM, 6.25 µM, 3.125 µM and 1.5 µM, compound **3b** emerged as the best one with an IC_{50} of 2.9 µM.

Table 6.2: *In vitro* biological activity results for the synthesized compounds**3a - 3o**.

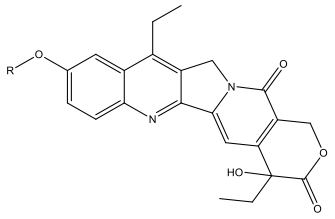

Comp no.	R	MIC in µM[a]		IC_{50} in µM[b]	Cytotoxicity (% inhibition)[c]
		MtbH37Rv	XDR		
Lead 1	H	7.96	15.92	6.25	57.32
3a	Benzyl	25.9	25.9	31.25	29.16
3b	1-Nitro benzyl	5.92	2.95	2.9	16.52
3c	2-Chloro benzyl	48.36	24.18	>100	27.54
3d	3-Fluoro benzyl	24.97	49.94	>100	22.78
3e	3,4-Difluoro benzyl	24.1	12.06	20	2.84
3f	2,3,4-Trifluoro benzyl	23.29	23.31	7.1	20.81
3g	2,3,4,5,6-Pentafluoro benzyl	5.46	5.46	4.8	23.01
3h	3-Chloro-5-fluoro benzyl	5.84	5.85	3.62	18.2
3i	4-Fluoro-2-(trifluoromethyl) benzyl	21.99	11	31.25	24.87
3j	2-(Trifluoro methyl) benzyl	11.32	11.32	12.5	23.65
3k	3-Fluoro-4-methoxy benzyl	23.56	23.56	62.5	4.87
3l	3-Methoxy benzyl	12.2	12.2	9.3	6.96
3m	2-Bromo benzyl	11.13	22.26	46.5	10.2
3n	2-Bromo-5-methoxy benzyl	26.3	21.18	62.5	16.17
3o	4-Iodobenzyl	20.55	20.55	31.25	22.32
	Isoniazid	0.72	45.57	nd	nd
	Rifampicin	0.15	30.37	nd	nd
	Ethambutol	7.64	244.7	nd	nd
	Moxifloxacin	2.16	34.59	nd	nd

IC_{50} – 50% inhibitory concentration; MIC – minimum inhibitory concentration; Mtb – *Mycobacterium tuberculosis*; XDR – Extensively drug resistant; nd – not determined.

a. MIC of the compounds on H37Rv and XDR-TB.

b. IC_{50} of the compounds against Mtb Topo I.

c. Cytotoxicity of compounds at 25 µM on Human embryonic kidney (HEK) cell line.

6.2.3. SAR of hydroxycamptothecin derivatives

The synthesized camptothecin derivatives were docked to the Mtb Topo 1 model developed so as to study their interaction pattern at the active site. With reference to the structure-activity relationship, the compounds were divided into three categories for convenience, based on their *in vitro* activity profiles i.e., active, moderately active and inactive. From the interaction behavior of hydroxycamptothecin at the active site, the hydrogen of hydroxyl group was replaced by various aromatic moieties so as increase the hydrophobic interactions with the adjacent residues. Of all, compound **3b** was found to be highly active with an IC_{50} of 2.9 µM and MIC of 5.92 µM. The compound exhibited six polar contacts with active site residues Ser10, Asp113, Gln309, Tyr319, Arg493 and Ser495 as shown in Figure 6.9. It was also found with strong non-polar interactions with Pro11, Tyr312, and Tyr319 and emerged to be with best docking score of -5.62. It was observed from the interaction profile of compound **3b**, the two oxygen atoms of nitro group were involved in polar contacts with Ser10 and Gln309 and the benzyl ring was involved in π-π stacking interactions with Tyr319 making the compound most potent. Compounds **3h**, **3g**, **3l** and **3f** were also found to be active *in vitro* next to compound **3b**. Of these, compounds **3h**, **3f** and **3g** were found to be fluoro benzyl substituted camptothecin derivatives. The presence of fluorine atoms over the phenyl ring (**3f** and **3g**) oriented the compounds such that the moiety was found stabilized by strong non-polar interactions with Tyr319, Ala362, Ala364. In case of compound **3h**, the presence of chlorine over the fluoro phenyl ring can be considered as a synergistic effect as seen from the activity profile (IC_{50} – 3.62 µM). The binding pattern of compound **3l** was found to be slightly different and interesting. The presence of methoxy group over phenyl ring imparted the lipophilicity to the compound and was found to be interacting with many residues like Pro11 and Tyr312. The methoxy group addition was also found to effect the orientation of compound making it align

close towards the residues Gln309, Met320 and Arg321 which were involved in non-bonded interactions with the compound.

Compounds **3o**, **3e**, **3i**, **3a** and **3j** were found to be moderately active with IC_{50} values ranging 12.5 - 31.25 µM. Of these, compound **3j** was found to be with better activity of 12.5 µM against Mtb Topo I enzyme. This compound when docked showed some polar contacts with Asp113 and Ser495. The trifluoro methyl group on 2^{nd} position of phenyl ring was found to be towards the solvent accessible surface area of protein showing least interactions with protein. This may be attributed for the reduced activity of the compound. Also compound **3i** was found with 2-trifluoro methyl group but with better activity profile compared to compound **3j**. This may be reasoned for the presence of 4-fluoro group in compound **3i** which was seen to be involved in non-bonded interactions.

The remaining ones, compounds **3m**, **3k**, **3n**, **3c** and **3d**, were found to be inactive against Mtb Topo I with IC_{50} ranging 46.5 to above 100 µM. Presence of bromine at 2-position of phenyl group, as seen in compounds **3m** and **3n**, can be considered as a non-favourable substitution as seen from their activity profile. The steric hindrance offered by bromine at the active site, due to its large atomic size, may be attributed to the corresponding compounds inactivity. Compound **3k** and **3d** were also found with similar substitution, 3-fluoro, suggesting the unsuitability of such moiety for Mtb Topo I activity.

In a nut shell, the substitution of hydrogen in hydroxycamptothecin (Lead **1**) by some hydrophobic moieties like substituted benzyl ring, revealed to be a suitable site for enhancement of Mtb Topo I inhibiting activity. However, not all the substitutions were found to give the positive impact. Of all, nitro group at 1-position of phenyl ring was found to be the most effective one (**3b**). 3-position of phenyl ring was found unfavorable for the substitution by halogens (**3m**, **3k**, **3e**, **3n** and **3d**) which were found to reduce the potency. Increased substitution of fluorine over phenyl ring was observed to enhance the potency of the

compounds gradually as observed in compounds **3d**, **3e**, **3f** and **3g**. Substitution of chlorine over fluoro benzyl group was found to be adding up for the activity (**3h**). Other substitutions like bromine, iodine and trifluoromethyl were observed to deteriorate the activity attributing to their steric bulk which hinders the efficient binding of compounds (**3i**, **3j**, **3m**, **3n** and **3o**).

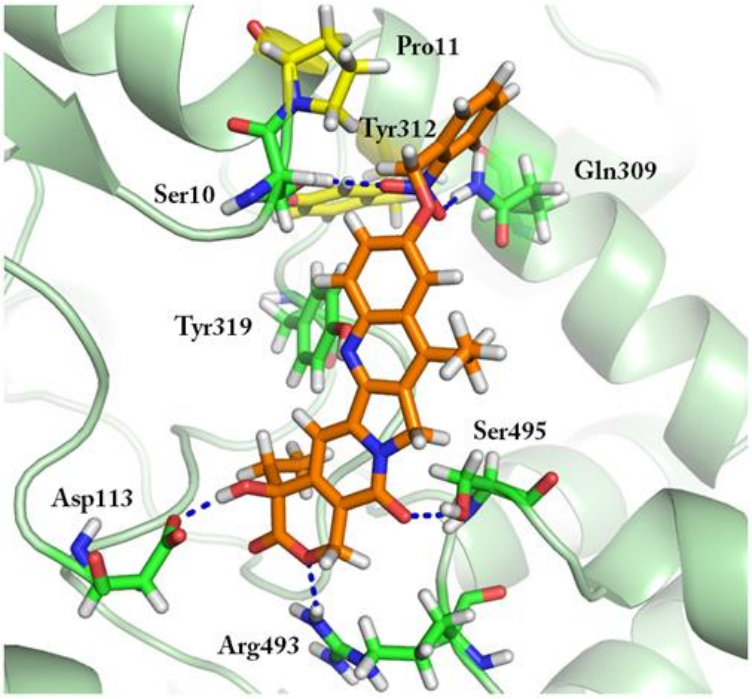

Figure 6.9: Interaction profile of compound **3b** at the Mtb Topo I model active site. Compound **3b** is shown in orange, residues involved in polar contacts shown in green, non-polar contacts shown in yellow. Blue color dashed lines indicate polar contacts.

6.2.4. *In vitro* active Mtb assay

All the synthesized drugs were treated with Mtb H37Rv and XDR strain to determine their anti-tubercular activity using microplate alamar blue assay (MABA) with drug concentrations ranging from 50 µg/ml to 0.78 µg/ml in duplicates. This assay is done by using a resarzurin-based oxidation-reduction indicator which measures colorimetric drug MICs for Mtb. The redox indicator alamar blue turns from blue to pink in the presence of mycobacterial growth. The minimum inhibitory concentration (MIC) was determined for each drug that is the

minimum concentration of the drug which prevents the color change from blue to pink. The MIC values of the synthesized compounds along with the standard drugs are given in Table 6.2. The synthesized compounds exhibited active Mtb MIC ranging from 5.46 to 48.36 µMand XDR-TB MIC ranging from 5.46 to 49.94 µM. Three compounds **3b, 3g** and **3h** were found with increased potency when compared to ethambutol (MIC - 7.82µM) and Lead 1(MIC - 7.96 µM) on Mtb H37Rv. On XDR strain, all the synthesized compounds except compound 3d were more potent than the standard drugs.

6.2.5. *In vitro* dormant Mtb assay

Though dormancy was not reported with respective to topoisomerase I protein expression in Mtb, yet to re-ascertain the efficiency of the inhibitors we screened them in the dormant induced forms. Dormancy was obtained by nutrient starvation, oxidative stress and nitrosative stress models. These methods trigger a dormancy response in the bacilli that is termed non-replicating persistence (NRP), a physiological state thought to mimic the one exhibited by *M. tuberculosis* during various stages of persistent infection [Joanna C.C., et al., 2002]. In nutrient starvation model, Mtb will be in slight or no replicating state but maintains long term viability. The bacteria in this model developed resistance towards isoniazid, rifampicin and moxifloxacin. In oxidative stress, caused due to hydrogen peroxide (H_2O_2), genes involved in DNA repair and recombination were selectively induced suggesting that DNA damage is the significant consequence in oxidative stress. Whereas in nitrosative stress model the reactive nitrogen was found to inhibit aerobic respiration in mitochondria there by inhibiting the growth of Mtb [Lamichhane G., 2011]. The assay of the dormant cultures was carried out with standard drugs like isoniazid, rifampicin and moxifloxacin along with synthesized drugs for 7 days at a concentration of 10 µg/ml. The bacterial log reductions for various standard and synthesized drugs are as depicted in Figure 6.10 and Table 6.3. All the 4 active compounds **3b, 3g, 3h and 3l** were screened and found to be more potent than moxifloxacin in nutrient starvation model

with bacterial log reduction ranging from ~2.7 to 3.1. Compound **3b** has exhibited most promising activity with ~3.1 bacterial log reduction and also inhibited Mtb Topo I with an IC_{50} of 2.9µM. In oxidative and nitrosative stress models, the above 4 active compounds were found to be potent than first line anti-tubercular drugs with bacterial log reduction ranging from ~0.8 to 2.1 which shows the efficiency of the camptothecin derived inhibitors.

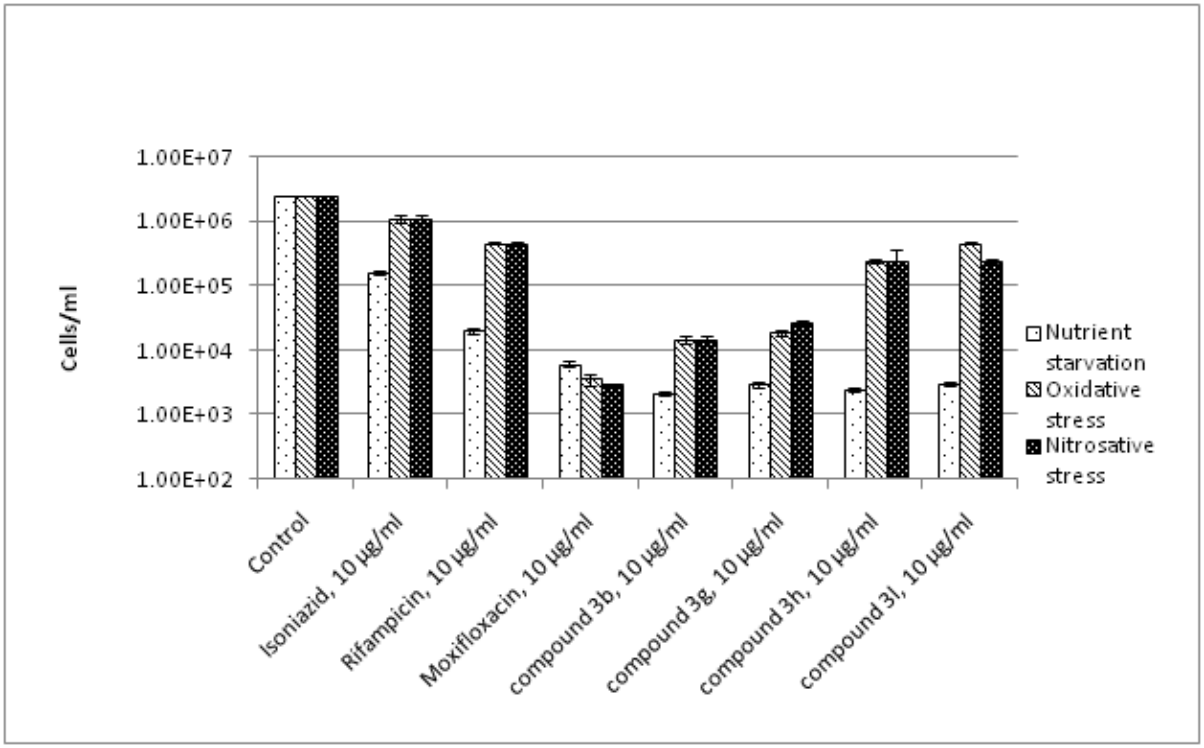

Figure 6.10: Bactericidal effect of **3b, 3g, 3h** and **3l** on dormant *M. tuberculosis* cells using nutrient starvation, oxidative stress and nitrosative stress models. Cells were treated with the compounds (10 µg/ml) for 7 days at 37°C. The viability of both treated and untreated cells was tested by MPN assay. The error bars represent standard deviation.

Table 6.3: Bacterial growth Log reduction values of active compounds with standard drugs

Drug	Nutrient starvation			Oxidative stress			Nitrosative stress		
	No. of bacteria	**SD***	**Log reduction values**	**No. of bacteria**	**SD***	**Log reduction values**	**No. of bacteria**	**SD***	**Log reduction values**
Control	2400000	0		2400000	0		2400000	0	
compound 3b, 10 µg/ml	2100	150	3.1	15000	2000	2.1	15000	1500	2.1
compound 3g, 10 µg/ml	3000	300	2.7	19000	2000	2	27000	1000	1.9
compound 3h, 10 µg/ml	2500	200	2.9	240000	10000	1	240000	120000	1
compound 3l, 10 µg/ml	3000	250	2.7	460000	15000	0.8	240000	10000	1
Isoniazid, 10 µg/ml	160000	15000	1.1	1100000	150000	0.2	1100000	150000	0.2
Rifampicin, 10 µg/ml	20000	1500	2	460000	15200	0.8	460000	14500	0.8
Moxifloxacin, 10 µg/ml	6100	700	2.6	3600	700	2.7	3000	100	2.9

*Standard Deviation

6.2.6. *In vitro* cytotoxicity screening

All the synthesized compounds were checked for their safety profile by using Human Embryonic Kidney cell line HEK 293 at 25µM. This test was carried out using MTT assay. Though, camptothecin is known to be cytotoxic, hydroxycamptothecin was found to be with non-cytotoxic which supports the selection of this compound for further derivatization. All the synthesized compounds showed very low inhibitory profile of 2.84 - 29.16% inhibition. The

most active compounds **3b, 3g, 3h** and **3l** had 6.96, 18.20, 23.01 and 16.52% inhibition respectively at 25µM drug concentrations. The results for cytotoxicity for all the compounds are given in Table 6.2. Substitution of camptothecin with various moieties at its 10^{th} position was found to result in reduced toxicity levels of the compound thereby resulting in drug-like compounds.

6.2.7. Anti-mycobacterial screening for most active compound using adult zebrafish

M.marinum when injected at higher bacterial counts into adult zebrafish always results in chronic granulomatous lesions. The pathology is logarithmically increased with increase in the bacterial count indicating dose dependency, making zebrafish model ideal to evaluate the virulence of various virulent bacterial species. Zebrafish acts as a natural host for *M.marinum* which is a commonly used laboratory animal for disease related studies. Adult zebrafish (*Daniorerio*) was infected with *M.marinum* and was assayed to estimate the infection recovery post-treatment. Granuloma-like lesions were observed on the dorsal side and around the fins as a sign of tuberculosis infection. The first line anti-tubercular agents, isoniazid (10mg/kg), rifampicin (5mg/kg) and ethambutol (10mg/kg) showed 1.8, 1.9 and 1.6 bacterial log reduction when compared to control whereas the second line anti-tubercular drug moxifloxacin (5mg/kg) showed 2.8 bacterial log reduction. The most active compound **3b** when administered at a dose of 5mg/kg body weight (10 mg/kg showed high mortality rate) showed a bacterial log reduction of 2.2 when compared to control (shown in Figure 6.11 and Table 6.4). The compound **3b** was found to be effectively inhibiting the pathogenesis when compared to that of isoniazid, rifampicin and ethambutol showing its potency towards mycobacteria. This study revealed the *in vivo* efficiency of the compound in addition to its *in vitro* tubercular inhibitory activity thereby suggesting its further optimization and development as an anti-tubercular agent.

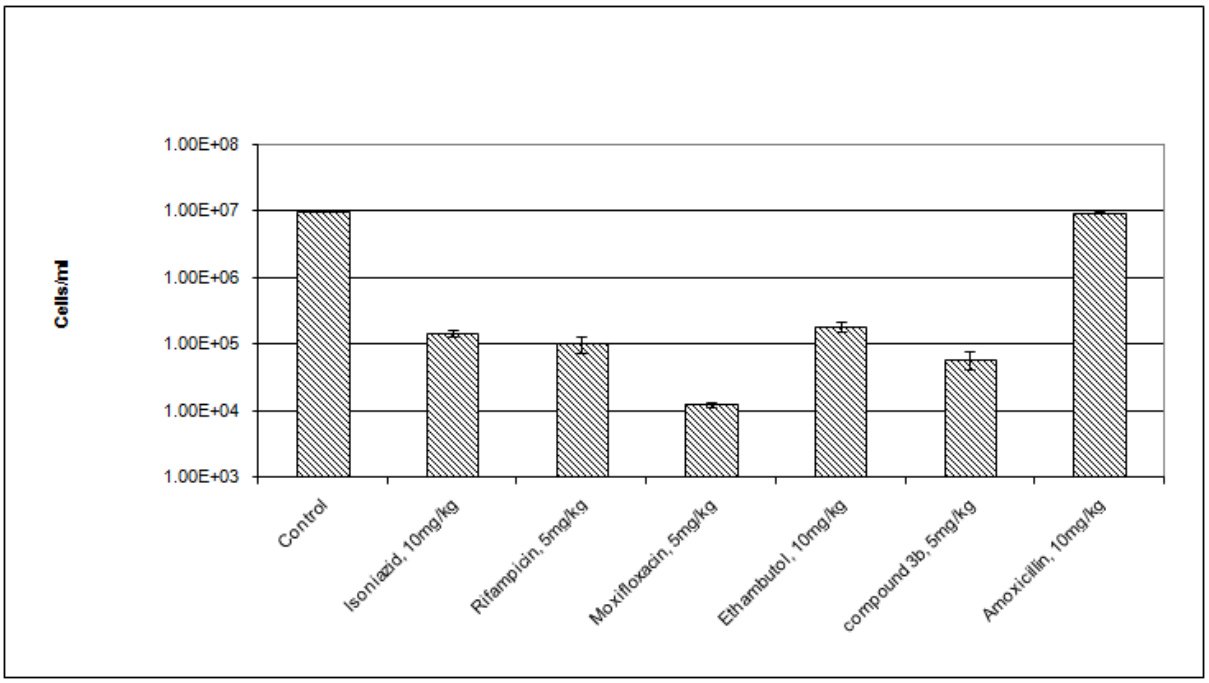

Figure 6.11: Bactericidal effect of **3b** on *M. marinum*. The drug is given at a dose of 5 mg/kg body weight for 7 days to *M. marinum* infected zebrafish. Bacterial count in both treated and untreated fish was determined using MPN assay. The error bars represents standard deviation.

Table 6.4: Bacterial growth Log reduction values of active compounds with standard drugs

Drug	No. of Bacteria	SD*	Log reduction values
Control	9600000	0	
Isoniazide, 10mg/kg	145000	15000	1.8
Rifampicin, 5mg/kg	102000	25000	1.9
Moxifloxacin, 5mg/kg	12600	1200	2.8
Ethambutol, 10mg/kg	184000	30000	1.6
compound **3b**, 5mg/kg	60000	1800	2.2
Amoxicillin, 10mg/kg	9400000	30000	-

*Standard Deviation

6.2.8. Differential scanning fluorimetry

Compound **3b** was further investigated for its binding affinity towards Mtb Topo I using differential scanning flourimetry. The native protein and protein-ligand complex, when subjected to an incremental increase in temperature from 25 ^{o}C to 95 ^{o}C, exhibited a T_m (melting temperature) of 36.5 ^{o}C and 38.7 ^{o}C respectively. A positive shift in T_m of about 2.2 ^{o}C was observed, as shown in Figure 6.12, indicating the increased stability of the protein over ligand binding. Thus, this biophysical characterization study revealed the efficient binding capacity of compound **3b** with topoisomerase I.

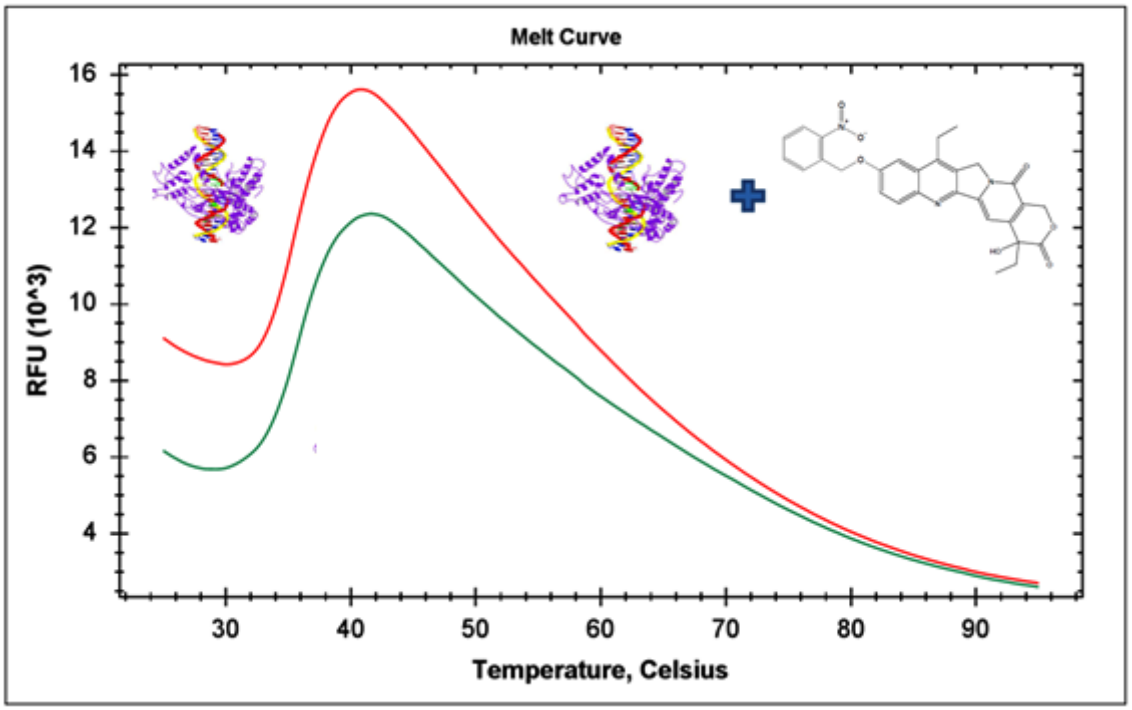

Figure 6.12: DSF experiment for compound **3b** complexed with Mtb Topo I (red) depicting a positive shift of 2.2 ^{o}C in T_m with reference to that of native Mtb Topo I protein (green).

6.2.9. ADME predictions for synthesized hydroxycamptothecin derivatives

Finally, 15 synthesized leads were analyzed for ADME prediction using QikProp module in Schrodinger. The predicted % human oral absorption and blood brain barrier for all the compounds were found to be good.

With regard to logP predictions all compounds were found to be in the acceptable range. HERG toxicity being crucial was predicted for all compounds and was expected to be below -5. All the compounds were found to be safe with no potential cardiotoxicity as predicted by the software.

The molecular weight of all these compounds except **3a** were high. This showed the violation from rule of five drug like property. The most active compound (**3b**) showed good predicted ADME properties. Further studies could be carried out for this compound to make this molecule a potent drug candidate. The ADME properties for the synthesized compounds are shown in Table 6.5.

Table 6.5: ADME predictions for the synthesized hydroxycamptothecin derivatives:

Compound ID	QPlogPo/w[a]	QPlogHERG[b]	QPPCaco[c]	QPlogBB[d]	% Human oral absorption[e]	Rule of 5[f]
Lead 1	2.39	-4.83	153.01	-1.48	80.02	0
3a	4.32	-6.74	533.78	-1.26	100	0
3b	3.68	-6.55	97.7	-2.18	71.13	1
3c	4.7	-6.6	533.32	-1.13	90.33	1
3d	4.48	-6.55	448.08	-1.24	87.65	1
3e	4.7	-6.43	461.83	-1.13	89.18	1
3f	4.94	-6.37	533.76	-0.98	91.73	1
3g	5.34	-6.22	532.65	-0.83	81.09	2
3h	5.05	-6.5	533.77	-1.01	79.39	2
3i	5.36	-6.4	537.11	-0.93	81.28	2
3j	5.13	-6.61	533.76	-1.05	79.85	2
3k	4.65	-6.54	533.78	-1.26	90.03	1
3l	4.4	-6.62	533.79	-1.35	88.54	1
3m	4.78	-6.62	533.77	-1.12	90.77	1
3n	4.83	-6.35	533.73	-1.19	91.1	1
3o	4.96	-6.66	533.33	-1.09	91.85	1

a.Predicted octanol/water partition coefficient logP (acceptable range: −2.0 to 6.5); b.Predicted IC50 value for blockage of HERG K+ channels.(below -5); c.Predicted apparent Caco-2 cell permeability in nm/sec (<25 poor; >500 great); d.Predicted brain/blood partition coefficient (-3.0 to 1.2);eh.Percent human oral absorption (<25% is poor and >80% is high); f.Rule of 5 violation (mol_MW < 500, QPlogPo/w < 5, donorHB ≤5, acceptHB ≤10)

6.3. Synthesis and biological assessment of Lead-II amsacarine derivatives

6.3.1. Lead optimization using medicinal chemistry

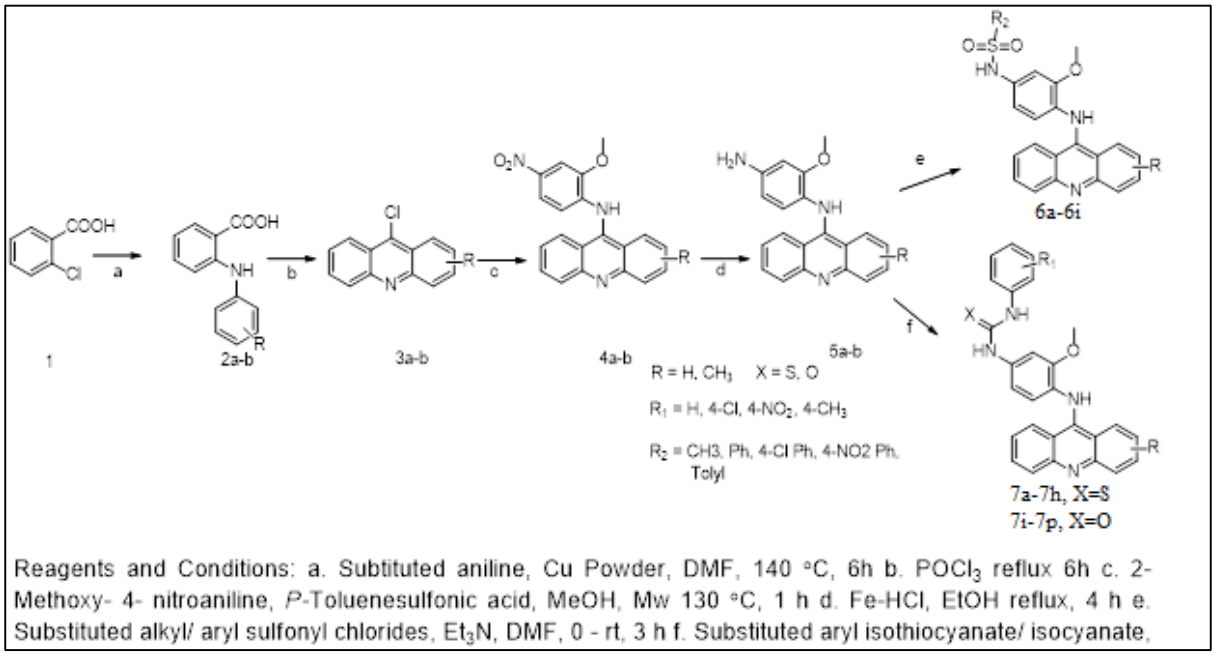

Figure 6.13: Synthetic protocol for Amsacrine derivatives (**6a-6i, 7a-7p**)

6.3.1.1. Preparation of substituted 2-(Phenylamino) benzoic acid derivatives (2a-b)

To a stirred solution of 2-chlorobenzoic acid (10g, 64 mmol) in DMF potassium carbonate (13.24g, 96 mmol) corresponding aniline (70.4 mmol) and copper powder was added and heated up to 140 °C for 6 h. Reaction progress was monitored by TLC after completion, reaction mass was filtered through celite, celite bed was washed with ethyl acetate. The combined organic layer was evaporated under reduced pressure obtained crude was purified by flash column chromatography using 5-20 % ethyl acetate: hexane as eluent in 100-200 mesh silica gel to get the corresponding phenylamino benzoic acid derivatives in good yield. The intermediates (**2a-b**) were confirmed by mass (ESI mode) and proceeded to next step.

6.3.1.2. Preparation of 9-Chloroacridine derivatives from substituted phenyl amino benzoic acid intermediates (**3a-b**)

The phenyl amino benzoic acid derivatives (47 mmol) (**2a-b**) were cyclised intramolecularly to 9-chloroacridine derivatives (**3a-b**) by refluxing them in 60 ml of $POCl_3$ for 4 h and the reaction was monitored by TLC. The excess POCl3 was removed by rota evaporator under reduced pressure. To this crushed ice was added and neutralised with saturated bicarbonate solution until pH reaches to ~7, the solid separated was filtered, dried and purified by flash column chromatography using 5-10% ethyl acetate: hexane as eluent in 60-120 mesh silica gel to get the corresponding 9-chloroacridine derivatives in good yield. These compounds were confirmed by mass and proceeded to next step.

6.3.1.3. Preparation of N-(2-Methoxy-4-nitrophenyl) acridin/2-methylacridine-9-amine intermediates (**4a-b**)

The 9-chloroacridine derivatives (10 mmol) (**3a-b**) were further reacted with 4-nitro *o*-anisidine (1.8g, 10.7 mmol) under microwave conditions in methanol using PTSA (Para-toluene sulphonic acid) as a catalyst (5-10 mg) at 130 °C for 1 h, reaction was monitored by TLC. After completion of reaction, methanol was evaporated under vacuum the crude was dissolved in ethyl acetate, washed with saturated bicarbonate solution. The organic layer was dried over anhydrous sodium sulphate and evaporated under vacuum obtained crude was further purified by flash column chromatography in 60-120 silica gel using 10-35% ethyl acetate: hexane as eluent to get an yellow solid.

6.3.1.4. Preparation of N^1-(Acridin/2-methylacridin-9-yl)-2-methoxybenzene-1,4-diamine intermediates (5a-b)

The corresponding nitro acridin derivatives (6 mmol) (**4a-b**) were converted to amine derivatives by reducing with Fe- HCl in ethanol by refluxing for 4 h. The crude reaction mixture diluted with ethyl acetate and filtered through celite bed, the organic layer was dried over sodium sulphate and concentrated under vacuo. The obtained crude was purified by flash column chromatography using ethyl acetate: hexane as eluent to get a brown solid in good yields.

6.3.1.5. Preparation of N-(3-Methoxy-4-((acridin/2-methylacridin-9-yl)amino)phenyl) methane/ substituted benzene sulfonamide derivatives (6a-6i)

For the preparation of sulphonamide derivatives corresponding acridin amine derivatives (0.6 mmol) (**5a-b**) were taken in 5 ml DMF (*N, N* dimethyl formamide) to this triethylamine (1.38 mmol) and corresponding substituted alkyl/ aryl sulphonyl chlorides (0.6 mmol) were added at 0 °C and allowed to stir at rt for 3 h. After completion of reaction crushed ice was added to the crude reaction mass the solid precipitated was filtered, dried and further purified by flash column chromatography using 5-10 % methanol: dichloromethane as eluent to fial sulphonamide derivatives in good yields.

6.3.1.6. Preparation of 1-(3-Methoxy-4-((acridin/2-methylacridin-9-yl)amino)phenyl)-3-phenylthiourea/ urea derivatives (7a-7p)

For preparation thiourea and urea derivatives corresponding acridin amine derivative (0.6 mmol), triethylamine (1.38 mmol) (Et_3N) and substituted phenyl isothiocyanate/isocyanate (0.6 mmol) were dissolved in ethanol and heated at 80 °C for 8 h. After completion of reaction

the solid precipitated was filtered, dried and recrystallized from ethanol to get the final corresponding thiourea and urea derivatives.

6.3.2. *In vitro* enzymatic assay of synthesized compounds

The Mtb Topo I assay was performed by gel based assays, with a range of inhibitor concentrations from 50 to 1.5 µM. The synthesized 24 compounds were screened at 50 µM, of which almost all the compounds showed more than 60% inhibition, except compounds **6f**, **7i**, **7j**, **7k** and **7l** showed lesser inhibitions. Further, all the compounds were screened at lower concentrations and their inhibitory concentrations (IC_{50}) were determined and given in Table 6.6. Of twenty four, compound **6b** and **6d** was found with better Mtb Topo I inhibitory profile followed by the other compounds. Finally, when tested at lower concentrations of 25 µM, 12.5 µM, 6.25 µM, 3.125 µM and 1.5 µM, compound **6b** and **6d** were emerged as the best compounds with an IC_{50} of 12.3 µM and 14.8 µM respectively.

Table 6.6: *In vitro* biological activity results for the synthesized amsacrine derivatives **6a-6i** and **7a-7p**

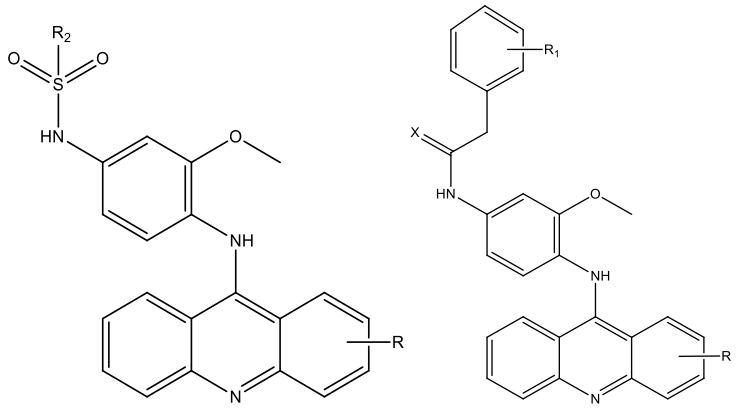

Compd.	R	R_1	R_2	X	IC_{50} in uM	MIC in uM[a]		Cytotoxicity (% inhibition)[b]
						H37Rv	XDR	
6a	H	-	CH3	-	25	8.6	17.2	48.56
6b	H	-	phenyl	-	14.8	1.56	1.56	2.84
6c	H	-	4-chloro phenyl	-	30.5	6.38	3.18	0.36
6d	H	-	4-nitro phenyl	-	12.3	0.86	0.86	11.82
6e	H	-	4-methyl phenyl	-	19.4	26.62	13.31	0.94
6f	CH3	-	phenyl	-	>50	13.31	13.31	11.24
6g	CH3	-	4-chloro phenyl	-	30.2	3.1	49.61	27.18
6h	CH3	-	4-nitro phenyl	-	34.1	48.59	48.59	21.85
6i	CH3	-	4-methyl phenyl	-	40.1	3.23	1.61	2.35
7a	H	H	-	S	23.3	55.49	111	1.09
7b	H	Cl	-	S	26.9	103.1	103.1	14.94
7c	H	NO_2	-	S	30.5	50.45	50.45	11.62
7d	H	CH_3	-	S	22.8	26.91	53.81	2.32
7e	CH_3	H	-	S	34.7	1.68	1.68	1.98
7f	CH_3	Cl	-	S	28.5	1.57	1.57	17.57
7g	CH_3	NO_2	-	S	32.8	0.77	1.53	17.33
7h	CH_3	CH_3	-	S	26.1	13.06	6.53	1.17
7i	H	H	-	O	>50	7.19	14.39	0.32
7j	H	Cl	-	O	45.6	13.33	13.33	21.57
7k	H	NO_2	-	O	48.3	52.14	52.14	23.28

7l	H	CH_3	-	O	>50	55.74	111.5	0.66
7m	CH_3	H	-	O	40.5	13.94	13.94	0.84
7n	CH_3	Cl	-	O	36.9	3.23	0.81	0.96
7o	CH_3	NO_2	-	O	31.2	3.16	6.33	13.85
7p	CH_3	CH_3	-	O	43.2	1.69	0.84	1.36
Isoniazid					nd	0.72	45.57	nd
Rifampicin					nd	0.15	30.37	nd
Ethambutol					nd	7.64	244.7	nd
Moxifloxacin					nd	2.16	34.59	nd

IC_{50} – 50% inhibitory concentration; MIC – minimum inhibitory concentration; Mtb – *Mycobacterium tuberculosis*; XDR – Extensively drug resistant; nd – not determined.

a. MIC of the compounds on H37Rv and XDR-TB.

b. IC_{50} of the compounds against Mtb Topo I.

c. Cytotoxicity of compounds at 25 µM on Human embryonic kidney (HEK) cell line.

6.3.3. SAR of amsacrine derivatives

The synthesized amsacrine derivatives were docked to the Mtb Topo 1 model developed so as to study their interaction pattern at the active site. For convenience, the compounds were divided into two series. From the interaction behavior of amsacrine (**6a**) at the active site, in the first series (**6b**-**6i**), the R_2 position was replaced by various aromatic moieties like phenyl, 4-chlore phenyl, 4-nitro phenyl and 4-methyl phenyl and hydrogen at R position is replaced by methyl group so as to increase the hydrophobic interactions with the adjacent residues. The compounds with hydrogen at R position (**6b**-**6e**) were found to be more active than compounds with methyl group at R position (**6f**-**6i**). Of all the compounds, compound **6d** with 4-nitro phenyl substitution at R_2 position and hydrogen at R position was found to be highly active with an IC_{50} of 12.3 µM and MIC of 0.86 µM. The compound exhibited five polar contacts with active site residues Asp111, Glu115, Arg168, Arg195, and Ser495 as shown in Figure 6.14 and emerged to be with best docking score of -4.78. The interaction profile of compound **6d** shows the polar contact of the oxygen atom of sulphonyl group with Arg168 and the oxygen group of nitro group involved in polar contact with Arg195 making the compound most potent.

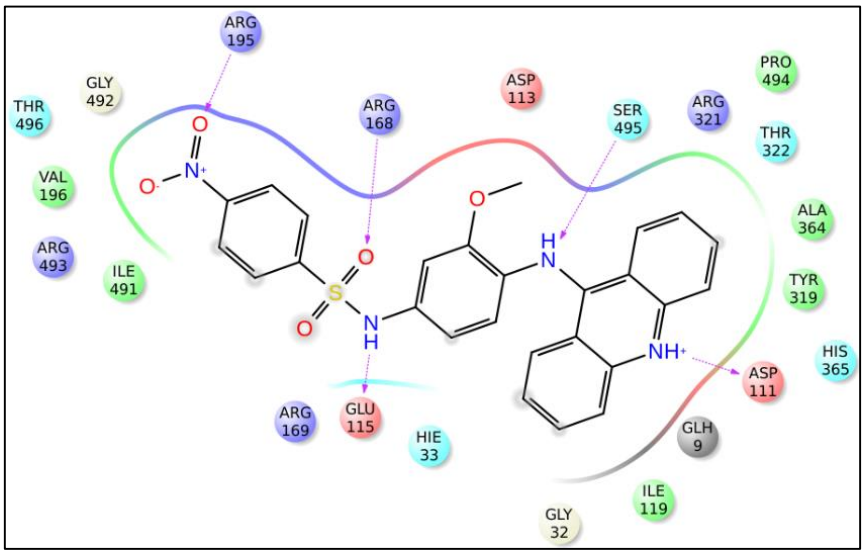

Figure 6.14: Ligand interaction diagram of most active compound **6d**.

Compounds **6b** and **6e** were also found to be active *in vitro* next to compound **6d**. Of this, compound 6b, with phenyl substitution was found to be next most active compound with IC_{50} 14.8 µM. In both compounds 6b and 6e, the strong non-polar interactions of phenyl ring with Arg493 made the moiety stable (Figure 6.15).

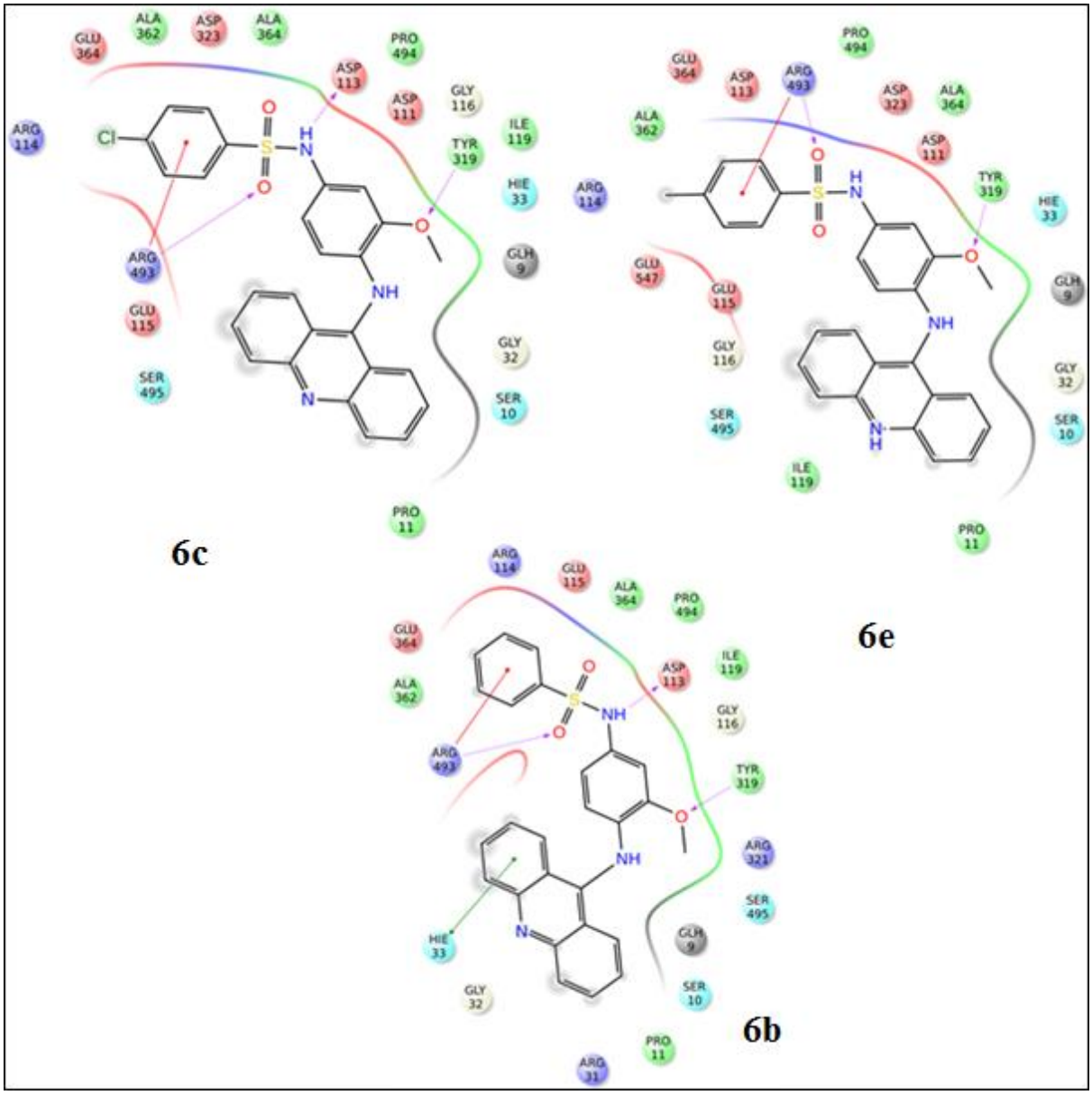

Figure 6.15: Ligand interaction diagram of compounds **6b**, **6c** and **6e**.

In the second series (**7a-7p**), the R_1 position is substituted with chloro, nitro and methyl substitution and the sulphonamide group is replaced with substituted ureas and thioureas. In this series, only one compound (7d) was found to more potent than Lead compound amsacrine. The ligand interaction picture of the compound 7d (Figure 6.16) shows the strong non-polar interactions of phenyl ring with Arg493 and the polar contacts of nitrogen and oxygen (of methoxy group) with active site residues, Asp113 and Tyr319 making the compound potent.

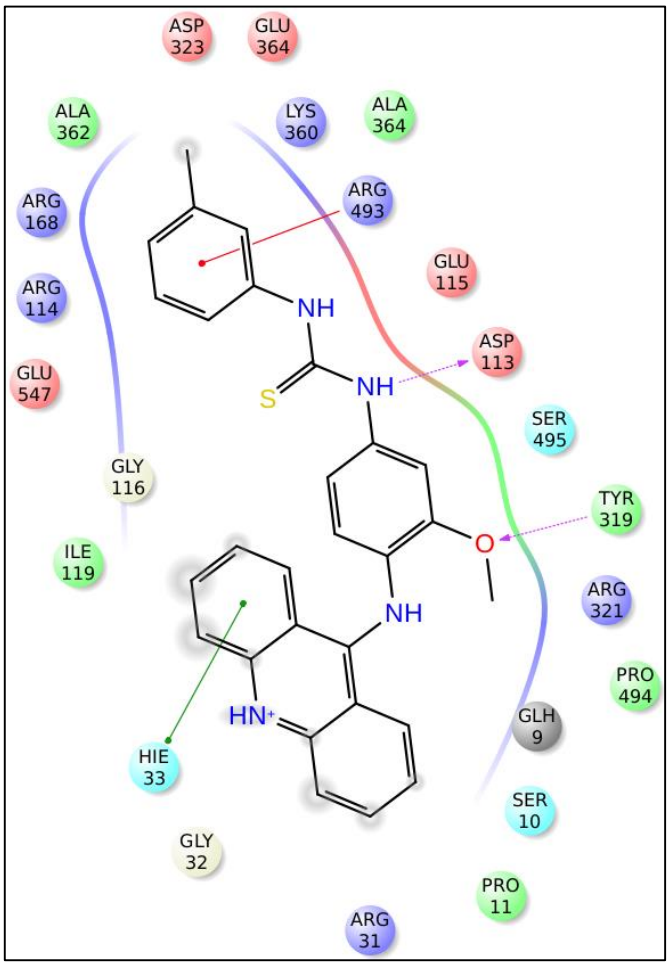

Figure 6.16: Ligand interaction diagram of compound **7d**.

6.3.4. *In vitro* active Mtb assay

All the synthesized drugs were treated with Mtb H37Rv and XDR strain to determine their anti-tubercular activity using microplate alamar blue assay (MABA) with drug concentrations ranging from 50 µg/ml to 0.78 µg/ml in duplicates. The MIC values of the synthesized compounds along with the standard drugs are given in Table 6.6. The synthesized compounds exhibited active Mtb MIC ranging from 0.77 to 103.1 µM and XDR-TB MIC ranging from 0.81 to 111.49 µM. Six compounds **6b, 6d, 7e, 7f, 7g** and **7p** were found with increased potency when compared to Moxifloxacin (MIC – 2.16µM), 12 compounds were found to be more active

than Ethambutol (MIC – 7.2 µM) and lead compound amsacrine (MIC- 8.6 µM). On XDR strain, almost all the synthesized compounds were more potent than the standard drug.

6.3.5. *In vitro* dormant Mtb assay

Dormancy was obtained by nutrient starvation, oxidative stress and nitrosative stress models. The nutrient starvation assay of the dormant cultures was carried out with standard drugs like isoniazid, rifampicin and moxifloxacin along with synthesized drugs for 7 days at a concentration of 10 µg/ml. The bacterial log reductions for various standard and synthesized drugs are as depicted in Figure 6.17 and Table 6.7. Out of 24 compounds, top 10 active compounds i.e., **6b, 6d, 6e, 6i, 7d, 7f, 7g, 7n, 7o** and **7p** were screened. Compounds **6b** and **6d** were found to be more potent than moxifloxacin in nutrient starvation model with bacterial log reduction 2.9 to 3.0. Compound **6d** has exhibited most promising activity with ~3.0 bacterial log reduction and also inhibited Mtb Topo I with an IC_{50} of 12.3µM. In oxidative and nitrosative stress models, MABA assay was performed and MIC was calculated using the dormant cultures. The synthesized compounds exhibited MIC ranging from 0.77 to 111.49 µM in oxidative stress model and MIC ranging from 0.77 to 115.09 µM in nitrosative stress model (Table 6.8). Seven compounds were found to be most active than standard compound Moxifloxacin (MIC-3.88 µM) in both Oxidative and nitrosative stress. Fourteen compounds were found to be more active than standard compound Rifampicin (MIC- 60.75 µM). Almost all the synthesized compounds were active than Isoniazid and Ethambutol. The most active compound **6d** was found to be more potent than all the standard compounds with MIC of 0.78 µM and 0.86 µM in oxidative and nitrosative stress models respectively.

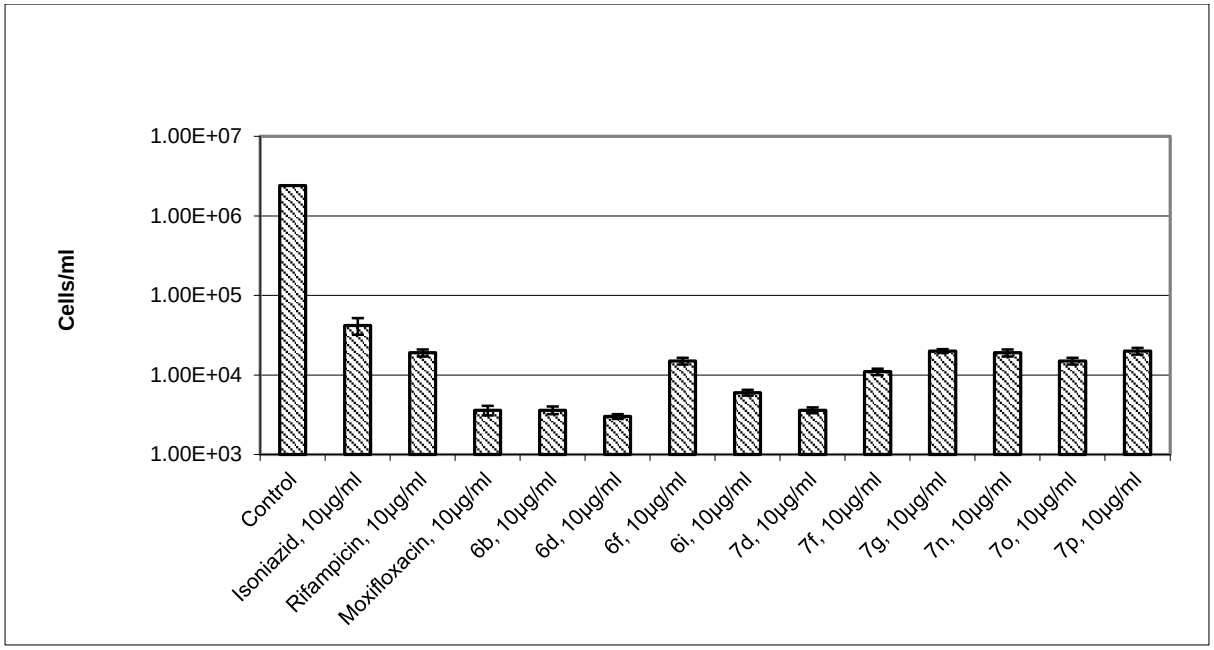

Figure 6.17: Bactericidal effect top 10 active compounds on dormant *M. tuberculosis* cells using nutrient starvation. Cells were treated with the compounds (10 µg/ml) for 7 days at 37°C. The viability of both treated and untreated cells was tested by MPN assay. The error bars represent standard deviation.

Table 6.7: Bacterial growth Log reduction values of active compounds with standard drugs

Compound	No. of Bacteria	SD*	Log reduction values
	2400000	0	
Isoniazid	42000	10000	1.7
Rifampicin	19000	1900	2
Moxifloxacin	3600	500	2.9
6b	3600	400	2.9
6d	3000	200	3
6f	15000	1500	2.1
6i	6000	500	2.6
7d	3600	300	2.9
7f	11000	1000	2.3
7g	20000	1200	2
7n	19000	1900	2
7o	15000	1500	2.1
7p	20000	2000	2

* Standard Deviation

Table 6.8: Dormant tb screening using oxidative and nitrosative stress models of synthesised amsacrine derivatives.

Compd.	R	R1	R2	X	MIC in uM on Dormant TB	
					Oxidative stress	Nitrosative stress
6a	H	-	CH3	-		
6b	H	-	phenyl	-	1.72	3.12
6c	H	-	4-chloro phenyl	-	6.38	12.76
6d	H	-	4-nitro phenyl	-	0.78	0.86
6e	H	-	4-methyl phenyl	-	106.49	106.49
6f	CH3	-	phenyl	-	53.24	106.49
6g	CH3	-	4-chloro phenyl	-	1.55	3.1
6h	CH3	-	4-nitro phenyl	-	97.18	97.18
6i	CH3	-	4-methyl phenyl	-	12.88	0.81
7a	H	H	-	S	110.98	110.98
7b	H	Cl	-	S	103.1	103.1
7c	H	NO_2	-	S	100.9	100.9
7d	H	CH_3	-	S	3.36	1.68
7e	CH_3	H	-	S	107.63	107.63
7f	CH_3	Cl	-	S	12.55	12.55
7g	CH_3	NO_2	-	S	0.77	0.77
7h	CH_3	CH_3	-	S	104.48	52.24
7i	H	H	-	O	57.54	115.09
7j	H	Cl	-	O	53.32	26.66
7k	H	NO_2	-	O	104.28	104.28
7l	H	CH_3	-	O	111.49	111.49
7m	CH_3	H	-	O	6.97	6.97
7n	CH_3	Cl	-	O	1.62	0.81
7o	CH_3	NO_2	-	O	3.16	1.58
7p	CH_3	CH_3	-	O	1.69	0.84
Isoniazid	-	-	-	-	182.22	182.22
Rifampicin	-	-	-	-	60.75	60.75
Ethambutol	-	-	-	-	244.72	244.72
Moxifloxacin	-	-	-	-	3.88	3.88

6.3.6. *In vitro* cytotoxicity screening

All the synthesized compounds were checked for their safety profile by using Human Embryonic Kidney cell line HEK 293 at 25µM. This test was carried out using MTT assay. Lead compound amsacrine had 48.56% inhibition (Table 6.6). All the synthesized compounds showed very low inhibitory profile of 0.36 – 27.18% inhibition. The most active compounds **6d** had 11.82% inhibition at 25µM drug concentrations. The results for cytotoxicity for all the compounds are given in table 6.6. Substitution of amsacrine with various moieties was found to result in reduced toxicity levels of the compound thereby resulting in drug-like compounds.

6.3.7. Anti-mycobacterial screening for most active compound using adult zebrafish

The first line anti-tubercular agents, isoniazid (10mg/kg), rifampicin (5mg/kg) and ethambutol (10mg/kg) showed 1.8, 1.9 and 1.6 bacterial log reduction when compared to control whereas the second line anti-tubercular drug moxifloxacin (5mg/kg) showed 2.8 bacterial log reduction. The most active compounds, **6b and 6d** when administered at a dose of 5mg/kg body weight showed a bacterial log reduction ranging from 2.8 to 3.1 when compared to control (shown in Figure 6.18 and Table 6.9). The compound **6d** was found to be most potent with bacterial log reduction of ~3.1 and was effectively inhibiting the pathogenesis when compared to that of isoniazid, rifampicin, moxifloxacin and ethambutol showing its potency towards mycobacteria. This study revealed the *in vivo* efficiency of the compound in addition to its *in vitro* tubercular inhibitory activity thereby suggesting its further optimization and development as an anti-tubercular agent.

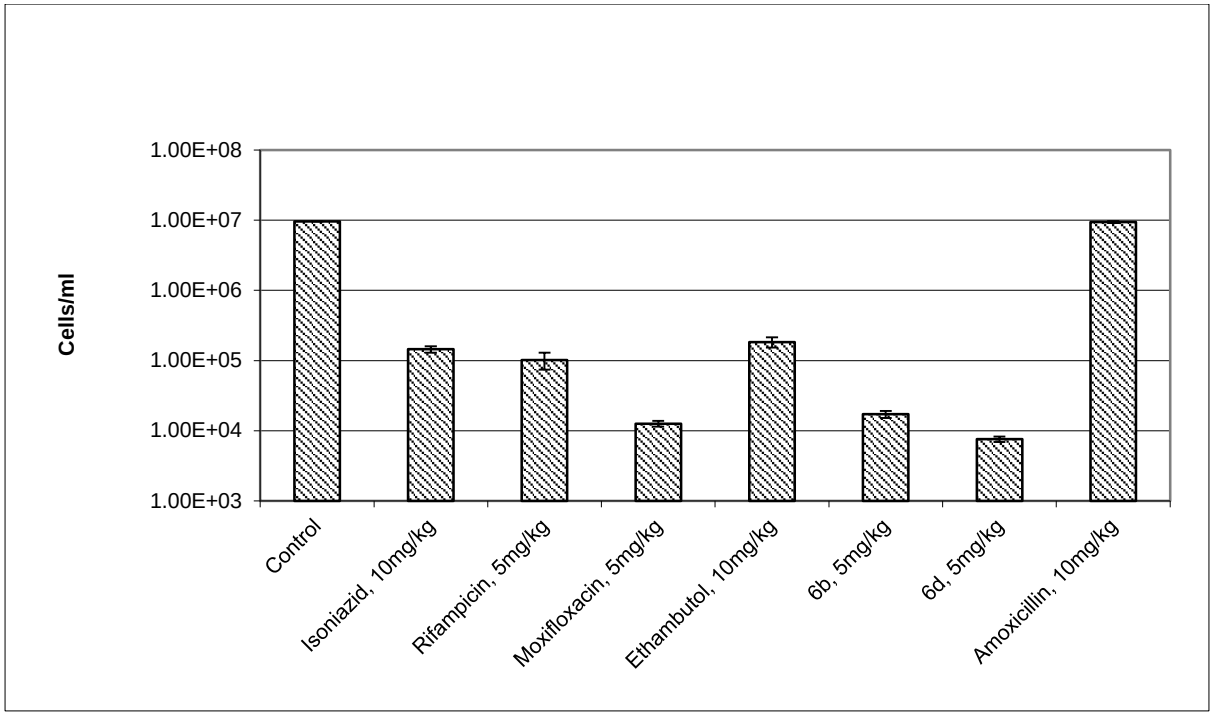

Figure 6.18: Bactericidal effect of compounds **6b** and **6d** on *M. marinum*. The drug is given at a dose of 5 mg/kg body weight for 7 days to *M. marinum* infected zebrafish. Bacterial count in both treated and untreated fish was determined using MPN assay. The error bars represents standard deviation.

Table 6.9: Bacterial growth Log reduction values of active compounds with standard drugs

Drug	No. of Bacteria	SD*	Log reduction Values
Control	9600000	0	
Isoniazid, 10mg/kg	145000	15000	1.8
Rifampicin, 5mg/kg	102000	25000	1.9
Moxifloxacin, 5mg/kg	12600	1200	2.8
Ethambutol, 10mg/kg	184000	30000	1.6
6b, 5mg/kg	12150	2000	2.8
6d, 5mg/kg	7566	700	3.1
Amoxicillin, 10mg/kg	9400000	30000	-

* Standard Deviation

6.3.8. ADME predictions for synthesized Amsacrine derivatives

ADME prediction was done using QikProp module in Schrodinger for 24 synthesized compounds. The predicted % human oral absorption and blood brain barrier for all the compounds were found to be good. With regard to logP predictions all compounds except **7b to 7f** were found to be in the acceptable range. HERG toxicity being crucial was predicted for all compounds and was expected to be below -5. All the compounds were found to be safe with no potential cardiotoxicity as predicted by the software.

The molecular weight of all these compounds except **6g and 6h** were in acceptable range. The violation from rule of five drug like property was mainly due to high molecular weight and logP values. The most active compound (**6d**) showed good predicted ADME properties. Further studies could be carried out for this compound to make this molecule a potent drug candidate. The ADME properties for the synthesized compounds are shown in Table 6.10.

Table 6.10: ADME predictions for the synthesized Amsacrine derivatives.

Compound ID	QPlogPo/w[a]	QPlogHERG[b]	QPPCaco[c]	QPlogBB[d]	% Human oral absorption[e]	Rule of 5[f]
6a	3.42	-6.51	701.99	-0.98	100	0
6b	4.74	-7.67	865.92	-1.01	100	0
6c	5.21	-7.55	930.88	-0.82	100	1
6d	3.75	-6.38	168.19	-1.66	75.76	1
6e	5.03	-7.58	931.78	-1	96.58	1
6f	5.02	-7.58	930.89	-1	96.52	1
6g	5.51	-7.47	929.64	-0.85	86.41	2
6h	4.32	-7.49	111.26	-2.22	75.91	1
6i	5.33	-7.49	930.57	-1.04	100	1
7a	6.23	-8.13	3074.28	-0.22	100	1
7b	6.72	-8.01	3081.73	-0.05	100	1
7c	5.54	-8	367.67	-1.42	92.36	1
7d	6.54	-8	3081.82	-0.23	100	1
7e	6.54	-8.04	3062.87	-0.24	100	1
7f	7.04	-7.96	3069.98	-0.07	100	1
7g	5.86	-7.94	367.09	-1.48	81.23	2
7h	6.86	-7.95	3078.56	-0.25	100	1
7i	5.23	-6.9	1088.47	-0.71	100	1
7j	5.94	-7.18	1088.38	-0.6	100	1
7k	4.56	-6.79	130.06	-1.95	91.46	0
7l	5.76	-7.18	1088.25	-0.78	100	1
7m	5.55	-6.85	1087.13	-0.75	100	1
7n	6.05	-6.74	1086.93	-0.59	100	1
7o	4.88	-6.74	129.89	-2.02	93.32	0
7p	5.87	-6.73	1084.81	-0.77	100	1

[a]Predicted octanol/water partition coefficient logP (acceptable range: −2.0 to 6.5); [b]Predicted IC_{50} value for blockage of HERG K+ channels.(below -5); [c]Predicted apparent Caco-2 cell permeability in nm/sec (<25 poor; >500 great); [d]Predicted brain/blood partition coefficient (-3.0 to 1.2); [e]Percent human oral absorption (<25% is poor and >80% is high); [f]Rule of 5 violation (mol_MW < 500, QPlogPo/w < 5, donorHB ≤5, accptHB ≤10)

6.4. Synthesis and biological assessment of Lead-III tryptanthrin derivatives

6.4.1. Lead optimization using Medicinal chemistry

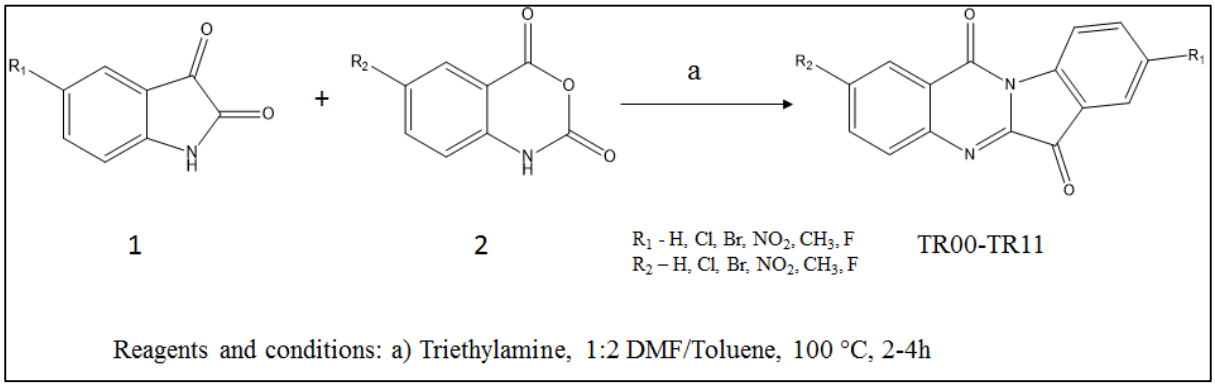

Figure 6.19: Synthetic protocol for Tryptanthrin derivatives (**TR00-TR13**).

The most efficient method for the synthesis of tryptanthrin and many of its analogues is the reaction of isatoic anhydride with isatin. Isatoic anhydride and isatin were taken in 1:2 ratio and heated at 100 °C in the presence of solvent 1:2 DMF/Toluene and trimethylamine for 2-4 hr. The reaction mixture was filtered and the filtrate was concentrated to get crude compound. Crude compound was triturated by using diisopropylether and dried to afford compound **TR00-TR13**. Synthetic protocol for the same is shown in Figure 6.19.

6.4.2. *In vitro* enzymatic assay of synthesized compounds

Thirteen derivatives synthesized were screened for their activity on Mtb Topo I using the gel based assay with concentrations ranging from 50 µM to 1.5 µM. Initially, all the compounds were screened at 50 µM, out of which 6 compounds showed more than 60% inhibition at 50 µM. These six compounds were subjected to further screening at lower concentrations. 4 compounds were found to be more potent than Lead compound Tryptanthrin, and compounds TR07 and TR11 were emerged to be most active compounds with IC_{50} 20.2 and 21.6 µM respectively. IC_{50} values for all the compounds were given in the Table 6.11.

Table 6.11: *In vitro* biological activity results for the synthesized tryptanthrin derivatives **TR00-TR13.**

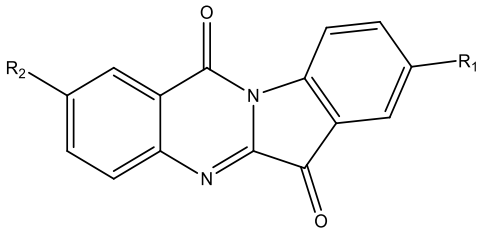

Compd.	R_1	R_2	IC_{50}	MIC in uM		Cytotoxicity (% inh) in uM
				MtbH37Rv	XDR	
TR00	H	H	42.3	1.57	1.57	57.83
TR01	H	Cl	>50	5.52	5.52	37.46
TR02	H	Br	>50	4.77	9.55	32.05
TR03	NO2	H	>50	21.31	42.63	34.76
TR04	F	H	>50	5.86	11.75	36.5
TR05	F	Cl	59.6	20.78	41.57	35.37
TR06	F	Br	>50	1.13	1.13	19.44
TR07	Cl	H	20.2	2.76	1.38	7.06
TR08	Cl	Cl	48.5	9.85	9.85	27.26
TR09	Cl	Br	41.5	34.57	17.29	31.99
TR10	Br	H	>50	76.42	152.84	9.67
TR11	Br	Cl	21.6	1.08	1.08	8.8
TR12	Br	Br	35.8	0.96	1.92	15.18
TR13	CH3	H	>50	11.93	47.71	29.89
Isoniazid	-	-	nd	0.72	45.57	nd
Rifampicin	-	-	nd	0.15	30.37	nd
Ethambutol	-	-	nd	7.64	244.7	nd
Moxifloxacin	-	-	nd	2.16	34.59	nd

IC_{50} – 50% inhibitory concentration; MIC – minimum inhibitory concentration;

Mtb – *Mycobacterium tuberculosis*; XDR – Extensively drug resistant; nd – not determined.

a. MIC of the compounds on H37Rv and XDR TB.

b. IC_{50} of the compounds against Mtb Topo I.

c. Cytotoxicity of compounds at 25 µM on Human embryonic kidney (HEK) cell line.

6.4.3. SAR of Tryptanthrin derivatives

The synthesized tryptanthrin derivatives were docked to the Mtb topo 1 model developed so as to study their interaction pattern at the active site. Thirteen derivatives were synthesized by substituting the R_1 and R_2 positions with Floro, Chloro, Bromo, Methyl and Nitro groups. Of all, compound **TR07 and TR11** were found to be highly active with an IC_{50} of 20.2 and 21.6 µM respectively. The compounds exhibited Mtb MIC of 2.6 and 1.08µM respectively. Compound TR07 and TR11 exhibited polar contact with active site residue Arg321 and strong non-polar interaction was seen with Lys502 (Figure 6.20 and 6.21**)**.

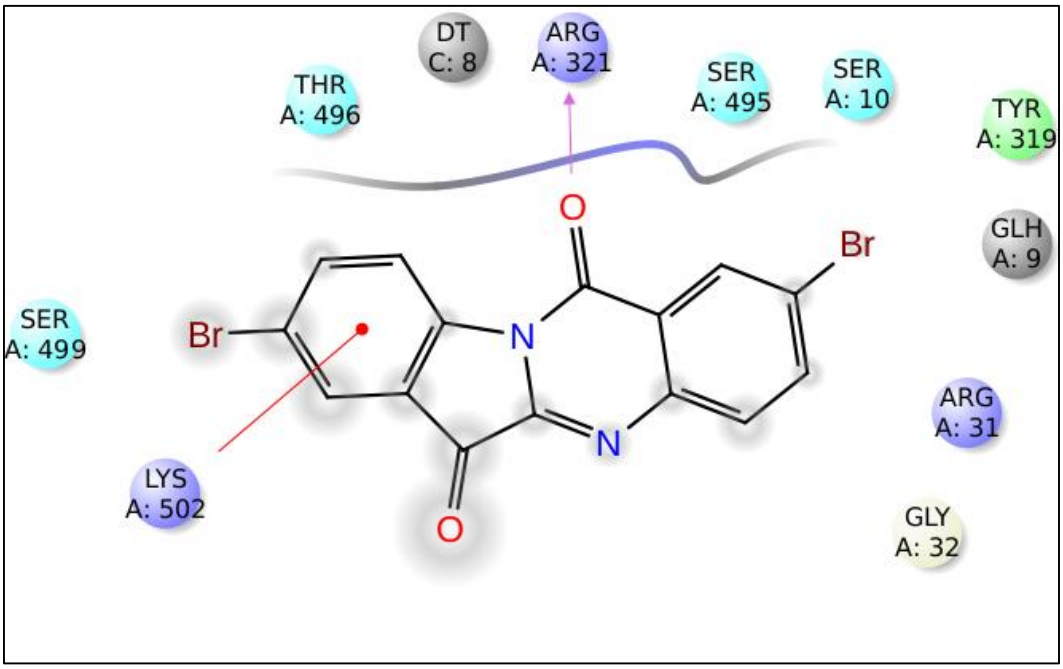

Figure 6.20: Ligand interaction diagram of compound **TR07**.

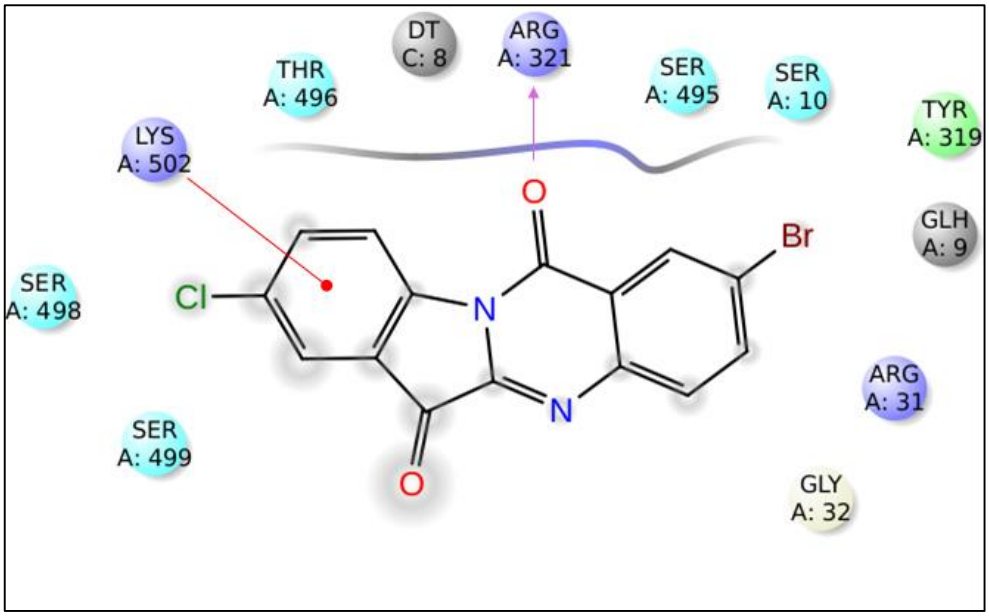

Figure 6.21: Ligand interaction diagram of compound **TR11**.

6.4.4. *In vitro* active Mtb assay

Thirteen synthesized drugs along with the Lead Tryptanthrin were treated with Mtb H37Rv and XDR strain to determine their anti-tubercular activity using microplate alamar blue assay (MABA) with drug concentrations ranging from 50 µg/ml to 0.78 µg/ml in duplicates. The MIC values of the synthesized compounds along with the standard drugs are given in Table 6.11. The synthesized compounds exhibited active Mtb MIC ranging from 0.96 to 76.42 µM and XDR-TB MIC ranging from 1.08 to 152.84 µM. Three compounds **TR07, TR11 and TR12** were found with increased potency when compared to Moxifloxacin (MIC – 2.16µM), 8 compounds were found to be more active than Ethambutol (MIC – 7.2 µM) and lead compound amsacrine (MIC- 8.6 µM). On XDR strain, almost all the synthesized compounds were more potent than the standard drug.

6.4.5. *In vitro* dormant Mtb assay

Dormancy was obtained by nutrient starvation, oxidative stress and nitrosative stress models. In Nutrient starvation model, top 3 active compounds along with the lead compound were

screened on the dormant bacilli by MPN assay method and the bacterial log reductions for various standard and synthesized drugs were depicted in Figure 6.22 and Table 6.12. All the 4 active compounds **TR00, TR07, TR11 and TR12** were screened and found to be more potent than standard compounds isoniazid and Rifampicin in nutrient starvation model with bacterial log reduction ranging from ~2.1 to 2.9. Compound **TR11** has exhibited most promising activity with ~2.9 bacterial log reduction and also inhibited Mtb topoisomerase I with an IC_{50} of 21.6 µM. In oxidative and nitrosative stress models, the above 3 active compounds TR07, TR11 and TR12 were found to be potent than the standard compounds including Moxifloxacin out of which TR11 was found to be more active with MIC of 1.08 µM in both oxidative stress and nitrosative stress models (Table 6.13).

Table 6.12: Bacterial growth Log reduction values of active compounds with standard drugs

Drug	No. of Bacteria	SD*	Log reduction values
Control	2400000	0	
TR00	6000	400	2.6
TR07	15000	300	2.1
TR11	3000	500	2.9
TR12	15000	1500	2.1
Isoniazid	42000	10000	1.7
Rifampicin	19000	1900	2
Moxifloxacin	3000	500	2.9

*Standard deviation

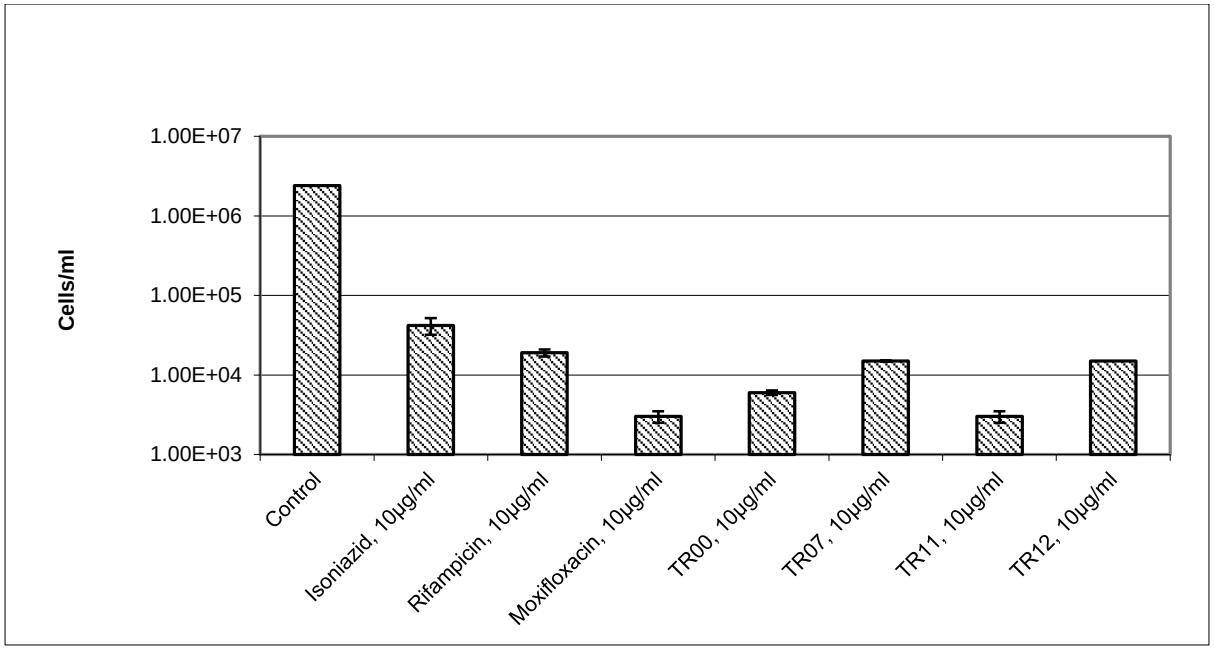

Figure 6.22: Bactericidal effect of **TR00, TR07, TR11 and TR12** on dormant *M. tuberculosis* cells using nutrient starvation. Cells were treated with the compounds (10 µg/ml) for 7 days at 37°C. The viability of both treated and untreated cells was tested by MPN assay. The error bars represent standard deviation.

Table 6.13: Dormant tb screening using oxidative and nitrosative stress models of synthesised amsacrine derivatives.

Compd.	R1	R2	MIC in uM on Dormant TB	
			Oxidative stress	Nitrosative stress
TR00	H	H	50.36	1.57
TR01	H	Cl	22.11	22.11
TR02	H	Br	38.21	76.42
TR03	NO2	H	2.66	2.66
TR04	F	H	2.93	2.93
TR05	F	Cl	41.57	41.57
TR06	F	Br	18.11	9.05
TR07	Cl	H	2.76	2.76
TR08	Cl	Cl	39.42	157.67
TR09	Cl	Br	138.29	138.29
TR10	Br	H	38.21	1.19
TR11	Br	Cl	1.08	1.08
TR12	Br	Br	2.98	2.98
TR13	CH3	H	30.79	30.79
Isoniazid	-	-	182.22	182.22
Rifampicin	-	-	60.75	60.75
Ethambutol	-	-	244.72	244.72
Moxifloxacin	-	-	3.88	3.88

6.4.6. *In vitro* cytotoxicity screening

All the synthesized compounds were checked for their safety profile by using Human Embryonic Kidney cell line HEK 293 at 25µM. Lead compound Tryptanthrin (TR00) showed an inhibitory percentage of 57.83%. All the synthesized compounds showed very low inhibitory profile of 7.06 – 37.46% inhibition (Table 6.11). The most active compounds **TR07, TR11** and **TR12** had 7.06, 8.8 and 15.18% inhibition respectively at 25µM drug concentrations. The results for cytotoxicity for all the compounds are given in table 6.10. Substitution of tryptanthrin with various moieties at its 2^{nd} and 8^{th} position was found to result in reduced toxicity levels of the compound thereby resulting in drug-like compounds.

6.4.7. Anti-mycobacterial screening for most active compound using adult zebrafish

The first line anti-tubercular agents, isoniazid (10mg/kg), rifampicin (5mg/kg) and ethambutol (10mg/kg) showed 1.8, 1.9 and 1.6 bacterial log reduction when compared to control whereas the second line anti-tubercular drug moxifloxacin (5mg/kg) showed 2.8 bacterial log reduction. The most active compounds, **TR00 and TR11** when administered at a dose of 5mg/kgbody weight showed a bacterial log reduction of 2.6 and 3.0 when compared to control (shown in Figure 6.23 and Table 6.14). The compound **TR11** was found to be effectively inhibiting the pathogenesis when compared to that of standard compound Moxifloxacin showing its potency towards mycobacteria. This study revealed the *in vivo* efficiency of the compound in addition to its *in vitro* tubercular inhibitory activity thereby suggesting its further optimization and development as an anti-tubercular agent.

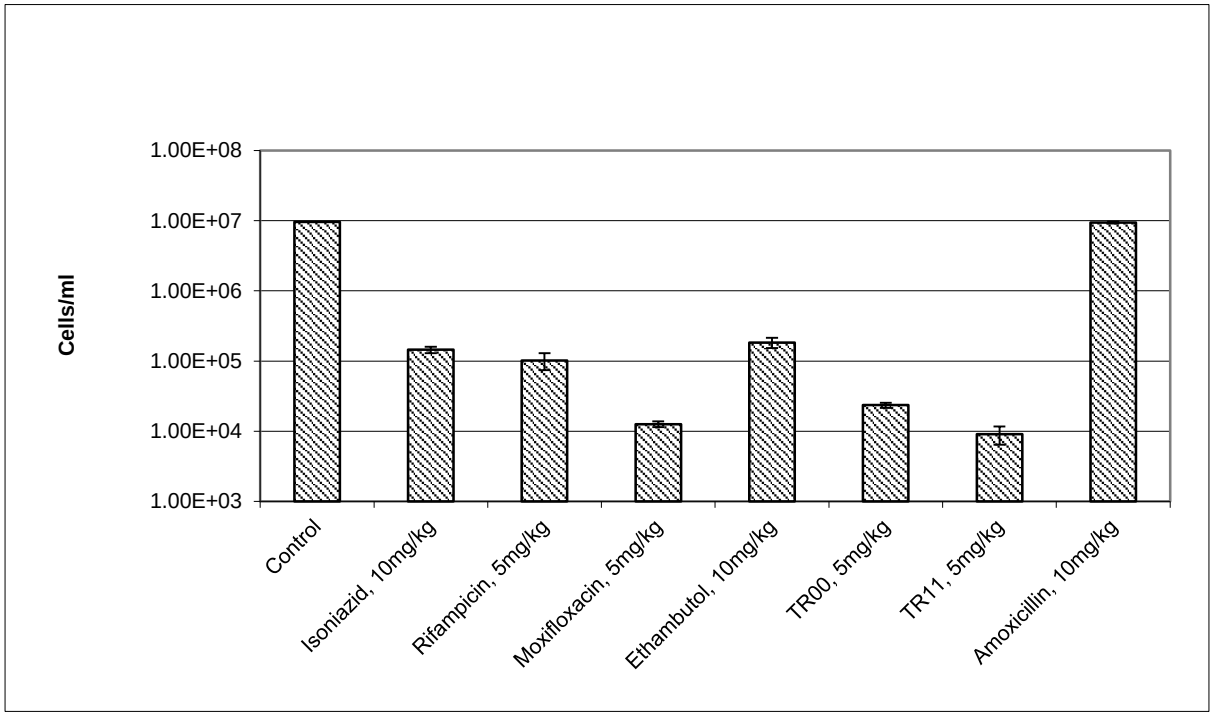

Figure 6.23: Bactericidal effect of **TR00** and **TR11** on *M. marinum*. The drug is given at a dose of 5 mg/kg body weight for 7 days to *M. marinum* infected zebrafish. Bacterial count in both treated and untreated fish was determined using MPN assay. The error bars represents standard deviation.

Table 6.14: Bacterial growth Log reduction values of active compounds with standard drugs

Drug	No. of Bacteria	SD*	Log reduction values
Control	9600000	0	
Isoniazid, 10mg/kg	145000	15000	1.8
Rifampicin, 5mg/kg	102000	25000	1.9
Moxifloxacin, 5mg/kg	12600	1200	2.8
Ethambutol, 10mg/kg	184000	30000	1.6
TR00, 5mg/kg	23500	2500	2.6
TR11, 5mg/kg	9000	2000	3
Amoxicillin, 10mg/kg	9400000	30000	-

*Standard Deviation

6.4.8. ADME predictions for synthesised tryptanthrin derivatives

ADME prediction was done using QikProp module in Schrodinger for 24 synthesized compounds. The predicted % human oral absorption and blood brain barrier for all the compounds were found to be good. With regard to logP predictions all compounds were found to be in the acceptable range. HERG toxicity being crucial was predicted for all compounds and was expected to be below -5. All the compounds except **TR02, TR08** and **TR09** were found to be safe with no potential cardiotoxicity as predicted by the software.

The molecular weight of all these compounds were in acceptable range. All the compounds were following Lipinski Rule of 5. The most active compound (**TR11**) showed good predicted ADME properties. Further studies could be carried out for this compound to make this molecule a potent drug candidate. The ADME properties for the synthesized compounds are shown in Table 6.15.

Table 6.15: ADME predictions for the synthesized Tryptanthrin derivatives.

Compound ID	QPlogPo/w[a]	QPlogHERG[b]	QPPCaco[c]	QPlogBB[d]	% Human oral absorption[e]	Rule of 5[f]
TR 00	1.01	-5.09	763.96	-0.44	84.44	0
TR 01	1.51	-5.06	764.1	-0.3	87.4	0
TR 02	1.25	-4.99	763.98	-0.34	85.84	0
TR 03	1.59	-5.1	764.05	-0.29	87.86	0
TR 04	1.33	-5.07	764.18	-0.48	86.34	0
TR 05	0.25	-5.08	91.17	-1.41	63.47	0
TR 06	2.02	-5.02	764.18	-0.15	90.36	0
TR 07	2.18	-5.09	764.08	-0.13	91.28	0
TR 08	1.83	-4.99	764.01	-0.18	89.26	0
TR 09	1.75	-4.95	764.06	-0.19	88.8	0
TR 10	2.1	-5.05	764.13	-0.14	90.82	0
TR 11	2.1	-5.05	764.13	-0.14	90.82	0
TR 12	1.59	-5.1	763.99	-0.29	87.86	0
TR 13	1.51	-5.06	764.04	-0.3	87.4	0

[a]Predicted octanol/water partition coefficient logP (acceptable range: −2.0 to 6.5); [b]Predicted IC_{50} value for blockage of HERG K+ channels.(below -5); [c]Predicted apparent Caco-2 cell permeability in nm/sec (<25 poor; >500 great); [d]Predicted brain/blood partition coefficient (-3.0 to 1.2); [e]Percent human oral absorption (<25% is poor and >80% is high); [f]Rule of 5 violation (mol_MW < 500, QPlogPo/w < 5, donorHB ≤5, accptHB ≤10).

6.5. Summary and conclusion

To conclude, this chapter focussed on homology modelling and virtual screening of in-house database using the model was attempted to identify novel inhibitors. Top fifteen hits identified were screened experimentally and three leads**, hydroxycamptothecin, amsacarine** and **tryptanthrine** with IC_{50}'s μM were found to be the primary molecule for further development. 15 optimized derivatives were synthesized for hydroxycamptothecin and evaluated for their ability to inhibit Mtb Topo 1, activity against Mtb (both H37Rv and XDR) and cytoxicity as steps towards the structure-activity relationships and lead optimization. Of these, compounds **3b**, **3g**, **3h** and **3l** were found with Mtb Topo I inhibitory activity below 10 μM with compound **3b** being most active with 2.9 μM. These four compounds, which also showed a better activity

profile against resistant form of TB (XDR strain) when compared to standard anti-tubercular agents, were further tested against dormant form of Mtb. The four compounds were found to be effective when compared to isoniazid and rifampicin against dormant form Mtb of which compound **3b** with nitro benzyl substitution was the best. Furthermore, it was observed that compound **3b** emerged to be effective against *in vivo* zebrafish model.

For lead-II, amsacrine, 24 derivatives were synthesised and evaluated for their activity on Mtb Topo I, Mtb H37Rv, XDR tb and cytotoxicity out of which compounds **6b**, **6d** and **6e** were found to be more active than the Lead compound amsacrine with compound **6d** being most active with 12.3 µM. Top 10 active compounds were screened for dormant model. Compounds 6b and 6d were found to be most active and were screened for *in vivo* zebrafish model. Compound **6d** with nitro phenyl substitution at R_2 position was found to be most active with ~3.1 bacterial log reduction.

For lead-III, tryptanthrine, 13 derivatives were synthesised and assessed for their activity Mtb Topo I, Mtb H37Rv, XDR tb and cytotoxicity out of which 3 compounds were more active than the Lead 3 Tryptanthrin. Top 4 active compounds were screened for dormant model. Compounds **TR11** was found to be most active and was screened for invivo zebrafish model. Compound **TR11** with bromo substitution at R_1 and chloro substitution at R_2 positions was found to be most active with ~3.0 bacterial log reduction.

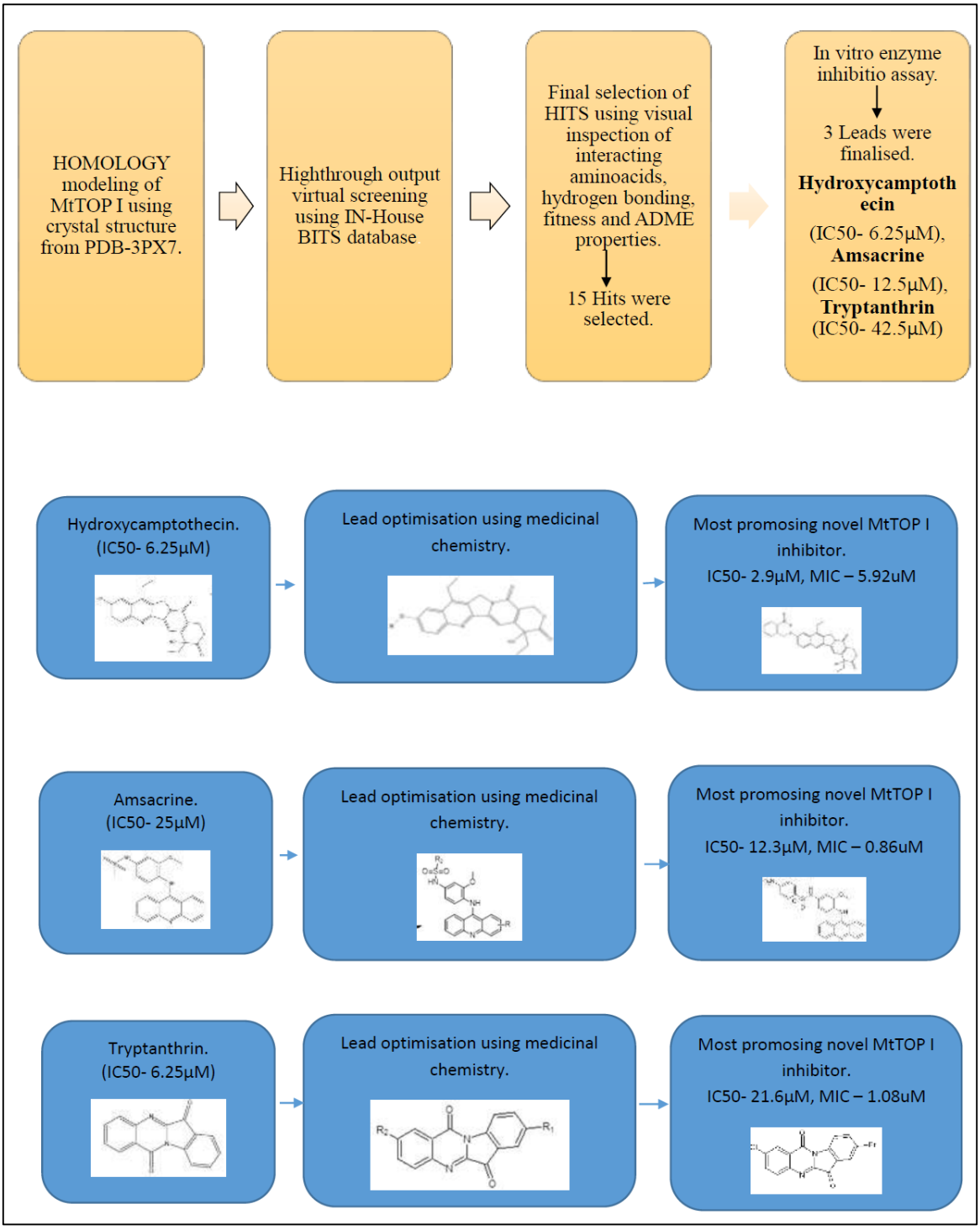

Figure 6.24: Flow chart showing the design and biological assessment of Mtb Topo I inhibitors

Chapter 7
Summary and Future perspectives

Based on the biological investigation and literature report, the Mtb Topo I was found to be an important target for the treatment of Mtb infection in both active and dormant model. Thus, the present study focused on the design of novel inhibitors for Mtb infection.

7.1. Development of mycobacterial Topo I inhibitors

In summary, homology model was prepared for Mtb Topo I as there is no crystal structure reported. High throughput virtual screening campaign against developed Mtb Topo I model using a library comprising 1000 compounds, we successfully identified three Leads Hydroxycamptothecin, Amsacrine and Tryptanthrin. These leads were further derivitised using medicinal chemistry approach. The derived compounds were screened for Invitro Mtb Topo I enzyme activity, active tb screening (both on H37Rv and XDR), dormant TB screening and *in vivo* anti-mycobacterial activity. Further, the biophysical characterization was evaluated using differential scanning flourimetry experiments. In series-I (Hydroxycamptothecin derivatives), Compound **3b** emerged as most potent Mtb Topo I inhibitor with Topo I inhibitory IC_{50} of 2.9 μM; Mtb MIC of 5.92μM and was not cytotoxic at 25 μM. The compound was further screened for dormant model and compound **3b** was found to be potent than standard anti-tubercular compounds exhibiting ~3.1 bacterial log reduction when compared to control. The compound **3b** was also found to be active when screened for *in vivo* anti-mycobacterial activity exhibiting ~2.6 bacterial log reduction.

Series-II (Amsacrine derivatives), Compound **6d** emerged as most potent Mtb Topo I inhibitor with Topo I inhibitory IC_{50} of 12.3 μM; Mtb MIC of 0.86μM and was not cytotoxic at 25 μM.

The compound was further screened for dormant model and compound **6d** was found to be potent than standard anti-tubercular compounds exhibiting ~3.0 bacterial log reduction when compared to control. The compound **6d** was also found to be active when screened for *in vivo* anti-mycobacterial activity exhibiting ~3.1 bacterial log reduction.

In series-III (Tryptanthrin derivatives), Compound **TR07** and **TR11** emerged as most potent Mtb Topo I inhibitor with Topo I inhibitory IC_{50} of 20.2 and 21.6 μM respectively; Mtb MIC of 2.76 and 1.08μM and were not cytotoxic at 25 μM. The compound **TR11** was further screened for dormant model and compound was found to be potent than First line anti-tubercular compounds exhibiting ~2.9 bacterial log reduction when compared to control. The compound **TR11** was also found to be active when screened for *in vivo* anti-mycobacterial activity exhibiting ~3.0 bacterial log reduction.

In conclusion, the class of compounds described here are the most promising lead compounds for further optimization and development to yield novel drugs for fast growing bacterial infections. The study also provides the basis for further chemical and biological optimization of these potent inhibitors as potential anti-tubercular agents.

7.2. Future perspectives

The Mtb Topo I is essential for the survival of bacterial populations, suggesting that it acts as potential targets for the development of novel anti-mycobacterial compounds.

The present study could be extended to resolve the x-ray crystallography of Mtb Topo I bound to these novel inhibitors as there was no crystal structure and there were no/not much reported inhibitors till date. The synthesized compounds were focussed to possess significant *in vitro* and *in vivo* activity; studies are still required to confirm pharmacokinetic and pharmacodynamics profiles of the active leads including safety profile. Also, further mutational studies and macrophage infection studies could be evaluated for the most promising leads

specific to Mtb Topo I. The advancement of any of the compound presented in the thesis along with the development path would require significant investment.

References

Adwait A.G., Leelaram M.N., Anuradha G.B., Paras J., Nagaraja V. Characterization of DNA topoisomerase I from *Mycobacterium tuberculosis*: DNA cleavage and religation properties and inhibition of its activity. *Archives of Biochemistry and Biophysics*. 2012, 528: 197-203.

Ahmed W., Menon S., Godbole A.A., Karthik P.V., Nagaraja V. Conditional silencing of topoisomerase I gene of Mycobacterium tuberculosis validates its essentiality for cell survival. *FEMS Microbiol Letters*. 2014, 353:116-23.

Ahmed W., Menon S., Karthik P.V., Nagaraja V. Reduction in DNA topoisomerase I level affects growth, phenotype and nucleoid architecture of *Mycobacterium smegmatis*. *Microbiology.* 2015, 161:341-53.

.Alderton W., Berghmans S., Butler P., Chassaing H., Fleming A., Golder Z. Accumulation and metabolism of drugs and CYP probe substrates in zebrafish larvae. *Xenobiotica*, 2010, 40: 547-557.

Altschul S.F., Gish W., Miller, W., Myers, E.W., Lipman, D.J. Basic local alignment search tool. *Journal of Molecular Biology.* 1990, 215: 403–410.

Annamalai T., Dani N., Cheng B., Tse-Dinh Y.C. Analysis of DNA relaxation and cleavage activities of recombinant *Mycobacterium tuberculosis* DNA topoisomerase I from a new expression and purification protocol. *BMC Biochemistry.* 2009, 10: 18.

ASINEX, ASINEX Platinum and Gold Collection, ASINECorp, Winston-Salem, NC, USA. http://www.asinex.com/

Banote R.K., Koutarapu S., Chennubhotla K.S., Chatti K., Kulkarni P. Oral gabapentin suppresses pentylenetetrazole-induced seizure-like behavior and cephalic field potential in adult zebrafish. *Epilepsy & Behavior*. 2013, 27: 212-219.

Bernstein J., Lott W.A., Steinberg B.A., Yale H.L. Chemotherapy of experimental tuberculosis. Isonicotinic acid hydrazide (Nydrazid) and related compounds, *American Review of Tuberculosis*. 1952, 65: 357-364.

Binda G., Domenichini E., Gottardi A., Orlandi B., Ortelli E., Pacini B., Fowst G. Rifampicin, a general review. *Arzneimittel-Forschung*. 1971, 12: 1907-1977.

Brannon M.K., Davis J.M., Mathias J.R., Hall C.J., Emerson J.C., Crosier P.S. *Pseudomonas aeruginosa* Type III secretion system interacts with phagocytes to modulate systemic infection of zebrafish embryos. *Cell Microbiology*. 2009, 11: 755-768.

Chao C.C., Hsu P.C., Jen C.F., Chen I.H., Wang C.H., Chan H.C. Zebrafish as a model host for *Candida albicans* infection. *Infection and Immunity*. 2010, 78: 2512-2521.

Chaudhari G.H., Chennubhotla K.S., Chatti K., Kulkarni P. Optimization of the adult zebrafish ECG method for assessment of drug-induced QTc prolongation. *Journal of Pharmacological and Toxicological Methods*. 2013, 67: 115-120.

Chopra P., Meena L.S., Singh Y. New drugs for *Mycobacterium tuberculosis*. *Indian Journal of Medical Research.* 2003, 117: 1-9.

Clark-Curtiss, Josephine E., and Shelley E.H. Molecular genetics of Mycobacterium tuberculosis pathogenesis. *Annual Reviews in Microbiology.* 2003, 57: 517-549.

Clatworthy A.E., Lee J.S., Leibman M., Kostun Z., Davidson AJ., Hung DT. *Pseudomonas aeruginosa* infection of zebrafish involves both host and pathogen determinants. *Infection and Immunity.* 2009, 77: 1293-1303.

Collins L.S., Franzblau S.G., MicroplateAlamar Blue assay versus BACTEC 460 system for high-throughput screening of compounds against *Mycobacterium tuberculosis* and *Mycobacterium avium*. *Antimicrobial Agents and Chemotherapy*. 1997, 41: 1004–1009.

Corbett E.L., Catherine J.W., Neff W., Dermot M., Brian G.W., Mario C.R., Christopher D. The growing burden of tuberculosis: global trends and interactions with the HIV epidemic. *Archives of Internal Medicine.* 2003, 163: 1009-1021.

Desmond Molecular Dynamics System, version 3.1, D. E. Shaw Research, New York, NY, 2012. Maestro-Desmond Interoperability Tools, version 3.1, Schrödinger, New York, NY, 2012.

Fattorini L., Piccaro G., Mustazzolu A., Giannoni F. Targeting dormant bacilli to fight tuberculosis. *Mediterranean Journal of Hematology and Infectious Diseases.* 2013, 5: e2013072.

Ferraris D.M., Diego S., Agnese P., Stefano M., Beat A., Massimo C., Peter S., . Menico R. Crystal structure of Mycobacterium tuberculosis zinc-dependent metalloprotease-1 (Zmp1), a metalloprotease involved in pathogenicity. *Journal of Biological Chemistry*. 2001, 286: 32475-32482.

Flynn J.L., John C. Tuberculosis: latency and reactivation. *Infection and Immunity*. 2001, 69: 4195-4201.

Franzblau S.G., Witzig R.S., McLaughlin J.C., Torres P. Rapid, low-technology MIC determination with clinical *Mycobacterium tuberculosis* isolates by using the microplatealamarblue assay. *Journal of Clinical Microbiology*. 1998, 36: 362-366.

Friesner R.A., Banks J.L., Murphy R.B., Halgren T.A., Klicic J.J., Mainz D.T., Repasky M. P., Knoll E. H., Shelley M., Perry J. K., Shaw D. E., Francis P., Shenkin P.S. Glide: a new approach for rapid, accurate docking and scoring. 1. Method and assessment of docking accuracy. *Journal of Medicinal Chemistry*. 2004, 47: 1739-1749.

Friesner R.A., Murphy R.B., Repasky M.P., Frye L.L., Greenwood J.R., Halgren T.A., Sanschagrin P.C., Mainz D.T. Extra precision glide: docking and scoring incorporating a model of hydrophobic enclosure for protein-ligand complexes. *Journal of Medicinal Chemistry*. 2006, 49: 6177-6196.

Fude Y., Guizhen L., Harvey R. Cloning, expression, purification and characterization of DNA topoisomerase I of Mycobacterium tuberculosis. *Gene.* 1996, 178: 63-69.

Glide, version 5.8, Schrödinger, LLC, New York, NY, 2012.

Godbole A.A., Ahmed W., Bhat R.S., Bradley E.K., Ekins S., Nagaraja V. Inhibition of *Mycobacterium tuberculosis* topoisomerase I by m-AMSA, a eukaryotic type II topoisomerase poison. *Biochemical and Biophysical Research Communications*. 2014, 446: 916-920.

Godbole AA, Ahmed W, Bhat RS, Bradley EK, Ekins S, Nagaraja V. Targeting Mycobacterium tuberculosis topoisomerase I by small-molecule inhibitors. *Antimicrobial Agents and Chemotherapy.* 2015, 59:1549-57.

.

Godbole A.A., Leelaram M.N., Bhat A.G., Jain P., Nagaraja V. Characterization of DNA topoisomerase I from *Mycobacterium tuberculosis*: DNA cleavage and relegation properties and inhibition of its activity. *Archives of Biochemistry and Biophysics*. 2012, 528: 197-203.

Goel M.K., Khanna P., Kishore J. Understanding survival analysis: Kaplan-Meier estimate. *International Journal of Ayurveda Research*. 2010, 1: 274-278.

Grant S.S., Kaufmann B.B., Chand N.S., Haseley N., Hung D.T. Eradication of bacterial persisters with antibiotic-generated hydroxyl radicals. *Proceedings of the National Academy of Sciences U.S.A.* 2012,109: 12147-52.

Green K.D., Garneau-Tsodikova S. Resistance in tuberculosis: what do we know and where can we go? *Frontiers in Microbiology.* 2013, 4: 208.

Houben E.N., Nguyen L., Pieters J. Interaction of pathogenic mycobacteria with the host immune system. *Current Opinion in Microbiology.* 2006, 9: 76-85.

J.C. de Man. The probability of most probable numbers. *European Journal of Applied Microbiology and Biotechnology*. 1975, 1: 67–78.

Jeankumar V.U., Renuka J., Santosh P., Soni V., Sridevi J.P., Suryadevara P., Yogeeswari P., and Sriram D. Thiazole-aminopiperidine hybrid analogues: design andsynthesis of novel *Mycobacterium tuberculosis* GyrB inhibitors. *European Journal of Medicinal Chemistry.* 2013, 70: 143-153.

Joanna C., Pauline T., Linda C., Ruth A., Ken D. Evaluation of a nutrient starvation model of *Mycobacterium tuberculosis* persistence by gene and protein expression profiling. *Molecular Microbiology.* 2002, 43: 717-731.

Jonathan, Benson. Totally drug-resistant' tuberculosis now sweeping India, 25% fatality rate so far [database on the Internet]. Updated January 2012.

Jones D., Metzger H.J., Schatz A., Waksman S.A. Control of gram-negative bacteria in experimental animals by streptomycin. *Science*. 1944, 100: 103-105.

Jorgensen W.L., Chandrasekhar J., Madura J.D., Impey R.W., Klein M.L. Comparison of Simple Potential Functions for Simulating Liquid Water. *Journal of Chemical Physics*. 1983, 79: 926-935.

Kawaji S., Zhong L., Whittington R.J. Partial proteome of *Mycobacterium aviumsubsp.*paratuberculosis under oxidative and nitrosative stress. *Veterinary Microbiology*. 2010, 145: 252-264.

Kimerling M.E, Kluge H., Vezhnina N., Iacovazzi T., Demeulenaere T., Portaels F., Inadequacy of the current WHO re-treatment regimen in a central Siberian prison: treatment failure and MDR-TB. *International Journal of Tuberculosis and Lung Disease*. 1999, 3 , 451-453.

Kinkel M.D., Eames S.C., Philipson L.H., Prince V.E. Intraperitoneal injection into adult zebrafish. *Journal of Visualized Experiments*. 2010, pii: 2126.

Koul A., Eric A., Nacer L., Jerome G., Koen A. The challenge of new drug discovery for tuberculosis. *Nature*. 2011, 469: 483-490.

Kräutler V., van Gunsteren W.F., Hünenberger P.H. A fast SHAKE algorithm to solve distance constraint equations for small molecules in molecular dynamics simulations. *Journal of Computational Chemistry.* 2001, 22: 501-508.

Kulkarni P., Chaudhari G.H., Vijaykumar S., Banote RK. Oral dosing in adult zebrafish: Proof-of-concept using pharmacokinetics and pharmacological evaluation of carbamazepine. *Pharmacological Reports*. 2014, 66: 179–183.

Lamichhane, G. *Mycobacterium tuberculosis* response to stress from reactiveoxygen and nitrogen species. *Frontiers in Microbiology*. 2011, 2: 176.

Laskowski R.A., MacArthur M.W., Moss D.S., Thornton J.M. PROCHECK: a program to check the stereochemical quality of protein structures. *Journal of Applied Crystallography.* 1993, 26: 283-291.

Leelaram M.N., Anuradha G.B., Shivanand M.H., Ramanathapuram M., Nagaraja V. Inhibition of type IA topoisomerase by a monoclonal antibody through perturbation of DNA cleavage–relegation equilibrium. *The FEBS Journal*. 2012, 279: 55-65

Lodish H., Berk A., Zipursky S.L. Molecular Cell Biology,fourth ed. W.H. Freeman, New York. 2000.

Manjunatha U.H., Madhusudan K., Unniraman S., Sikder D., Chatterjee M., Bhaduri T., Radha D.R., Nagaraja V. DNA topoisomerases from *Mycobacterium tuberculosis and Mycobacterium smegmatis*. *Journal of the Indian Institute of Science.* 2003, 86: 751-761.

Mudi A., Chakravarty C. Effect of the Berendsen thermostat on dynamical properties of water. *Molecular Physics.* 2004, 102: 681-685.

Nagaraja V., Sikder D., Jain P. DNA topoisomerase I from mycobacteria—a potential drug target. *Current Pharmaceutical Design*. 2002, 8:1995-2007.

Niesen F.H., Berglund H., Vedadi M. The use of differential scanning fluorimetry to detect ligand interactions that promotes protein stability. *Nature Protocols*. 2007, 2: 2212-2221.

Pieters J., *Mycobacterium tuberculosis* and the macrophage: maintaining a balance. *Cell Host & Microbe*, 2008, 3: 399–407.

Petrovic A.G., Chen Y., Pescitelli G., Berova N., Proni G. CD-sensitive Zn-porphyrin tweezer host-guest complexes, part 1: MC/OPLS-2005 computational approach for predicting preferred inter-porphyrin helicity. *Chirality*. 2010, 22: 129-139.

Prajsnar T.K., Cunliffe V.T., Foster S.J., Renshaw S.A. A novel vertebrate model of Staphylococcus aureus infection reveals phagocyte-dependent resistance of zebrafish to non-host specialized pathogens. *Cell Microbiology,* 2008, 10: 2312-2325.

Prime, version 3.1, Schrödinger, LLC, New York, NY, 2012.

Ramakrishnan L. The Zebrafish Guide to Tuberculosis Immunity and Treatment. *Cold Spring Harbor Symposia on Quantitative Biology*. 2013, 78: 179-192.

Rohit S., Rajni, Anita M., Laxman S.M. Multidrug resistant and extensively drug resistant TB: A Nuisance to Medical Science. *Journal of Bacteriology & Parasitology*2011, 2: 1.

Salina E., Ryabova O., Kaprelyants A., Makarov V. New 2-thiopyridines as potential candidates for killing both actively growing and dormant *Mycobacterium tuberculosis* cells. *Antimicrobial Agents and Chemotherapy.* 2014, 58: 55-60.

Schatz A., Bugie E., Waksman S.A. Streptomycin, a substance exhibiting antibiotic activity against Gram-positive and Gram negative bacteria. *Proceedings of the society for experimental biology and medicine*1944, *55,* 66–69.

SiteMap, version 2.6, Schrödinger, LLC, New York, NY, 2012.

Skrahin A., Ahmed R.K., Ferrara G., Rane L., Poiret T., Isaikina Y., Skrahina A., Zumla A., Maeurer M.J. Autologous mesenchymal stromal cell infusion as adjunct treatment in patients with multidrug and extensively drug resistant tuberculosis: an open-label phase 1 safety trial. *The Lancet Respiratory Medicine.* 2014, 2: 108-122

Stewart A., Cachat J.M., Suciu C., Hart P.C., Gaikwad S., Utterback E. Neurophenotyping of adult zebrafish using the light/dark box paradigm. In A. V. Kalueff, & J. Cachat (Eds.), *Zebrafish neurobehavioral protocols*. 2012: 169–179.

Swaim L.E., Connolly L.E., Volkman H.E., Humbert O., Born D.E., Ramakrishnan L. Mycobacterium marinum infection of adult zebrafish causes caseating granulomatous tuberculosis and is moderated by adaptive immunity. *Infection and Immunity.* 2006, 74: 6108-6117.

Szabady R.L., Lokuta M.A., Walters K.B., Huttenlocher A., Welch R.A. Modulation of neutrophil function by a secreted mucinase of Escherichia coli O157:H7. *PLoS Pathogens.* 2009, 5, e1000320.

Takaki K., Cosma C.L., Troll M.A., Ramakrishnan L. An *in vivo* platform for rapid high-throughput anti-tubercular drug discovery. *Cell Reports*. 2012, 2: 175-184.

Thomas J.P, Baughn C.O., Wilkinson R.G., Shepherd R.G. A new synthetic compound with antituberculous activity in mice: ethambutol (dextro-2,2'-(ethylenediimino)-di-l-butanol). *American Review of Respiratory Disease.* 1961, 83: 891-893.

Tisha B., Shashwati B., Devanjan S., Nagaraja V. Inhibition of Mycobacterium smegmatis topoisomerase I by specific oligonucleotides. *FEBS Letters*. 2000, 486: 126-130.

Tobin D.M., Ramakrishnan L. Comparative pathogenesis of *Mycobacterium marinum* and *Mycobacterium tuberculosis*. *Cellular Microbiology*, 2008, 10: 1027-1039.

Trauner A., Borrell S., Reither K., Gagneux S. Evolution of Drug Resistance in Tuberculosis: Recent Progress and Implications for Diagnosis and Therapy. *Drugs*, 2014, 74: 1063–1072.

VanMeerloo J., Kaspers G.J., Cloos J. Cell sensitivity assays: the MTT assay. *Methods in Molecular Biology*. 2011, 731: 237-245.

Veneman W.J., Marín-Juez R., de Sonneville J., Ordas A. Establishment and Optimization of a High Throughput Setup to Study *Staphylococcus epidermidis* and *Mycobacterium marinum* Infection as a Model for Drug Discovery. *Journal of Visualized Experiments*, 2014

Vergne I., Fratti R.A., Hill P.J., Chua J., Belisle J., Deretic V. *Mycobacterium tuberculosis* phagosome maturation arrest: mycobacterial phosphatidylinositol analog phosphatidylinositol mannoside stimulates early endosomal fusion. *Molecular Biology of the Cell*. 2012, 15: 751–760.

Vergunst A.C., Meijer A.H., Renshaw S.A., O'Callaghan D. Burkholderia cenocepacia creates an intramacrophage replication niche in zebrafish embryos, followed by bacterial dissemination and establishment of systemic infection. *Infection and Immunity*. 2010, 78: 1495-1508.

Villemagne B., Crauste C., Flipo M., Baulard A.R., Deprez B., Willand N., Tuberculosis: the drug development pipeline at a glance. *European Journal of Medicinal Chemistry*. 2012, 51: 1-16

Wang Z., Du J., Lam S.H., Mathavan S., Matsudaira P., Gong Z. Morphological and molecular evidence for functional organization along the rostrocaudal axis of the adult zebrafish intestine. *BMC Genomics*, 2010, 11: 392.

Westerfield M. The zebrafish book. A guide for the laboratory use of zebrafish (Danio rerio) (5th ed.). Eugene University of Oregon Press. 2007.

Wiles T.J., Bower J.M., Redd M.J., Mulvey M.A.mUse of zebrafish to probe the divergent virulence potentials and toxin requirements of extraintestinal pathogenic Escherichia coli. *PLoS Pathogens*, 2009, 5.

World Health Organization (WHO) - Global Tuberculosis Control 2011 report [cited 24 February2012].

Yang F., Lu G., Rubin H. Cloning, expression, purification and characterization of DNA topoisomerase I of *Mycobacterium tuberculosis*. *Gene*. 1996, 178: 63-69.

Zahrt T.C, Deretic V. Reactive nitrogen and oxygen intermediates and bacterial defenses: unusual adaptations in *Mycobacterium tuberculosis*. *Antioxidants & Redox Signaling.* 2002, 4: 141–159.

Zhang Y. The magic bullets and tuberculosis drug targets. *Annual Review of Pharmacology and Toxicology.* 2005, 45: 529-564.

Zumla A.I., Gillespie S.H., Hoelscher M., Philips P.P., Cole S.T., Abubakar I., McHugh T.D., Schito M., Marurer M., Nunn A.J. New antituberculosis drugs, regimens, and adjunct therapies: needs, advances, and future prospects. *The Lancet Infectious Diseases.* 2014. 14: 327-34

Annexures

Annexure I: Synthesis of Hydroxycamptothecin derivatives (3a-3o):

The procedures and characterization data are given for all the synthesized compounds.

Preparation of Hydroxycamptothecin derivatives (3a-3o):

To a solution of 7-Ethyl-10-hydroxycamptothecin (0.02 g, 0.0510 mmol) in 1,4-dioxane (5 mL) was added Cs_2CO_3 (0.019 g, 0.0612 mmol) followed by corresponding benzylbromide derivative (0.0561 mmol) and the resulting solution was heated under reflux for 12 h under inert atmosphere. The reaction mixture was filtered and the filtrate was concentrated to get crude compound. Crude compound was triturated by using diisopropylether and dried to afford compound 3a – 3o.

9-(Benzyloxy)-4,11-diethyl-4-hydroxy-1H-pyrano[3',4':6,7]indolizino[1,2-b] quinoline-3,14(4H,12H)-dione (3a):

Yellow solid; Yield (65%); mp: 232-234°C. ^{1}H NMR (DMSO-*d*$_6$):δ_H . 0.87(t, 3H, J = 7.2Hz), 1.26(t, 3H, J = 7.6Hz), 1.84-1.88(m, 2H), 3.20(q, 2H, J = 8.0 Hz), 5.28(s, 2H), 5.36(s, 2H), 5.42(s, 2H), 6.50(s, 1H), 7.29-7.45(m, 4H), 7.54(m, 4H), 8.08(d, 1H, J = 9.9 Hz).^{13}C NMR (DMSO-*d*$_6$): δ_C 190.5, 172.5, 162.3, 160.1, 151.9, 150.5, 144.2, 140.3, 134.2, 131.9, 129.2, 128.6, 125.7, 123.2, 120.9, 119.8, 114.4, 111.5, 109.7, 105.4, 78.9, 71.7, 69.7, 51, 39.3, 29.4, 21.5, 15.5. ESI-MS m/z 483 $(M + H)^+$. Anal calcd for $C_{29}H_{26}N_2O_5$:C, 72.18; H, 5.43; N, 5.81; Found: C, 72.19; H, 5.44; N, 5.82.

4,11-Diethyl-4-hydroxy-9-((2-nitrobenzyl)oxy)-1H-pyrano[3',4':6,7]indolizino[1,2-b]quinoline-3,14(4H,12H)-dione (3b):

Brown solid; Yield (78%); mp: 219-221°C. ^{1}H NMR ($CDCl_3$):δ_H. 1.03(t, 3H, J = 7.6Hz), 1.33(t, 3H, J = 7.6Hz), 1.83-1.95(m, 2H), 3.12(q, 2H, J = 7.6 Hz), 3.88(s, 1H), 5.23(s, 2H), 5.30(d, 1H, J = 16 Hz), 5.67(s, 2H), 5.74(d, 1H, J = 16 Hz), 7.40(d, 1H, J = 2.8 Hz), 7.52-7.58(m, 2H), 7.60(s, 1H), 7.72(t, 2H, J = 8.0 Hz), 7.94(d, 1H, J =16 Hz), 8.19(t, 1H, J = 8.4 Hz).^{13}C NMR (DMSO-*d_6*): δ_C 190.5, 172.5, 162.3, 160.1, 154.9, 152.5, 149.2, 147.1, 145.8, 143.9, 140.2, 138.9, 132.6, 129.8, 127.2, 126.7, 124.8, 120.5, 109.7, 105.4, 78.9, 71.7, 69.7, 51, 39.3, 29.4, 21.5, 15.5. ESI-MS m/z 528 $(M + H)^+$. Anal calcd for $C_{29}H_{25}N_3O_7$:C, 66.03; H, 4.78; N, 7.97; Found: C, 66.05; H, 4.76; N, 7.96.

9-((2-Chlorobenzyl)oxy)-4,11-diethyl-4-hydroxy-1H-pyrano[3',4':6,7]indolizino[1,2-b]quinoline-3,14(4H,12H)-dione (3c):

Yellow solid; Yield (64%); mp: 232-234°C. ^{1}H NMR (DMSO-*d_6*):δ_H. 0.88(t, 3H, J = 7.2Hz), 1.26(t, 3H, J = 7.6Hz), 1.85-1.89(m, 2H), 3.20(q, 2H, J = 8.0 Hz), 5.26(s, 2H), 5.41(s, 2H), 5.42(s, 2H), 6.51(s, 1H), 7.27(s, 2H), 7.40-7.45(m, 2H), 7.54-7.58(m, 3H), 7.68-7.71(m, 1H), 8.08(d, 1H, J = 9.9 Hz).^{13}C NMR (DMSO-*d_6*): δ_C 190.5, 172.5, 162.3, 160.1, 151.9, 150.5, 148.2, 146, 142.3, 139.2, 137.9, 135.2, 131.6, 129.8, 127.2, 124.9, 122.8, 117.5, 109.7, 105.4, 78.9, 71.7, 69.7, 51, 39.3, 29.4, 21.5, 15.5. ESI-MS m/z 518 $(M + H)^+$. Anal calcd for $C_{29}H_{25}ClN_2O_5$:C, 67.38; H, 4.87; N, 5.42; Found: C, 67.39;H, 4.88; N, 5.43.

4,11-Diethyl-9-((3-fluorobenzyl)oxy)-4-hydroxy-1H-pyrano[3',4':6,7]indolizino[1,2-b]quinoline-3,14(4H,12H)-dione (3d):

Off-white solid; Yield (62%); mp: 217-219°C. ^{1}H NMR (DMSO-*d_6*):δ_H. 0.88(t, 3H, J = 7.2Hz), 1.26(t, 3H, J = 7.2Hz), 1.79-1.92(m, 2H), 3.17(q, 2H, J = 7.6 Hz), 5.24(s, 2H), 5.33(s, 2H), 5.42(s, 2H), 6.52(s, 1H), 7.11-7.21(m, 1H), 7.26(s, 2H), 7.34-7.46(m, 3H), 7.51-7.58(m, 1H),

8.06(d, 1H, J = 9.0 Hz).^{13}C NMR (DMSO-d_6): δ_C 190.5, 172.5, 162.3, 160.1, 151.9, 150.5, 148.2, 146.1, 143.8, 142.3, 139.2, 137.9, 131.6, 129.8, 127.2, 124.9, 122.8, 117.5, 109.7, 105.4, 78.9, 71.7, 69.7, 51, 39.3, 29.4, 21.5, 15.5. ESI-MS m/z 501 $(M + H)^+$. Anal calcd for $C_{29}H_{25}FN_2O_5$:C, 69.59; H, 5.03; N, 5.60; Found: C, 69.58; H, 5.01; N, 5.58.

9-((3,4-Difluorobenzyl)oxy)-4,11-diethyl-4-hydroxy-1H-pyrano[3',4':6,7]indolizino [1,2-b]quinoline-3,14(4H,12H)-dione (3e):

Brown solid; Yield (58%); mp: 233-235°C. ^{1}H NMR (DMSO-d_6):δ_H . 0.87(t, 3H, J = 7.2Hz), 1.26(t, 3H, J = 7.6Hz), 1.84-1.88(m, 2H), 3.20(q, 2H, J = 8.0 Hz), 5.30(s, 2H), 5.36(s, 2H), 5.42(s, 2H), 6.48(s, 1H), 7.27(s, 2H), 7.40-7.52(m, 2H), 7.59-7.68(m, 2H), 8.10(d, 1H, J = 7.2 Hz).^{13}C NMR (DMSO-d_6):δ_C 190.5, 172.5, 162.3, 160.1, 151.9, 150.5, 149.2, 147, 145.3, 142.2, 141.6, 137.9, 135.2, 134.6, 132.7, 126.2, 119.8, 111.5, 109.7, 105.4, 78.9, 71.7, 69.7, 51, 39.3, 29.4, 21.5, 15.5. ESI-MS m/z 519 $(M + H)^+$. Anal calcd for $C_{29}H_{24}F_2N_2O_5$:C, 67.18; H, 4.67; N, 5.40; Found: C, 67.19; H, 4.65; N, 5.42.

4,11-Diethyl-4-hydroxy-9-((2,3,4-trifluorobenzyl)oxy)-1H-pyrano[3',4':6,7] indolizino[1,2-b]quinoline-3,14(4H,12H)-dione (3f):

Brown solid; Yield (58%); mp: 181-183°C. ^{1}H NMR (DMSO-d_6):δ_H . 0.89(t, 3H, J = 7.2Hz), 1.29(t, 3H, J = 7.6Hz), 1.84-1.88(m, 2H), 3.20(q, 2H, J = 8.0 Hz), 5.31(s, 2H), 5.38(s, 2H), 5.42(s, 2H), 6.51(s, 1H), 7.28(s, 2H), 7.41-7.52(m, 1H), 7.59-7.68(m, 2H), 8.10(d, 1H, J = 7.2 Hz).^{13}C NMR (DMSO-d_6): δ_C 190.5, 172.5, 162.3, 160.1, 157.9, 155.5, 152.2, 150.8, 147, 145.3, 142.2, 141.6, 137.9, 135.2, 134.6,132.7, 119.8, 111.5, 109.7, 105.4, 78.9, 71.7, 69.7, 51, 39.3, 29.4, 21.5, 15.5. ESI-MS m/z 537 $(M + H)^+$. Anal calcd for $C_{29}H_{23}F_3N_2O_5$:C, 64.92; H, 4.32; N, 5.22; Found: C, 64.94; H, 4.29; N, 5.23.

4,11-Diethyl-4-hydroxy-9-((perfluorophenyl)methoxy)-1H-pyrano[3',4':6,7] indolizino[1,2-b]quinoline-3,14(4H,12H)-dione (3g):

Yellow solid; Yield (65%); mp:226-228°C. ^{1}H NMR (DMSO-d_6): δ_H . 0.87(t, 3H, J = 7.2Hz), 1.26(t, 3H, J = 7.6Hz), 1.84-1.88(m, 2H), 3.20(q, 2H, J = 8.0 Hz), 5.28(s, 1H), 5.32(s, 2H), 5.42(s, 2H), 5.50(s, 1H), 6.51(s, 1H), 7.28(s, 1H), 7.42(s, 1H), 7.72(d, 1H, J = 7.4 Hz), 8.10(d, 1H, J = 9.0 Hz).^{13}C NMR (DMSO-d_6): δ_C 190.5, 172.5, 162.3, 160.1, 157.9, 155.5, 152.2, 151.9, 150.8, 147, 145.3, 142.2, 141.6, 137.9, 135.2, 134.6, 132.7, 121.5, 119.7, 112.4, 82.9, 71.7, 69.7, 51, 39.3, 29.4, 21.5, 15.5. ESI-MS m/z 573 $(M + H)^+$. Anal calcd for $C_{29}H_{21}F_5N_2O_5$:C, 60.84; H, 3.70; N, 4.89; Found: C, 60.83; H, 3.69; N, 4.87.

9-((3-Chloro-5-fluorobenzyl)oxy)-4,11-diethyl-4-hydroxy-1H-pyrano[3',4':6,7] indolizino[1,2-b]quinoline-3,14(4H,12H)-dione (3h):

Brown solid; Yield (72%); mp:225-227°C. ^{1}H NMR (DMSO-d_6):δ_H . 0.88(t, 3H, J = 7.2Hz), 1.26(t, 3H, J = 7.2Hz), 1.79-1.92(m, 2H), 3.17(q, 2H, J = 7.6 Hz), 5.28(s, 2H), 5.40(s, 2H), 5.42(s, 2H), 6.47(s, 1H), 7.28(s, 3H), 7.39-7.43(m, 2H), 7.52(m, 1H), 8.10(d, 1H, J = 9.2 Hz). ^{13}C NMR (DMSO-d_6):δ_C 190.5, 172.5, 162.3, 160.1, 151.9, 150.5, 148.2, 146, 142.3, 139.2, 137.9, 135.2, 134.6, 132.7, 126.2, 122.9, 119.8, 111.5, 109.7, 105.4, 78.9, 71.7, 69.7, 51, 39.3, 29.4, 21.5, 15.5.ESI-MS m/z 536 $(M + H)^+$. Anal calcd for $C_{29}H_{24}ClFN_2O_5$:C, 65.11; H, 4.52; N, 5.24; Found: C, 65.13; H, 4.53; N, 5.23.

4,11-Diethyl-9-((4-fluoro-2-(trifluoromethyl)benzyl)oxy)-4-hydroxy-1H-pyrano [3',4':6,7]indolizino[1,2-b]quinoline-3,14(4H,12H)-dione (3i):

Brown solid; Yield (72%); mp: 221-223°C.^{1}H NMR (DMSO-d_6):δ_H . 0.88(t, 3H, J = 7.2Hz), 1.26(t, 3H, J = 7.2Hz), 1.79-1.92(m, 2H), 3.17(q, 2H, J = 7.6 Hz), 5.28(s, 2H), 5.40(s, 2H), 5.42(s, 2H), 6.47(s, 1H), 7.28(s, 2H), 7.36-7.41(m, 2H), 7.42(s, 1H), 7.54-7.59(m, 1H), 8.10(d, 1H, J = 9.2 Hz).^{13}C NMR (DMSO-d_6): δ_C 190.5, 172.5, 162.3, 160.1, 151.9, 150.5, 149.2, 147,

142.2, 141.6, 137.9, 135.2, 134.6, 132.7, 129.4, 126.2, 122.7, 119.8, 111.5, 109.7, 105.4, 78.9, 71.7, 69.7, 51, 39.3, 29.4, 21.5, 15.5. ESI-MS m/z 570 $(M + H)^+$. Anal calcd for $C_{30}H_{24}F_4N_2O_5$:C,63.38; H, 4.26; N, 4.93; Found: C, 63.39; H, 4.25; N, 4.95.

4,11-Diethyl-4-hydroxy-9-((2-(trifluoromethyl)benzyl)oxy)-1H-pyrano[3',4':6,7] indolizino[1,2-b]quinoline-3,14(4H,12H)-dione (3j):

Brown solid; Yield (53%); mp: 223-225°C. ^{1}H NMR (DMSO-*d*$_6$):$\delta_{H\ .}$ 0.88(t, 3H, J = 7.2Hz), 1.26(t, 3H, J = 7.4Hz), 1.84-1.88(m, 2H), 3.19(q, 2H, J = 8.0 Hz), 5.25(s, 2H), 5.39(s, 2H), 5.41(s, 2H), 6.49(s, 1H), 7.27(s, 1H), 7.40-7.45(m, 2H), 7.54-7.58(m, 3H), 7.60-7.69(m, 1H), 8.08(d, 1H, J = 9.9 Hz).^{13}C NMR (DMSO-*d*$_6$): δ_C 190.5, 172.5, 162.3, 160.1, 151.9, 150.5, 149.2, 142.2, 141.6, 137.9, 135.2, 134.6, 132.7, 129.4, 126.2, 125.6, 122.7, 119.8, 111.5, 109.7, 105.4, 78.9, 71.7, 69.7, 51, 39.3, 29.4, 21.5, 15.5. ESI-MS m/z 551 $(M + H)^+$. Anal calcd for $C_{30}H_{25}F_3N_2O_5$:C, 65.45; H,4.58; N, 5.09; Found: C, 65.44; H, 4.56; N, 5.08.

4,11-Diethyl-9-((3-fluoro-4-methoxybenzyl)oxy)-4-hydroxy-1H-pyrano[3',4':6,7] indolizino[1,2-b]quinoline-3,14(4H,12H)-dione (3k):

Yellow solid; Yield (59%); mp: 171-173°C.^{1}H NMR (DMSO-*d*$_6$): $\delta_{H\ .}$ 0.89(t, 3H, J = 7.2Hz), 1.24(t, 3H, J = 7.6Hz), 1.82-1.89(m, 2H), 3.18(q, 2H, J = 7.6 Hz), 3.76(s, 3H), 5.29(s, 2H), 5.30(s, 2H), 5.43(s, 2H), 6.49(s, 1H), 6.92(dd, 1H, J = 3.2 Hz, J = 8.8 Hz), 7.25(dd, 2H, J = 3.4 Hz, J = 8.8 Hz), 7.56-7.61(m, 3H), 8.10(d, 1H, J = 9.2 Hz). ^{13}C NMR (DMSO-*d*$_6$):δ_C 190.5, 172.5, 168.9, 162.3, 160.1, 153.9, 152.3, 150.5, 148.2, 146, 142.3, 139.2, 137.9, 135.2, 131.6, 127.7, 119.8, 111.5, 109.7, 105.4, 78.9, 71.7, 69.7, 59.8, 51, 39.3, 29.4, 21.5, 15.5. ESI-MS m/z 531 $(M + H)^+$. Anal calcd for $C_{30}H_{27}FN_2O_6$:C, 67.92; H, 5.13; N, 5.28; Found: C, 67.93; H, 5.11; N, 5.26.

4,11-Diethyl-4-hydroxy-9-((3-methoxybenzyl)oxy)-1H-pyrano[3',4':6,7] indolizino[1,2-b]quinoline-3,14(4H,12H)-dione (3l):

Yellow solid; Yield (65%); mp: 228-230°C. ^{1}H NMR (DMSO-d_6):$\delta_{H.}$ 0.88(t, 3H, J = 7.2Hz), 1.27(t, 3H,J = 7.6Hz), 1.83-1.88(m, 2H), 3.18(q, 2H,J = 7.6Hz), 3.75(s, 3H), 5.29(s, 2H), 5.34(s, 2H), 5.42(s, 2H), 6.47(s, 2H), 6.92(dd, 1H, J = 3.2 Hz, J = 8.8 Hz), 7.25-7.28(m, 2H), 7.56-7.1(m, 3H), 8.10(d, 1H, J = 9.2 Hz). ^{13}C NMR (DMSO-d_6):δ_C 190.5, 172.5, 168.9, 162.3, 160.1, 151.9, 150.5, 148.2, 146, 142.3, 139.2, 137.9, 135.2, 131.6, 127.7, 122.9, 119.8, 111.5, 109.7, 105.4, 78.9, 71.7, 69.7, 59.8, 51, 39.3, 29.4, 21.5, 15.5. ESI-MS m/z 514 $(M + H)^+$. Anal calcd for $C_{30}H_{28}N_2O_6$:C, 70.30; H, 5.51; N, 5.47; Found: C, 70.31; H, 5.50; N, 5.45.

9-((2-Bromobenzyl)oxy)-4,11-diethyl-4-hydroxy-1H-pyrano[3',4':6,7]indolizino[1,2-b]quinoline-3,14(4H,12H)-dione (3m):

Brown solid; Yield (68%); mp: 236-238°C. ^{1}H NMR (DMSO-d_6): $\delta_{H.}$ 0.88(t, 3H, J = 7.2Hz), 1.26(t, 3H, J = 7.6Hz), 1.85-1.89(m, 2H), 3.19(q, 2H,J = 8.0 Hz), 5.26(s, 2H), 5.41(s, 2H), 5.42(s, 2H), 6.51(s, 1H), 7.27(s, 1H), 7.39-7.45(m, 2H), 7.54-7.58(m, 3H), 7.68-7.71(m, 1H), 8.09(d, 1H, J = 9.8 Hz). ^{13}C NMR (DMSO-d_6):): δ_C 190.5, 172.5, 162.3, 160.1, 151.9, 150.5, 148.2, 146, 142.3, 139.2, 137.9, 135.2, 131.6, 127.7, 126.2, 122.9, 119.8, 111.5, 109.7, 105.4, 78.9, 71.7, 69.7, 51, 39.3, 29.4, 21.5, 15.5. ESI-MS m/z 562 $(M + H)^+$. Anal calcd for $C_{29}H_{25}BrN_2O_5$:C, 62.04; H, 4.49; N, 4.99; Found: C, 62.05; H, 4.47; N, 4.50.

9-((2-Bromo-5-methoxybenzyl)oxy)-4,11-diethyl-4-hydroxy-1H-pyrano[3',4':6,7] indolizino[1,2-b]quinoline-3,14(4H,12H)-dione (3n):

Yellow solid; Yield (65%); mp: 164-166°C. ^{1}H NMR (DMSO-d_6): $\delta_{H.}$ 0.89(t, 3H, J = 7.2Hz), 1.28(t, 3H, J = 7.6Hz), 1.84-1.89(m, 2H), 3.19(q, 2H, J = 7.6 Hz), 3.78(s, 3H), 5.30(s, 2H), 5.34(s, 2H), 5.42(s, 2H), 6.50(s, 1H), 6.92(dd, 1H, J = 3.2 Hz, J = 8.8 Hz), 7.25-7.28(m, 3H), 7.56-7.61(m, 2H), 8.10(d, 1H, J = 9.2 Hz).^{13}C NMR (DMSO-d_6): δ_C 190.5, 172.5, 168.9, 162.3,

160.1, 153.9, 152.3, 151.9, 150.5, 148.2, 146, 142.3, 139.2, 137.9, 135.2, 131.6, 121.7, 119.8, 111.5, 109.7, 105.4, 78.9, 71.7, 69.7, 51, 39.3, 29.4, 21.5, 15.5.ESI-MS m/z 592 $(M + H)^+$. Anal calcd for $C_{30}H_{27}BrN_2O_6$:C, 60.92; H, 4.60; N, 4.74; Found: C, 60.91; H, 4.59; N, 4.75.

4,11-Diethyl-4-hydroxy-9-((4-iodobenzyl)oxy)-1H-pyrano[3',4':6,7]indolizino[1,2-b] quinoline-3,14(4H,12H)-dione (3o):

Brown solid; Yield (58%); mp: 161-163°C. ^{1}H NMR (DMSO-d_6):δ_H . 0.87(t, 3H, J = 7.2Hz), 1.26(t, 3H, J = 7.6Hz), 1.84-1.88(m, 2H), 3.20(q, 2H, J = 8.0 Hz), 5.30(s, 2H), 5.36(s, 2H), 5.42(s, 2H), 6.48(s, 1H), 7.27(s, 3H), 7.40-7.52(m, 2H), 7.59-7.68(m, 2H), 8.10(d, 1H, J = 7.2 Hz). ^{13}C NMR (DMSO-d_6):δ_C 190.5, 172.5, 168.9, 162.3, 160.1, 151.9, 150.5, 148.2, 146, 142.3, 139.2, 137.9, 135.2, 131.6, 127.7, 119.8, 114.4, 111.5, 109.7, 105.4, 78.9, 71.7, 69.7, 51, 39.3, 29.4, 21.5, 15.5. ESI-MS m/z 610 $(M + H)^+$. Anal calcd for $C_{29}H_{25}IN_2O_5$:C, 57.25; H, 4.14; N, 4.60; Found: C, 57.23; H, 4.15; N, 4.61.

Annexure II: Synthesis of Amsacrine derivatives (6a-6i, 7a-7p):

Preparation of substituted 2-(Phenylamino)benzoic acid derivatives (2a-b):

To a stirred solution of 2-chlorobenzoic acid (10g, 64 mmol) in DMF potassium carbonate (13.24g, 96 mmol) corresponding aniline (70.4 mmol) and copper powder was added and heated up to 140 C for 6 h. Reaction progress was monitored by TLC after completion, reaction mass was filtered through celite, celite bed was washed with ethyl acetate. The combined organic layer was evaporated under reduced pressure obtained crude was purified by flash column chromatography using 5-20 % ethyl acetate: hexane as eluent in 100-200 mesh silica gel to get the corresponding phenylamino benzoic acid derivatives in good yield. The intermediates (**2a-b**) were confirmed by mass (ESI mode) and proceeded to next step.

2-(Phenylamino)benzoic acid (**2a**):

Off-white solid; Yield 75%; ESI-MS was found at 212$(M-H)^-$.

2-(p-Tolylamino)benzoic acid (**2b**):

Pale brown solid; Yield 77%; ESI-MS was found at 228 $(M+H)^+$.

Preparation of 9-Chloroacridine derivatives from substituted phenyl amino benzoic acid intermediates (**3a-b**):

The phenyl amino benzoic acid derivatives (47 mmol) (**2a-b**) were cyclised intramolecularly to 9-chloroacridine derivatives (**3a-b**) by refluxing them in 60 ml of $POCl_3$ for 4 h and the reaction was monitored by TLC. The excess POCl3 was removed by rota evaporator under reduced pressure. To this crushed ice was added and neutralised with saturated bicarbonate solution until pH reaches to ~7, the solid separated was filtered, dried and purified by flash column chromatography using 5-10% ethyl acetate: hexane as eluent in 60-120 mesh silica gel

to get the corresponding 9-chloroacridine derivatives in good yield. These compounds were confirmed by mass and proceeded to next step.

9-Chloroacridine (**3a**):

Pale orange solid; Yield 69%; ESI-MS was found at 228 $(M+H)^+$.

9-Chloro-2-methylacridine (**3b**):

Pale brown solid; Yield 71%; ESI-MS was found at 228 $(M+H)^+$.

Preparation of N-(2-Methoxy-4-nitrophenyl)acridin/2-methylacridine-9-amine intermediates (**4a-b**):

The 9-chloroacridine derivatives (10 mmol) (**3a-b**) were further reacted with 4-nitro *o*-anisidine (1.8g, 10.7 mmol) under microwave conditions in methanol using PTSA (Para-toluene sulphonic acid) as a catalyst (5-10 mg) at 130 °C for 1 h, reaction was monitored by TLC. After completion of reaction, methanol was evaporated under vacuum the crude was dissolved in ethyl acetate, washed with saturated bicarbonate solution. The organic layer was dried over anhydrous sodium sulphate and evaporated under vacuum obtained crude was further purified by flash column chromatography in 60-120 silica gel using 10-35% ethyl acetate: hexane as eluent to get an yellow solid.

N-(2-Methoxy-4-nitrophenyl) acridin-9-amine (**4a**):

Brown solid; Yield 69%; ESI-MS was found at 346 $(M+H)^+$.

N-(2-Methoxy-4-nitrophenyl)-2-methylacridin-9-amine (**4b**):

Pale brown solid; Yield 68%; ESI-MS was found at 358 $(M-H)^-$.

Preparation of N^1-(Acridin/2-methylacridin-9-yl)-2-methoxybenzene-1,4-diamine intermediates (**5a-b**):

The corresponding nitro acridin derivatives (6 mmol) (**4a-b**) were converted to amine derivatives by reducing with Fe- HCl in ethanol by refluxing for 4 h. The crude reaction mixture diluted with ethyl acetate and filtered through celite bed, the organic layer was dried over sodium sulphate and concentrated under vacuo. The obtained crude was purified by flash column chromatography using ethyl acetate: hexane as eluent to get a brown solid in good yields.

N^1-(Acridin-9-yl)-2-methoxybenzene-1,4-diamine:

Brown solid; Yield 68%; ESI-MS was found at 316 $(M+H)^+$.

2-Methoxy-N^1-(2-methylacridin-9-yl)benzene-1,4-diamine:

Pale brown solid; Yield 64%; ESI-MS was found at 330 $(M+H)^+$.

Preparation of N-(3-Methoxy-4-((acridin/2-methylacridin-9-yl)amino)phenyl) methane/ substituted benzene sulfonamide derivatives (**6a-6i**) :

For the preparation of sulphonamide derivatives corresponding acridin amine derivatives (0.6 mmol) (**5a-b**) were taken in 5 ml DMF (*N, N* dimethyl formamide) to this triethylamine (1.38 mmol) and corresponding substituted alkyl/ aryl sulphonyl chlorides (0.6 mmol) were added at 0 C and allowed to stir at rt for 3 h. After completion of reaction crushed ice was added to the crude reaction mass the solid precipitated was filtered, dried and further purified by flash column chromatography using 5-10 % methanol: dichloromethane as eluent to fial sulphonamide derivatives in good yields.

N-(4-(Acridin-9-ylamino)-3-methoxyphenyl)methanesulfonamide (6a):

Orange solid; Yield 80%; mp 234-236 °C; ^{1}H NMR (DMSO-d_6)**:** δ_H. 2.89 (s, 3H), 3.87 (s, 3H), 5.91-5.94 (m, 2H), 6.41 (d, 1H, J = 7.8 Hz), 7.55-7.97 (m, 6H), 8.19 (m, 2H), 9.94 (s, 1H), 10.81 (s, 1H). ^{13}C NMR (DMSO-d_6): δ_C. 150.3, 148.5, 142.8(2C), 128.9(2C), 128.4, 127.8(2C), 126.1(2C), 122.7, 130.1(2C), 118.3, 114.9(2C), 109.5, 100.6, 55.8, 40.1. EI-MS m/z 392 $(M-H)^-$. Anal Calcd. for $C_{21}H_{19}N_3O_3S$:C, 64.10; H, 4.87; N, 10.68; O, 12.20; S, 8.15; Found: 64.08, H, 4.82, N, 10.61.

N-(4-(Acridin-9-ylamino)-3-methoxyphenyl)benzenesulfonamide (6b):

Brown solid; Yield 64%; mp 125-127 °C; ^{1}H NMR (DMSO-d_6)**:** δ_H. 3.86 (s, 3H), 5.92-5.96 (m, 2H), 6.31 (d, 1H, J = 8.1 Hz), 7.56-7.94 (m, 11H), 8.19 (m, 2H), 9.96 (s, 1H), 10.71 (s, 1H). ^{13}C NMR (DMSO-d_6): δ_C. 150.4, 148.7, 142.9(2C), 140.3, 132.2, 130.6(2C), 129.8(2C), 129.0, 128.1(2C), 127.8(2C), 126.9(2C), 123.2, 121.5(2C), 118.8, 115.4(2C), 109.8, 100.6, 56.2. EI-MS m/z 454 $(M-H)^-$. Anal Calcd. for $C_{26}H_{21}N_3O_3S$: C, 68.55; H, 4.65; N, 9.22; Found: C, 68.52; H, 4.67; N, 9.19.

N-(4-(Acridin-9-ylamino)-3-methoxyphenyl)-4-chlorobenzenesulfonamide (6c):

Pale brown solid; yield 74%; mp 118-120 °C; ^{1}H NMR (DMSO-d_6)**:** δ_H. 3.86 (s, 3H), 5.92-5.96 (m, 2H), 6.29 (d, 1H, J = 7.8 Hz), 7.61-7.96 (m, 10H), 8.15 (m, 2H), 9.87 (s, 1H), 10.67 (s, 1H). ^{13}C NMR (DMSO-d_6): δ_C. 150.2, 148.8, 142.8(2C), 138.4(2C), 130.5(2C), 129.7(2C), 129.4(2C), 128.6(3C), 126.9(2C), 123.0, 121.4(2C), 119.0, 115.5(2C), 110.1, 100.9, 56.3. EI-MS m/z 490 $(M+H)^+$. Anal Calcd. for $C_{26}H_{20}ClN_3O_3S$: C, 63.73; H, 4.11; N, 8.58; Found: C, 63.69; H, 4.16; N, 8.61.

N-(4-(Acridin-9-ylamino)-3-methoxyphenyl)-4-nitrobenzenesulfonamide (6d):

Brown solid; Yield 70%; mp 127-129 °C; ^{1}H NMR (DMSO-d_6)**:** δ_H. 3.84 (s, 3H), 5.92 (m, 2H), 6.32 (d, 1H, J = 8.1 Hz), 7.57-7.93 (m, 6H), 8.10-8.41 (m, 6H), 9.91 (s, 1H), 10.74 (s, 1H). ^{13}C NMR (DMSO-d_6): δ_C. 152.7, 150.5, 148.5, 146.2, 142.9(2C), 130.4(2C), 129.2, 128.7(2C), 128.1(2C), 127.0(2C), 124.7(2C), 123.1, 121.5(2C), 118.5, 115.3(2C), 110.0, 100.7, 56.5. EI-MS m/z 499 $(M-H)^-$. Anal Calcd. for $C_{26}H_{20}N_4O_5S$: C, 62.39; H, 4.03; N, 11.19; Found: C, 62.42; H, 4.06; N, 11.15.

N-(4-(Acridin-9-ylamino)-3-methoxyphenyl)-4-methylbenzenesulfonamide (6e):

Brown solid; Yield 71%; mp 136-138 °C; ^{1}H NMR (DMSO-d_6)**:** δ_H. 2.36 (s, 3H), 3.79 (s, 3H), 5.94 (m, 2H), 6.25 (d, 1H, J = 7.8 Hz), 7.43-7.92 (m, 10H), 8.21 (m, 2H), 9.87 (s, 1H), 10.71 (s, 1H). ^{13}C NMR (DMSO-d_6): δ_C. 150.4, 148.9, 142.8(2C), 138.3, 137.5, 130.5(2C), 129.9(2C), 129.0(2C), 128.6(3C), 128.0(2C), 123.4, 121.4(2C), 118.7, 115.4(2C), 109.8, 100.6, 56.3, 22.0. EI-MS m/z 470 $(M+H)^+$. Anal Calcd. for $C_{27}H_{23}N_3O_3S$: C, 69.06; H, 4.94; N, 8.95; Found: C, 69.09; H, 4.81; N, 8.97.

N-(3-Methoxy-4-((2-methylacridin-9-yl)amino)phenyl)benzenesulfonamide (6f):

Brown solid; yield 68%; mp 147-149 °C; ^{1}H NMR (DMSO-d_6)**:** δ_H. 2.35 (s, 3H), 3.85 (s, 3H), 5.95 (m, 2H), 6.29 (d, 1H, *J* = 7.8 Hz), 7.52-7.83 (m, 10H), 8.01-8.19 (m, 2H), 9.92 (s, 1H), 10.57 (s, 1H). ^{13}C NMR (DMSO-d_6): δ_C. 149.9, 148.7, 142.7, 140.4(2C), 135.6, 132.7(3C), 130.5, 129.8(3C), 129.1, 128.0(3C), 122.9, 122.0, 121.2, 119.8, 118.9, 109.9, 108.5, 100.5, 56.2, 22.4. EI-MS m/z 470 $(M+H)^+$. Anal Calcd. for $C_{27}H_{23}N_3O_3S$: C, 69.06; H, 4.94; N, 8.95; Found: C, 69.02; H, 4.79; N, 8.91.

4-Chloro-N-(3-methoxy-4-((2-methylacridin-9-yl)amino)phenyl)benzenesulfonamide (6g):

Pale brown solid; Yield 69%; mp 136-138 °C; ^{1}H NMR (DMSO-d_6)**:** δ_H. 2.32 (s, 3H), 3.82 (s, 3H), 5.92 (m, 2H), 6.31 (d, 1H, *J* = 8.1 Hz), 7.53-7.87 (m, 9H), 8.02-8.22 (m, 2H), 9.97 (s, 1H), 10.77 (s, 1H). ^{13}C NMR (DMSO-d_6): δ_C. 150.0, 148.5, 142.8, 140.2, 138.5(2C), 135.7, 132.2(2C), 130.6, 130.0(3C), 129.4(3C), 127.5, 123.1, 122.0, 121.4, 119.8, 118.9, 109.7, 108.3, 100.8, 56.4, 22.3. EI-MS m/z 502 $(M-H)^-$. Anal Calcd. for $C_{27}H_{22}ClN_3O_3S$: C, 64.34; H, 4.40; N, 8.34; Found: C, 64.37; H, 4.36; N, 8.39.

N-(3-Methoxy-4-((2-methylacridin-9-yl)amino)phenyl)-4-nitrobenzenesulfonamide (6h): Brown solid; Yield 68%; mp 109-111 °C; ^{1}H NMR (DMSO-d_6)**:** δ_H. 2.36 (s, 3H), 3.86 (s, 3H), 5.92 (m, 2H), 6.29 (d, 1H, *J* = 7.8 Hz), 7.53-7.97 (m, 6H), 8.14-8.41 (m, 5H), 9.93 (s, 1H), 10.74 (s, 1H). ^{13}C NMR (DMSO-d_6): δ_C. 151.9, 149.7, 148.9, 146.3, 142.6, 140.1, 135.4, 132.0(2C), 130.3(2C), 128.8(3C), 127.7, 124.9(2C), 123.2, 121.9, 121.0, 119.7, 118.5, 109.8, 108.4, 100.5, 56.1, 22.6. EI-MS m/z 515 $(M+H)^+$. Anal Calcd. for $C_{27}H_{22}N_4O_5S$: C, 63.02; H, 4.31; N, 10.89; Found: C, 63.04; H, 4.35; N, 10.91.

N-(3-Methoxy-4-((2-methylacridin-9-yl)amino)phenyl)-4-methylbenzenesulfonamide (6i):

Pale brown solid; Yield 69%; mp 140-142 °C; ^{1}H NMR (DMSO-d_6)**:** δ_H. 2.32 (s, 6H), 3.84 (s, 3H), 5.93 (m, 2H), 6.27 (d, 1H, *J* = 8.2 Hz), 7.39-7.83 (m, 9H), 8.01 -8.23 (m, 2H), 9.88 (s, 1H), 10.77 (s, 1H). ^{13}C NMR (DMSO-d_6): δ_C. 149.9, 148.5, 142.7, 140.1, 138.3, 137.2, 135.4, 132.6(2C), 130.7, 130.1(3C), 129.0(3C), 127.9, 123.1, 121.9, 121.2, 119.8, 118.9, 109.8, 108.3, 100.6, 56.3, 22.6(2C). EI-MS m/z 484 $(M+H)^+$. Anal Calcd. for $C_{28}H_{25}N_3O_3S$: C, 69.54; H, 5.21; N, 8.69; Found: C, 69.49; H, 5.25; N, 8.73.

Preparation of 1-(3-Methoxy-4-((acridin/2-methylacridin-9-yl)amino)phenyl)-3-phenylthiourea/ urea derivatives (**7a-7p**) :

For preparation thiourea and urea derivatives corresponding acridin amine derivative (0.6 mmol), triethylamine (1.38 mmol) (Et_3N) and substituted phenyl isothiocyanate/isocyanate (0.6 mmol) were dissolved in ethanol and heated at 80 °C for 8 h. After completion of reaction the solid precipitated was filtered, dried and recrystallized from ethanol to get the final corresponding thiourea and urea derivatives.

1-(4-(Acridin-9-ylamino)-3-methoxyphenyl)-3-phenylthiourea (7a):

Brown solid; Yield 70%; mp 150-152 °C; ^{1}H NMR (DMSO-d_6)**:** δ_H. 3.85 (s, 3H), 5.74-5.89 (m, 2H), 6.25-6.78 (2H, J = 7.5Hz), 7.23-7.71 (m, 8H), 7.97-8.15 (m, 4H), 8.89 (s, 2H), 10.5 (s, 1H, J = 7.6Hz). ^{13}C NMR (DMSO-d_6): δ_C. 180.2, 150.4, 148.6, 143.0(2C), 139.1, 130.3(2C), 129.9(2C) 129.5(2C), 128.7(3C), 128.1(2C), 127.0(2C), 126.8(2C), 121.4(2C), 120.2, 118.6, 115.3(2C), 110.9, 56.3. EI-MS m/z: 451 $(M+H)^+$. Anal Calcd. for $C_{27}H_{22}N_4OS$: C, 71.98; H, 4.92; N, 12.44; Found: C, 72.01; H, 4.87; N, 12.49.

1-(4-(Acridin-9-ylamino)-3-methoxyphenyl)-3-(4-chlorophenyl)thiourea (7b):

Pale brown solid; Yield 73%; mp 116-118 °C; ^{1}H NMR (DMSO-d_6)**:** δ_H. 3.87 (s, 3H), 5.71-5.99 (m, 2H), 6.29-6.56 (m, 3H), 7.27-7.81 (m, 6H), 7.99-8.19 (m, 4H, J = 7.6Hz), 9.01 (s, 2H), 9.98 (s, 1H, J = 8.2Hz). ^{13}C NMR (DMSO-d_6): δ_C. 180.4, 150.5, 142.9(2C), 142.5, 137.3, 134.2, 131.8(2C), 130.4(2C), 129.7(2C), 129.1, 128.5(2C), 127.9(2C), 126.7(2C), 121.4(2C), 118.3(2C), 111.5(2C), 56.1. EI-MS m/z 483 $(M-H)^-$. Anal Calcd. for $C_{27}H_{21}ClN_4OS$: C, 66.86; H, 4.36; N, 11.55; Found: C, 66.83; H, 4.38; N, 11.51.

1-(4-(Acridin-9-ylamino)-3-methoxyphenyl)-3-(4-nitrophenyl)thiourea (7c):

Yellow solid; Yield 71%; mp 120-122 °C; ^{1}H NMR (DMSO-d_6)**:** δ_H. 3.89 (s, 3H). 5.72-5.87 (m, 2H, J = 7.26Hz), 6.22-6.65 (m, 3H), 7.61-7.92 (m, 6H), 8.04-8.19 (m, 4H, J = 7.26Hz), 8.89 (s, 2H), 9.97 (s, 1H). ^{13}C NMR (DMSO-d_6): δ_C. 180.2, 150.4, 148.5, 145.0, 144.5, 143.1(2C), 130.4(2C), 129.1(2C), 128.3(2C), 126.9(2C), 125.6(2C), 124.8(2C), 121.5(2C), 120.2, 118.1, 115.2(2C), 110.7, 56.2. EI-MS m/z 496 $(M+H)^+$. Anal Calcd. for $C_{27}H_{21}N_5O_3S$: C, 65.44; H, 4.27; N, 14.13; Found: C, 65.47; H, 4.22; N, 14.06.

1-(4-(Acridin-9-ylamino)-3-methoxyphenyl)-3-(p-tolyl)thiourea (7d):

Pale brown solid; Yield 71%; mp 137-139 °C; ^{1}H NMR (DMSO-d_6)**:** δ_H. 2.36 (s, 3H), 3.86 (s, 3H), 5.74-5.89 (m, 2H), 6.23-6.97 (m, 5H), 7.57-7.96 (m, 6H), 8.19 (d, 2H, *J* = 7.8 Hz), 8.87 (s, 2H), 10.3 (s, 1H, J = 8.1Hz). ^{13}C NMR (DMSO-d_6): δ_C. 180.3, 150.4, 148.2, 142.9(2C), 137.7, 136.2, 130.6(2C), 129.8(2C), 128.7(2C), 128.2(2C), 126.9(2C), 126.7(2C), 121.5(2C), 120.3, 118.3, 115.5(2C), 110.8, 55.4, 21.7. EI-MS m/z 465 $(M+H)^+$. Anal Calcd. for $C_{28}H_{24}N_4OS$: C, 72.39; H, 5.21; N, 12.06; Found: C, 72.36; H, 5.23; N, 12.11.

1-(3-Methoxy-4-((2-methylacridin-9-yl)amino)phenyl)-3-phenylthiourea (7e):

Brown solid; Yield 69%; mp 142-145 °C; ^{1}H NMR (DMSO-d_6)**:** δ_H. 2.36 (s, 3H), 3.86 (s, 3H), 5.97-5.85 (m, 2H), 6.79-6.24 (m, 2H, J = 7.6Hz), 7.81-7.21 (m, 9H), 8.19-8.01 (m, 2H, J = 7.6Hz), 8.98 (s, 2H), 9.98 (s, 1H). ^{13}C NMR (DMSO-d_6): δ_C. 180.3, 149.7, 148.4, 142.4, 139.9, 138.8, 135.6, 131.7(2C), 130.1(2C), 129.5(2C), 128.9(3C), 127.7, 127.1(2C), 122.0, 121.2, 119.9(2C), 118.3, 110.7, 108.5, 56.1, 22.2. EI-MS m/z 463 $(M-H)^-$. Anal Calcd. for $C_{28}H_{24}N_4OS$: C, 72.39; H, 5.21; N, 12.06; Found: C, 72.41; H, 5.24; N, 12.09.

1-(4-Chlorophenyl)-3-(3-methoxy-4-((2-methylacridin-9-yl)amino)phenyl)thiourea (7f):

Pale brown solid; Yield 67%; mp 124-126 °C; ^{1}H NMR (DMSO-d_6)**:** δ_H. 2.32 (s, 3H), 3.85 (s, 3H), 3.85 (s, 3H), 3.85 (s, 3H), 5.79-5.89 (m, 2H), 6.19-6.56 (m, 3H), 7.25-7.84 (m, 7H), 8.00-8.17 (d, 2H, *J* = 7.9 Hz), 9.01 (s, 2H), 9.98 (s, 1H), ^{13}C NMR (DMSO-d_6): δ_C. 180.1, 149.8, 148.3, 142.5, 140.1, 137.2, 135.7, 134.1, 132.0, 131.8(3C), 130.1(2C), 129.8(2C), 128.8(2C), 127.9, 121.9, 121.0, 120.1(2C), 118.4, 110.7, 108.3, 56.3, 22.1. EI-MS m/z 499 $(M+H)^+$. Anal Calcd. for $C_{28}H_{23}ClN_4OS$: C, 67.39; H, 4.65; N, 11.23; Found: C, 67.35; H, 4.68; N, 11.21.

1-(3-Methoxy-4-((2-methylacridin-9-yl)amino)phenyl)-3-(4-nitrophenyl)thiourea (7g):

Pale brown solid; Yield 68%; mp 136-138 °C; ^{1}H NMR (DMSO-d_6)**:** δ_H. 2.35 (s, 3H), 3.86 (s, 3H), 5.78-5.94 (m, 2H), 6.23-6.67 (m, 3H), 7.58-7.89 (m, 6H, J = 7.5Hz), 8.03-8.18 (m, 3H), 9.08 (s, 2H, J = 8.1Hz), 10.6 (s, 1H), ^{13}C NMR (DMSO-d_6): δ_C. 180.3, 149.6, 148.2, 145.0, 144.4, 142.7, 140.0, 135.6, 131.9(2C), 130.2(2C), 128.9(2C), 127.8, 125.6(2C), 124.9(2C), 122.0, 121.7, 120.2(2C), 118.4, 110.8, 108.5, 55.3, 22.3. EI-MS m/z 508 $(M-H)^-$. Anal Calcd. for $C_{28}H_{23}N_5O_3S$:: C, 66.00; H, 4.55; N, 13.74; Found: C, 66.03; H, 4.49; N, 13.77.

1-(3-Methoxy-4-((2-methylacridin-9-yl)amino)phenyl)-3-(p-tolyl)thiourea (7h):

Pale brown solid; Yield 65%; mp 163-165 °C; ^{1}H NMR (DMSO-d_6)**:** δ_H. 2.36 (s, 6H), 3.82 (s, 3H), 5.74-5.86 (m, 2H), 6.26-6.94 (m, 5H), 7.51-7.95 (m, 6H), 8.16 (d, 1H, *J* = 8.4 Hz), 9.04 (s, 2H), 9.89 (s, 1H). ^{13}C NMR (DMSO-d_6): δ_C. 180.5, 149.8, 148.6, 142.3, 140.1, 137.7, 135.9(2C), 132.2(2C), 130.5(2C), 129.8(2C), 129.0(2C), 127.5, 126.8(2C), 121.7, 121.3, 119.6(2C), 118.2, 110.8, 108.4, 55.7, 22.5(2C). EI-MS m/z 479 $(M+H)^+$. Anal Calcd. for $C_{29}H_{26}N_4OS$: C, 72.78; H, 5.48; N, 11.71; Found: C, 72.75; H, 5.52; N, 11.74.

1-(4-(Acridin-9-ylamino)-3-methoxyphenyl)-3-phenylurea (7i):

Brown solid; Yield 68%; mp 184-186 °C; ^{1}H NMR (DMSO-d_6)**:** δ_H. 3.83 (s, 3H), 6.51-6.97 (m, 2H, J = 7.5Hz), 7.19-7.59 (m, 8H), 7.81-8.15 (m, 6H, J = 7.8Hz), 8.98 (s, 2H), 10.5 (s, 1H). ^{13}C NMR (DMSO-d_6): δ_C. 153.4, 150.2, 148.2, 142.9(2C), 139.8, 130.3(2C), 129.5(2C), 128.7(2C), 28.3(2C), 127.4(3C), 122.1(2C), 121.5(2C), 117.9, 115.4(3C), 106.1, 55.7. EI-MS m/z 435 $(M+H)^+$. Anal Calcd. for $C_{27}H_{22}N_4O_2$: C, 74.64; H, 5.10; N, 12.89; Found: C, 74.61; H, 5.05; N, 12.93.

1 1-(4-(Acridin-9-ylamino)-3-methoxyphenyl)-3-(4-chlorophenyl)urea (7j):

Brown solid; Yield 71%; mp 174-176 °C; ^{1}H NMR (DMSO-d_6)**:** δ_H. 3.31 (s, 3H), 6.59-6.98 (m, 2H), 7.16-7.92 (m, 11H), 8.19 (d, 2H, J = 7.8 Hz), 8.97 (s, 2H), 9.97 (s, 1H). ^{13}C NMR (DMSO-d_6): δ_C. 153.6, 150.4, 147.3, 143.1(2C), 138.2, 133.8, 130.5(2C), 129.5(2C), 128.9, 128.2(2C), 127.7, 127.2(2C), 121.4(2C), 121.0(2C), 118.3, 115.5(3C), 106.1, 55.9. EI-MS m/z 467 $(M-H)^-$. Anal Calcd. for $C_{27}H_{21}ClN_4O_2$: C, 69.15; H, 4.51; N, 11.95; Found: C, 69.11; H, 4.54; N, 11.98.

1-(4-(Acridin-9-ylamino)-3-methoxyphenyl)-3-(4-nitrophenyl)urea (7k):

Pale yellow solid; Yield 64%; mp 190-192 °C; ^{1}H NMR (DMSO-d_6)**:** δ_H. 3.85 (s, 3H), 6.62-7.03 (m, 2H), 7.15-7.94 (m, 9H), 8.15-8.27 (m, 4H), 8.89 (s, 2H, J = 8.1Hz), 9.98 (s, 1H). ^{13}C NMR (DMSO-d_6): δ_C. 153.5, 150.3, 147.9, 146.1, 144.3, 142.9(2C), 130.5(2C), 129.0, 128.3(2C), 127.5, 127.0(2C), 124.8(2C), 121.6(2C), 120.4(2C), 118.1, 115.3(3C), 106.2, 55.5. EI-MS m/z 480 $(M+H)^+$. Anal Calcd. for $C_{27}H_{21}N_5O_4$: C, 67.63; H, 4.41; N, 14.61; Found: C, 67.67; H, 4.39; N, 14.63.

1-(4-(Acridin-9-ylamino)-3-methoxyphenyl)-3-(p-tolyl) urea (7l):

Pale brown solid; Yield 64%; mp 197-199 °C; ^{1}H NMR (DMSO-d_6)**:** δ_H. 2.31 (s, 3H, J = 7.26Hz), 3.84 (s, 3H), 6.55-7.01 (m, 2H), 7.19-7.74 (m, 9H), 7.98-8.15 (m, 4H, J = 8.1Hz), 8.97 (s, 2H), 10.6 (s, 1H, J = 8.1Hz). ^{13}C NMR (DMSO-d_6): δ_C. 153.4, 150.2, 148.2, 142.9(2C), 137.3(2C), 130.5(2C), 129.9(2C), 129.0, 128.3(2C), 127.5, 127.0(2C), 122.8(2C), 121.6(2C), 118.3, 115.6(3C), 106.0, 56.2, 21.9. EI-MS 449 $(M+H)^+$. Anal Calcd. for $C_{28}H_{24}N_4O_2$: C, 74.98; H, 5.39; N, 12.49; Found: C, 74.95; H, 5.41; N, 12.46.

1-(3-Methoxy-4-((2-methylacridin-9-yl)amino)phenyl)-3-phenylurea (7m):

Pale brown solid; Yield 68%; mp 200-202 °C; ^{1}H NMR (DMSO-d_6)**:** δ_H. 2.31 (s, 3H), 3.85 (s, 3H), 6.53-6.88 (m, 2H), 7.14-7.95 (m, 11H), 8.19 (d, 1H, J = 8.1 Hz), 9.06 (s, 2H), 10.7 (s, 1H). ^{13}C NMR (DMSO-d_6): δ_C. 153.5, 149.7, 148.1, 142.3, 140.1(2C), 135.6, 132.0(2C), 130.4, 129.5(2C), 128.9(2C), 128.6(2C), 127.4, 122.9(3C), 121.3, 119.9, 118.4, 115.2, 108.6, 106.1, 56.4, 22.3. EI-MS m/z 447 $(M-H)^-$. Anal Calcd. for $C_{28}H_{24}N_4O_2$: C, 74.98; H, 5.39; N, 12.49; Found: C, 75.02; H, 5.35; N, 12.48.

1-(4-Chlorophenyl)-3-[3-methoxy-4-((2-methylacridin-9-yl)amino)phenyl]urea (7n):

Brown solid; Yield 63%; mp 210-212 °C; ^{1}H NMR (DMSO-d_6)**:** δ_H. 2.35 (s, 3H), 3.81 (s, 3H, J = 7.5Hz), 6.59-6.97 (m, 2H), 7.19-7.96 (m, 11H, J = 7.6Hz), 8.21 (m, 1H), 9.07 (s, 2H), 9.97 (s, 1H, J = 8.1Hz). ^{13}C NMR (DMSO-d_6): δ_C. 153.6, 149.7, 148.4, 142.3, 140.1, 138.3, 135.8, 133.9, 132.1(2C), 130.5(2C), 129.7(2C), 128.9, 127.5(2C), 122.1, 121.4(3C), 119.8, 118.1, 115.4, 108.3, 106.0, 56.2, 22.5. EI-MS m/z 483 $(M+H)^+$. Anal Calcd. for $C_{28}H_{23}ClN_4O_2$: C, 69.63; H, 4.80; N, 11.60; Found: C, 69.61; H, 4.83; N, 11.57.

1-(3-Methoxy-4-((2-methylacridin-9-yl)amino)phenyl)-3-(4-nitrophenyl)urea (7o):

Pale brown solid; Yield 68%; mp 191-192 °C; ^{1}H NMR (DMSO-d_6)**:** δ_H. 2.32 (s, 3H), 3.79 (s, 3H), 6.62-6.94 (m, 2H), 7.12-7.89 (m, 9H), 8.19-8.27 (m, 3H, J = 7.6Hz), 9.04 (s, 2H), 10.2 (s, 1H, J = 7.6Hz). ^{13}C NMR (DMSO-d_6): δ_C. 153.4, 149.8, 148.3, 146.1, 144.3, 142.6, 140.1, 135.6, 131.8(2C), 130.5(2C), 128.7, 127.3(2C), 124.7(2C), 122.3, 121.6, 120.3(2C), 119.6, 118.2, 115.3, 108.5, 106.1, 56.4, 22.2. EI-MS m/z 492 $(M-H)^-$. Anal Calcd. for $C_{28}H_{23}N_5O_4$: C, 68.14; H, 4.70; N, 14.19; Found: C, 68.17; H, 4.74; N, 14.16.

1-(3-Methoxy-4-((2-methylacridin-9-yl)amino)phenyl)-3-(p-tolyl)urea (7p):

Pale brown solid; Yield 62%; mp 189-190 °C; ^{1}H NMR (DMSO-d_6)**:** δ_H. 2.32 (s, 6H), 3.81 (s, 3H), 6.48-6.96 (m, 2H), 7.15-7.61 (m, 8H, J = 7.8Hz), 7.80-8.21 (m, 4H), 8.99 (s, 2H), 9.89 (s, 1H, J = 7.6Hz). ^{13}C NMR (DMSO-d_6): δ_C. 153.6, 149.7, 148.4, 142.3, 140.1, 137.3(2C), 135.8, 132.0(2C), 130.7, 129.9(3C), 128.7, 127.4(2C), 122.1(3C), 121.3, 119.8, 118.4, 114.5, 108.3, 106.2, 56.4, 22.5(2C). EI-MS m/z 463 $(M+H)^+$. Anal Calcd. for $C_{29}H_{26}N_4O_2$: C, 75.30; H, 5.67; N, 12.11; Found: C, 75.32; H, 5.61; N, 12.15.

Annexure III: Synthesis of Tryptanthrin derivatives (TR00-TR13):

The most efficient method for the synthesis of tryptanthrin and many of its analogues is the reaction of isatoic anhydride with isatin. Isatoic anhydride and isatin were taken in 1:2 ratio and heated at 100 °C in the presence of solvent 1:2 DMF/Toluene and trimethylamine for 2-4 hr. The reaction mixture was filtered and the filtrate was concentrated to get crude compound. Crude compound was triturated by using diisopropylether and dried to afford compound **TR00-TR13.**

Indolo[2,1-b]quinazoline-6,12-dione (TR00):

Yellow solid; Yield 48%; mp 189-190 °C; ^{1}H NMR (DMSO-d_6): δ_H 7.30(t, 1H, J = 7.5Hz), 7.65(q, 2H), 7.72(m, 1H, J = 7.5Hz), 7.99-8.05(m, 3H), 8.49(d, 1H, J = 7.5Hz); ^{13}C NMR (DMSO-d_6): δ_C 187.4, 160.6, 151.7, 146.2, 145.5, 134.7, 133.4, 130.0, 129.9, 127.3, 126.7, 126.6, 125.7, 120.8,117.7. ESI-MS m/z 249 $(M + H)^+$.Anal Calcd. for $C_{15}H_8N_2O_2$: C, 72.58; H, 3.25; N, 11.28; O, 12.89; Found: C, 72.60; H, 3.24; N, 11.29; O, 12.88.

2-Chloro-indolo[2,1-b]quinazoline-6,12-dione (TR01):

Yellow solid; Yield 57.6%; mp 252-253 °C; 1H NMR (DMSO-d6): δ_H 7.40(m, 2H, J = 7.26Hz), 7.75(d, 1H), 7.99-8.05(m, 3H), 8.49(d, 1H, J = 7.2.6Hz); 13C NMR (DMSO-d6): δ_C 187.4, 160.6, 151.7, 146.2, 143.6, 134.7, 133.5, 132.9, 130.0, 129.9, 127.7, 127.7, 125.7, 122.2, 117.7. ESI-MS m/z 283 $(M + H)^+$. Anal Calcd. for $C_{15}H_7ClN_2O_2$: C, 63.73; H, 2.50; Cl, 12.54; N, 9.91; O, 11.32; Found: C, 63.74; H, 2.49; N, 11.28; O, 12.89.

2-Bromo-indolo[2,1-b]quinazoline-6,12-dione (TR02):

Pale yellow solid; Yield 47%; mp 258-259 °C; 1H NMR (DMSO-d6): δ_H 7.40(m, 1H, J = 7.26Hz), 7.71(d, 1H), 7.99-8.05(q, 3H), 8.25(s, 1H, J = 7.26Hz), 8.49(d, 1H, J = 7.2.6Hz); 13C NMR (DMSO-d6): δ_C 187.4, 160.6, 151.7, 146.2, 144.5, 136.3, 134.7, 132.3, 130.0, 129.9,

125.7, 124.6, 123.0, 121.7, 117.7. ESI-MS m/z 328 $(M + H)^+$. Anal Calcd. for $C_{15}H_7BrN_2O_2$: C, 55.07; H, 2.16; Br, 24.43; N, 8.56; O, 9.78; Found: C, 55.08; H, 2.15; Br, 24.44; N, 8.54; O, 9.79.

8-Nitro-indolo[2,1-b]quinazoline-6,12-dione (TR03):

Light green solid; Yield 30%; mp 276-277 °C; 1H NMR (DMSO-d6): δ_H 7.64-7.71(m, 3H, J = 7.5Hz), 8.05(d, 1H), 8.25(d, 1H, J = 7.5Hz), 8.44(s, 1H, J = 7.5Hz), 8.53(d, 1H); 13C NMR (DMSO-d6): $\delta_{C.}$ 187.4, 160.6, 152.3, 151.7, 145.5, 144.0, 133.4, 129.9, 127.3, 126.7, 126.6,123.7, 123.0, 120.8, 118.6 ESI-MS m/z 294 $(M + H)^+$. Anal Calcd. for $C_{15}H_7N_3O_4$: C, 61.44; H, 2.41; N, 14.33; O, 21.82; Found: C, 61.42; H, 2.42; Br, 24.43; N, 8.53; O, 9.78.

8-Fluoro-indolo[2,1-b]quinazoline-6,12-dione (TR04):

Yellow solid; Yield 82.6%; mp 271-272 °C; 1H NMR (DMSO-d6): δ_H 7.44-7.51(m, 2H, J = 8.0Hz), 7.63-7.75(m, 3H), 7.98-8.05(q, 2H, J = 7.5Hz); 13C NMR (DMSO-d6): $\delta_{C.}$ 187.4, 164.5, 160.6, 151.7, 145.5, 141.8, 133.4, 127.3, 126.7, 126.6, 123.7, 121.5, 120.8, 119.3, 112.6. ESI-MS m/z 267 $(M + H)^+$. Anal Calcd. for $C_{15}H_7FN_2O_2$: C, 67.67; H, 2.65; F, 7.14; N, 10.52; O, 12.02; Found: C, 67.65; H, 2.64; F, 7.15; N, 10.51; O, 12.01.

2-Chloro-8-Fluoro-indolo[2,1-b]quinazoline-6,12-dione (TR05):

Yellow solid; Yield 61.3%; mp 278-279 °C; 1H NMR (DMSO-d6): δ_H 7.44-7.51(m, 3H, J = 8.0Hz), 7.75(d, 1H), 7.94-7.99(t, 2H, J = 7.5Hz); 13C NMR (DMSO-d6): $\delta_{C.}$ 187.4, 164.5, 160.6, 151.7, 143.6, 141.8, 133.5, 132.9, 127.7, 127.7, 123.7, 122.2, 121.5, 119.3, 112.6. ESI-MS m/z 301 $(M + H)^+$. Anal Calcd. for $C_{15}H_6ClFN_2O_2$: C, 59.92; H, 2.01; Cl, 11.79; F, 6.32; N, 9.32; O, 10.64; Found: C, 59.95; H, 2.02; Cl, 11.78; F, 6.31; N, 8.53; O, 9.78.

2-Bromo-8-Fluoro-indolo[2,1-b]quinazoline-6,12-dione (TR06):

Yellow solid; Yield 67%; mp 281-282 °C; 1H NMR (DMSO-d6): δ_H 7.44-7.51(m, 2H, J = 8.0Hz), 7.67(d, 1H), 7.45-8.02(q, 3H, J = 8.0Hz), 8.22(d, 1H, J = 7.5Hz); 13C NMR (DMSO-d6): $\delta_{C.}$ 187.4, 164.5, 160.6, 151.7, 144.5, 141.8, 136.3, 132.3, 124.6, 123.7, 123.0, 121.7, 121.5, 119.3, 112.6. ESI-MS m/z 346 $(M + H)^+$. Anal Calcd. for $C_{15}H_6BrFN_2O_2$: C, 52.20; H, 1.75; Br, 23.15; F, 5.50; N, 8.12; O, 9.27; Found: C, 52.18; H, 1.73; Br, 23.16; F, 5.51; N, 8.13; O, 9.28.

8-Chloro-indolo[2,1-b]quinazoline-6,12-dione (TR07):

Brown solid; Yield 63%; mp 287-288 °C; 1H NMR (DMSO-d6): δ_H 7.62-7.80(m, 5H, J = 7.5Hz), 7.96(d, 1H), 8.05(d, 1H, J = 7.5Hz); 13C NMR (DMSO-d6): $\delta_{C.}$ 187.4, 160.6, 151.7, 145.5, 144.3, 138.2, 134.8, 133.4, 127.3, 126.9, 126.7,126.6, 124.7, 120.8, 119.1.ESI-MS m/z 283 $(M + H)^+$. Anal Calcd. for $C_{15}H_7ClN_2O_2$: C, 63.73; H, 2.50; Cl, 12.54; N, 9.91; O, 11.32; Found: C, 63.71; H, 2.51; Cl, 12.55; N, 9.93; O, 9.77.

2,8-Dichloro-indolo[2,1-b]quinazoline-6,12-dione (TR08):

Yellow solid; Yield 72%; mp 288-289 °C; 1H NMR (DMSO-d6): δ_H 7.45(d, 1H, J = 7.5Hz), 7.73-7.80(q, 3H), 7.95(d, 2H, J = 7.5Hz); 13C NMR (DMSO-d6): $\delta_{C.}$ 187.4, 160.6, 151.7, 144.3, 143.6, 138.2, 134.8, 133.5, 132.9, 127.7, 127.7, 126.9, 124.7, 122.2, 119.1. ESI-MS m/z 318 $(M + H)^+$. Anal Calcd. for $C_{15}H_6Cl_2N_2O_2$: C, 56.81; H, 1.19; Cl, 22.36; N, 8.83; O, 10.09; Found: C, 56.78; H, 1.18; Cl, 22.38; N, 8.84; O, 10.10.

2-Bromo-8-Chloro-indolo[2,1-b]quinazoline-6,12-dione (TR09):

Pale yellow solid; Yield 42.9%; mp 283-284 °C; 1H NMR (DMSO-d6): δ_H 7.65(d, 1H, J = 7.5Hz), 7.74-7.80(q, 2H), 7.94-8.03(m, 2H, J = 7.5Hz), 8.23(s, 1H); 13C NMR (DMSO-d6): $\delta_{C.}$ 187.4, 160.6, 151.7, 144.5, 144.3, 138.2, 136.3, 134.8, 132.3, 126.9, 124.7, 124.6, 123.0,

121.7, 119.1.ESI-MS m/z 362 $(M + H)^+$. Anal Calcd. for $C_{15}H_6BrClN_2O_2$: C, 49.83; H, 1.67; Br, 22.10; Cl, 9.81; N, 7.75; O, 8.85; Found: C, 49.81; H, 1.65; Br, 22.12; Cl, 9.82; N, 7.74; O, 8.87

8-Bromo-indolo[2,1-b]quinazoline-6,12-dione (TR10):

Brown solid; Yield 48.6%; mp 276-277 °C; 1H NMR (DMSO-d6): δ_H 7.62-7.70(m, 3H, J = 7.5Hz), 7.85-7.89(q, 2H), 8.03-8.08(t, 2H, J = 7.5Hz); 13C NMR (DMSO-d6): $\delta_{C.}$ 187.4, 160.6, 151.7, 145.5, 145.2, 137.6, 133.6, 133.4, 127.3, 126.7, 126.6, 124.3, 120.8, 119.9, 119.2. ESI-MS m/z 326 $(M + H)^+$. Anal Calcd. for $C_{15}H_7BrN_2O_2$: C, 55.07; H, 2.16; Br, 24.43; N, 8.56; O, 9.78; Found: C, 55.04; H, 2.15; Br, 24.45; N, 8.57; O, 9.79.

2-Chloro-8-Bromo-indolo[2,1-b]quinazoline-6,12-dione (TR11):

Yellow solid; Yield 48%; mp 272-273 °C; 1H NMR (DMSO-d6): δ_H 7.45(d, 1H, J = 7.5Hz), 7.75(d, 1H), 7.85-7.96(m, 3H, J = 7.5Hz), 8.06(d, 1H); 13C NMR (DMSO-d6): $\delta_{C.}$ 187.4, 160.6, 151.7, 145.2, 143.6, 137.6, 133.6, 133.5, 132.9, 127.7, 127.7, 124.3, 122.2, 119.9, 119.2. ESI-MS m/z 362 $(M + H)^+$. Anal Calcd. for $C_{15}H_6BrClN_2O_2$: C, 49.83; H, 1.67; Br, 22.10; Cl, 9.81; N, 7.75; O, 8.85; Found: C, 49.80; H, 1.68; Br, 22.09; Cl, 9.82; N, 7.77; O, 8.86.

2,8-Dibromo-indolo[2,1-b]quinazoline-6,12-dione (TR12):

Yellow solid; Yield 32%; mp 281-282 °C; 1H NMR (DMSO-d6): δ_H 7.65(d, 1H, J = 7.5Hz), 7.85-7.90(m, 2H), 8.01-8.07(m, 2H, J = 7.5Hz), 8.22(d, 1H); 13C NMR (DMSO-d6): $\delta_{C.}$ 187.4, 160.6, 151.7, 145.2, 144.5, 137.6, 136.3, 133.6, 132.3, 124.6, 124.3, 123.0, 121.7, 119.9, 119.2. ESI-MS m/z 407 $(M + H)^+$. Anal Calcd. for $C_{15}H_6Br_2N_2O_2$: C, 44.37; H, 1.49; Br, 39.36; N, 6.90; O, 7.88; Found: C, 44.34; H, 1.48; Br, 39.38; N, 6.91; O, 7.89.

8-Methyl-indolo[2,1-b]quinazoline-6,12-dione (TR13):

Yellow solid; Yield 52.2%; mp 270-271 °C; 1H NMR (DMSO-d6): δ_H 2.35(s, 1H, J = 7.5Hz), 7.48(d, 1H), 7.57-7.71(m, 4H), 7.87(d, 1H, J = 7.5Hz), 8.02(d, 1H); 13C NMR (DMSO-d6): $\delta_{C.}$ 187.4, 160.6, 151.7, 145.5, 143.2, 137.4, 135.0, 133.4, 127.3, 126.7, 126.6, 124.0, 122.0, 120.8, 117.6, 21.3. ESI-MS m/z 263 $(M + H)^+$. Anal Calcd. for $C_{16}H_{10}N_2O_2$: C, 73.27; H, 3.84; N, 10.68; O, 12.20; Found: C, 73.29; H, 3.83; N, 10.66; O, 7.92

Appendix
List of publications

From thesis work:

1. **Jonnalagadda Padma Sridevi**, Hasitha Shilpa Anantaraju, Pushkar Kulkarni, Perumal Yogeeswari, Dharmarajan Sriram. Optimization and validation of *Mycobacterium marinum*-induced adult zebrafish model for evaluation of oral anti-tuberculosis drugs. **International Journal of Mycobacteriology,** 2014. 3, 259-267.
2. **Jonnalagadda Padma Sridevi** , Priyanka Suryadevara, Renuka Janupally, Jogula Sridhar, Vijay soni, Hasitha Shilpa Anantaraju, Perumal Yogeeswari, Dharmarajan Sriram. Identification of potential Mycobacterium tuberculosis topoisomerase I inhibitors: a study against active, dormant and resistant tuberculosis. **European Journal of Pharmaceutical Sciences.** 2015. 72, 81-92.

Other Publications:

1. Parthiban Brindha Devi, Shalini Saxena, Manoj Chandran, **Jonnalagadda Padma Sridevi**, Renu Yadav, Rudraraju Reshma Srilakshmi, Perumal Yogeeswari, Dharmarajan Sriram. Design and Development of Mycobacterium tuberculosis Lysine ε-Aminotransferase Inhibitors for Latent Tuberculosis Infection. Chemical Biology and Drug Design. 2015. doi: 10.1111/cbdd.12655. [Epub ahead of print]
2. Parthiban Brindha Devi, **Jonnalagadda Padma Sridevi,** Shruti Singh Kakan, Shalini Saxena, Variam Ullas Jean Kumar, Vijay Soni, Hasitha Shilpa Anantaraju, Perumal Yogeeswari, Dharmarajan Sriram. Discovery of novel lysine ε-aminotransferase inhibitors: An intriguing potential target for latent tuberculosis. Tuberculosis (Edinb). 2015. 95, 786-94. doi: 10.1016/j.tube.2015.04.010.
3. Ahmed Kamal, B.V. Subba Reddy, Bhima Sridevi, A. Ravikumar, A. Venkateswarlu, G. Sravanthi, **Jonnalagadda Padma Sridevi**, Perumal Yogeeswari, Dharmarajan Sriram. Synthesis and biological evaluation of phaitanthrin congeners as anti-mycobacterial agents. Bioorganic and Medicinal Chemistry Letters. 2015. 25, 3867-72. doi: 10.1016/j.bmcl.2015.07.057.
4. Brahmam Medapi, Priyanka Suryadevara, Renuka Janupally, **Jonnalagadda Padma Sridevi**, Perumal Yogeeswari, Dharmarajan Sriram. 4-Aminoquinoline derivatives as novel Mycobacterium tuberculosis GyrB inhibitors: Structural optimization, synthesis and biological evaluation. European Journal of Medicinal Chemistry. 2015. 103, 1-16. doi: 10.1016/j.ejmech.2015.06.032.
5. Kummetha Indrasena Reddy, C. Aruna, K. Sudhakar babu, M. Manisha, **Jonnalagadda Padma Sridevi**, Perumal Yogeeswari, Dharmarajan Sriram. ChemInform Abstract: General and Efficient Synthesis of Benzoxazol-2(3H)-ones: Evolution of Their Anticancer and Anti-mycobacterial Activities. ChemInform. 2015. doi: 10.1002/chin.201518158.
6. Manoj Chandran, Renuka Janupally, **Jonnalagadda Padma Sridevi**, Ganesh S Pedgaonkar, Vanaparthi Asmitha, Perumal Yogeeswari, Dharmarajan Sriram. Benzothiazinone-piperazine derivatives as efficient Mycobacterium tuberculosis DNA gyrase inhibitors. International Journal of Mycobacteriology. 2015. 3. doi: 10.1016/j.ijmyco.2015.02.002.
7. Brahmam Medapi, Janupally Renuka, Shalini Saxena, **Jonnalagadda Padma Sridevi**, Raghavendra Medishetti, Pushkar Kulkarni, Perumal Yogeeswari, Dharmarajan Sriram. Design and synthesis of novel quinoline-aminopiperidine hybrid analogues as Mycobacterium tuberculosis DNA gyraseB inhibitors. Bioorganic and Medicinal Chemistry. 2015. 23, 2062-78. doi: 10.1016/j.bmc.2015.03.004.
8. Shalini Saxena, Ganesh Samala, **Jonnalagadda Padma Sridevi**, Parthiban Brindha Devi, Perumal Yogeeswari, Dharmarajan Sriram. Design and development of novel Mycobacterium tuberculosis L-alanine dehydrogenase inhibitors. European Journal of Medicinal Chemistry. 2015. 92, 401-14. doi: 10.1016/j.ejmech.2014.12.046.
9. Shalini Saxena, Ganesh Samala, Janupally Renuka, **Jonnalagadda Padma Sridevi**, Perumal Yogeeswari, Dharmarajan Sriram. Development of 2-amino-5-phenylthiophene-3-carboxamide

derivatives as novel inhibitors of Mycobacterium tuberculosis DNA GyrB domain. Bioorganic and Medicinal Chemistry. 2015. 23, 1402-12. doi: 10.1016/j.bmc.2015.02.032.

10. Variam Ullas Jean Kumar, Rudraraju Reshma Srilakshmi, Janupally Renuka, Shalini Saxena, **Jonnalagadda Padma Sridevi**, Brahmam Medapi, Pushkar Kulkarni, Perumal Yogeeswari, Dharmarajan Sriram. Enabling the (3 + 2) cycloaddition reaction in assembling newer anti-tubercular lead acting through the inhibition of the gyrase ATPase domain: lead optimization and structure activity profiling. Organic and Biomolecular Chemistry. 2015. 13, 2423-31. doi: 10.1039/c4ob02049a.
11. Variam Ullas Jean Kumar, Sonali Kotagiri, Janupally Renuka, Priyanka Suryadevara, **Jonnalagadda Padma Sridevi**, Raghavendra Medishetti, Pushkar Kulkarni, Perumal Yogeeswari, Dharmarajan Sriram. Exploring the gyrase ATPase domain for tailoring newer anti-tubercular drugs: hit to lead optimization of a novel class of thiazole inhibitors. Bioorganic and Medicinal Chemistry. 2015. 23, 588-601. doi: 10.1016/j.bmc.2014.12.001.
12. Parthiban Brindha Devi, Ganesh Samala, **Jonnalagadda Padma Sridevi**, Shalini Saxena, Mallika Alvala, Salina EG, Dharmarajan Sriram, Perumal Yogeeswari. Structure-guided design of thiazolidine derivatives as Mycobacterium tuberculosis pantothenate synthetase inhibitors. ChemMedChem. 2014. 9, 2538-47. doi: 10.1002/cmdc.201402171.
13. Gilish Jose, T.H. Suresha Kumara, G. Nagendrappa, H.B. Sowmya, Dharmarajan Sriram, Perumal Yogeeswari, **Jonnalagadda Padma Sridevi**, Tayur N. Guru Row, Amar Hosamani , P.S. Sujan Ganapathy, N. Chandrika, L.V. Narendra. Synthesis, molecular docking and anti-mycobacterial evaluation of new imidazo[1,2-a]pyridine-2-carboxamide derivatives. European Journal of Medicinal Chemistry. 2015. 9, 616-27. doi: 10.1016/j.ejmech.2014.10.079.
14. Vijayaprthasarathi Vijayakumar, Kummetha Indrasena Reddy, Aruna Chuppala, K. Sudhakar Babu, M.Manisha**, Jonnalagadda Padma Sridevi**, Perumal Yogeeswari, Dharmarajan Sriram. General and an efficient synthesis of benzoxazol-2(3H)-ones: Evolution of its anti-cancer and anti-mycobacterial activities. RSC Advances. 2014. doi: 10.1039/C4RA07123A.
15. Kummetha Indrasena Reddy, K. Srihari, Janupally Renuka, Sree KS, Chuppala Aruna, Variam Ullas Jean Kumar, **Jonnalagadda Padma Sridevi**, K. Sudhakar Babu, Perumal Yogeeswari, Dharmarajan Sriram. An efficient synthesis and biological screening of benzofuran and benzo[d]isothiazole derivatives for Mycobacterium tuberculosis DNA GyrB inhibition. Bioorganic and Medicinal Chemistry. 2014. 22, 6552-63.
16. Ganesh S Pedgaonkar, **Jonnalagadda Padma Sridevi**, Variam Ullas Jean Kumar, Shalini Saxena, Parthiban Brindha Devi, Janupally Renuka, Perumal Yogeeswari, Dharmarajan Sriram. Development of 2-(4-oxoquinazolin-3(4H)-yl)acetamide derivatives as novel enoyl-acyl carrier protein reductase (InhA) inhibitors for the treatment of tuberculosis, Eur. J. Med. Chem, DOI: 10.1016/j.ejmech.2014.09.028.
17. Asit Kumar Chakraborti, Parth Shah, Tejas M.Dhameliya, Rohit Bansal, Manesh Nautiyal, Damodara Naidu Kommi, Pradeep Jadhavar, **Jonnalagadda Padma Sridevi**, Perumal Yogeeswari, Dharmarajan Sriram. N-Arylalkylbenzo[d]thiazole-2-carboxamides as anti-mycobacterial agents: Design, new methods of synthesis and biological evaluation. Medicinal Chemistry Communications. 2014. doi: 10.1039/C4MD00224E.

18. Ganesh Samala, Chunduri Madhuri, **Jonnalagadda Padma Sridevi**, Radhika Nallangi, Perumal Yogeeswari, Dharmarajan Sriram. Synthesis and anti-tubercular evaluation of 2-iminothiazolidine-4-ones. European Journal of Chemistry. 2014. doi: 10.5155/eurjchem.5.3.550-556.1059.
19. Karyakulam Andrews Bobesh, Janupally Renuka, Variam Ullas Jeankumar, Singh Kakan Shruti · **Jonnalagadda Padma Sridevi**, Perumal Yogeeswari, Dharmarajan Sriram. Extending the N-linked aminopiperidine class to the mycobacterial gyrase domain: Pharmacophore mapping from known antibacterial leads. European Journal of Medicinal Chemistry. 2014. 85, 593-604. doi:10.1016/j.ejmech.2014.08.018.
20. Ganesh S Pedgaonkar, **Jonnalagadda Padma Sridevi**, Variam Ullas Jean Kumar, Shalini Saxena, Parthiban Brindha Devi, Janupally Renuka, Perumal Yogeeswari, Dharmarajan Sriram, Development of benzy[*d*]oxazol-2(3*H*)-ones derivatives as novel inhibitors of *Mycobacterium tuberculosis* InhA, Bioorg. Med. Chem., DOI: 10.1016/j.bmc.2014.08.031.
21. Lakshmi Reddy Pagadala, Lakshmi Devi Mukkara, Satyanarayana Singireddi, Ashita Singh, Veera Reddy Thummaluru, **Jonnalagadda Padma Sridevi**, Raja Sekhar Guttala, Yogeeswari Perumal, Sriram Dharmarajan, Suryanarayana Murty Upadhyayula, Ramesh Ummanni, Venkata Subba Reddy Basireddy, Narender Ravirala. Design, synthesis and anti-mycobacterial activity of 1,2,3,5-tetrasubstituted pyrrolyl-N-acetic acid derivatives. European Journal of Medicinal chemistry. 2014. 84, 118-26. DOI:10.1016/j.ejmech.2014.06.075.
22. Janupally Renuka, Kummetha Indrasena Reddy, Konduri Srihari, Variam Ullas Jeankumar, Morla Shravan, **Jonnalagadda Padma Sridevi**, Perumal Yogeeswari, Kondra Sudhakar Babu, Dharmarajan Sriram. Design, synthesis, biological evaluation of substituted benzofurans as DNA gyraseB inhibitors of Mycobacterium tuberculosis. Bioorganic and Medicinal Chemistry. 2014. doi: 10.1016/j.bmc.2014.06.041.
23. Variam Ullas Jeankumar, Janupally Renuka, Sonali Kotagiri, Shalini Saxena, Shruti Singh Kakan · **Jonnalagadda Padma Sridevi**, Swapna Yellanki, Pushkar Kulkarni, Perumal Yogeeswari, Dharmarajan Sriram. Gyrase ATPase Domain as an Anti-tubercular Drug Discovery Platform: Structure-Based Design and Lead Optimization of Nitrothiazolyl Carboxamide Analogues. ChemMedChem. 2014. doi: 10.1002/cmdc.201402035.
24. Ganesh Samala, Shruti Singh Kakan, Radhika Nallangi, Parthiban Brindha Devi, **Jonnalagadda Padma Sridevi**, Shalini Saxena, Perumal Yogeeswari, Dharmarajan Sriram, Investigating structure-activity relationship and mechanism of action of anti-tubercular 1-(4-chlorophenyl)-4-(4-hydroxy-3-methoxy-5-nitrobenzylidene) pyrazolidine-3,5-dione [CD59], International Journal of Mycobacteriology, **2014** 3(2):117-126. doi:10.1016/j.ijmyco.2014.02.006.
25. Ganesh Samala, Radhika Nallangi, Parthiban Brindha Devi, Shalini Saxena, Renu Yadav**, Jonnalagadda Padma Sridevi**, Perumal Yogeeswari, Dharmarajan Sriram, Identification and development of 2-methylimidazo[1,2-a] pyridine-3-carboxamides as Mycobacterium tuberculosis pantothenate synthetase Inhibitors, Bioorganic and Medicinal Chemistry. 2014. DOI: 10.1016/j.bmc.2014.05.038.

26. Mahesh Akula, **Jonnalagadda Padma Sridevi**, Perumal Yogeeswari, Dharmarajan Sriram, Anupam Bhattacharya · New class of anti-tubercular compounds: Synthesis and anti-tubercular activity of 4-substituted pyrrolo[2,3-c]quinolines. Monatshefte fuer chemie/Chemical mothly. 2014. 145, 811-819. doi: 10.1007/s00706-013-1141-1.

27. Variam Ullas Jeankumar, Reshma Alokam, **Jonnalagadda Padma Sridevi**, Priyanka Suryadevara, Siddharth Sai Matikonda, Santosh Peddi, Seedarala Sahithi, Mallika Alvala, Perumal Yogeeswari, Dharmarajan Sriram · Discovery and Structure Optimization of a Series of Isatin Derivatives as Mycobacterium tuberculosis Chorismate Mutase Inhibitors. Chemical Biology and Drug Design. 2014. 83, 498-506. doi: 10.1111/cbdd.12265.

28. Radhika Nallangi, Ganesh Samala, **Jonnalagadda Padma Sridevi**, Perumal Yogeeswari, Dharmarajan Sriram. Development of anti-mycobacterial tetrahydrothieno[2,3-c]pyridine-3- carboxamides and hexahydrocycloocta[b]thiophene-3-carboxamides: Molecular modification from known anti-mycobacterial lead. European Journal of Medicinal Chemistry. 2014. 76, 110-117. doi: 10.1016/j.ejmech.2014.02.028.

29. Ganesh Samala, Parthiban Brindha Devi**,** Radhika Nallangi, **Jonnalagadda Padma Sridevi**, Shalini Saxena, Perumal Yogeeswari, Dharmarajan Sriram, Development of Novel tetrahydrothieno[2,3-c] pyridine-3-carboxamide based *Mycobacterium tuberculosis* pantothenate synthetase inhibitors: Molecular hybridization from known anti-mycobacterial leads, Bioorg. Med. Chem., **2014**, 22(6); 1938-1947. doi: 10.1016/j.bmc.2014.01.030.

30. Hunsur Nagendra Nagesh, Narva Suresh, Kalaga Mahalakshmi Naidu, Boyineni Arun, **Jonnalagadda Padma Sridevi,** Dharmarajan Sriram, Perumal Yogeeswari, Kondapalli Venkata Gowri Chandra Sekhar. Synthesis and evaluation of anti-tubercular activity of 6-(4-substitutedpiperazin-1-yl) phenanthridine analogues. European Journal of Medicinal Chemistry. 2014. 74, 333-39. doi: 10.1016.j.ejmech.2014.01.005.

31. Parthiban Brindha Devi, Shalini saxena, Sridhar Jogula, Asireddy Parameshwar reddy, **Jonnalagadda Padma Sridevi**, Dharmarajan Sriram, Perumal Yogeeswari. Design of Novel Mycobacterium tuberculosis Pantothenate Synthetase Inhibitors: Virtual Screening, Synthesis and *In Vitro* Biological Activities. Molecular Informatics. 2014. 34, 2-3. doi: 10.1002/minf.20140012.

32. Variam Ullas Jeankumar, Janupally Renuka, Venkat Koushik Pulla, Vijay Soni, **Jonnalagadda Padma Sridevi**, Priyanka Suryadevara, Morla Shravan, Raghavender Medishetti, Pushkar Kulkarni, Perumal Yogeeswari, Dharmarajan Sriram. Development of Novel N-linked Aminopiperidine based Mycobacterial DNA Gyrase B inhibitors: Scaffold hoping from known Antibacterial leads. Internation Journal of Antimicrobial Agents. 2013, 43. doi: 10.1016/j.ijantimicag.2013.12.006.

33. Thirumal Yempala, **Jonnalagadda Padma Sridevi**, Perumal Yogeeswari, Dharmarajan Sriram, Srinivas Kantevari. ChemInform Abstract: Rational Design and Synthesis of Novel Dibenzo[b,d]furan-1,2,3-triazole Conjugates as Potent Inhibitors of Mycobacterium tuberculosis. European Journal of Medicinal Chemistry. 2013. 71, 160-67. doi: 10.1016/j.ejmech.2013.10.082.

34. Hunsur Nagendra Nagesh, Kalaga Mahalakshmi Naidu, Damarla Harika Rao, **Jonnalagadda Padma Sridevi**, Dharmarajan Sriram, Perumal Yogeeswari, Kondapalli Venkata Gowri Chandra Sekhar. Design, synthesis and evaluation of 6-(4-((substituted-1H-1,2,3-triazol-4-yl)methyl)piperazin-1-yl)phenanthr idine analogues as anti-mycobacterial agents. Bioorganic and Medicinal Chemistry Letters. 2013. 23. doi: 10.1016/j.bmcl.2013.10.016.

35. Variam Ullas Jeankumar, Janupally Renuka, Peddi Santosh, Vijay Soni, **Jonnalagadda Padma Sridevi**, Priyanka Suryadevara, Perumal Yogeeswari, Dharmarajan Sriram. Thiazole-aminopiperidine hybrid analogues: Design and synthesis of novel Mycobacterium tuberculosis GyrB inhibitors. European Journal of Medicinal Chemistry. 2013. 70, 143-53. doi: 10.1016/j.ejmech.2013.09.025.

36. Reshma Alokam, Variam Ullas Jeankumar, **Jonnalagadda Padma Sridevi**, Siddharth Sai Matikonda, Santosh Peddi, Mallika Alvala, Perumal Yogeeswari, Dharmarajan Sriram. Identification and structure-activity relationship study of carvacrol derivatives as Mycobacterium tuberculosis chorismate mutase inhibitors. Journal of Enzyme Inhibition and Medicinal Chemistry. 2013. 29. doi: 10.3109/14756366.2013.823958.

37. Thirumal Yempala, **Jonnalagadda Padma Sridevi**, Perumal Yogeeswari, Darmarajan Sriram, Srinivas Kantevari. ChemInform Abstract: Design, Synthesis and Anti-tubercular Evaluation of Novel 2-Substituted-3H-benzofuro Benzofurans via Palladium-Copper Catalyzed Sonogashira Coupling Reaction. Bioorganic and Medicinal Chemistry. 2013. doi: 10.1016/j.bmcl.2013.07.048.

BIOGRAPHY OF PADMA SRIDEVI J.

Padma Sridevi J. completed her Bachelor of Pharmacy from The Tamilnadu Dr. M.G.R. Medical University, Chennai, Tamilnadu. She was awarded "Prof.K.Chinnaswamy GOLD MEDAL" for securing highest percentage in B.Pharmacy. She was also awarded "IDMA J.B. Mody Best Student's Excellence Award" for the academic year 2011 by INDIAN DRUG MANUFACTURERS' ASSOCIATION (IDMA). She has been appointed as DST INSPIRE Fellow from 2013-2016, at BITS-Pilani Hyderabad campus, under the supervision of Prof. D. Sriram. She has joined as DST-INSPIRE JRF in Jan 2013 and has been promoted to DST-INSPIRE SRF in Sep 2015. She has published 39 scientific publications in well-renowned international journals.

BIOGRAPHY OF Prof. D. SRIRAM

Prof. D. Sriram is presently working in the capacity of Professor at Pharmacy Group, Birla Institute of Technology and Science, Pilani, Hyderabad campus. He received his Ph. D. in 2000 from Banaras Hindu University, Varanasi. He has been involved in teaching and research for last 16 years. He has collaborations with various national and international organizations such as Karolinska institute, Sweden; National Institute of Immunology, New Delhi; IIT Kanpur; Institute of Science and technology for Tuberculosis, Porto alegre, Brazil etc.,. He has guided 16 Ph.D. students and 9 students are pursuing Ph.D currently.